Coupled-cluster theory for infinite matter

Gustav Baardsen

January 15, 2014

Contents

Chapter 1

Introduction

- Why infinite nuclear matter?

Nucleosynthesis.
Core-collapse supernovae and colliding neutron stars are candidates for r-processes, which is believed to be the process that has created a large portion of the heaviest elements [1,2]. Neutron star equation of state important here (including symmetry energy and stiffness of EOS). [3]

- Why the electron gas?
- Why coupled-cluster theory?
- What I have done
- An outline of the thesis
- Nuclear physics long range plan: `http://science.energy.gov/np/nsac/`

Computational physics, a third way beside experiments and theory. High-performance computing plays a crucial role.

Chapter 2

Background

The subject of this thesis is related to fields as different as nuclear astrophysics and nanotechnology. On a general level, we are interested in questions considering, for example, the origin of the chemical elements, the stability of nuclear matter [4], and physical properties of technological devices on a nanoscale [5]. To get a deeper understanding of these problems, we can study complex systems such as neutron stars, supernovae, atomic nuclei, and nanoscale transistors. The way to approach complicated systems in physics is by using simplified models. Hopefully, the models can tell us something essential about the behaviour of the real physical objects. The focus of this thesis is on one such class of models: infinite matter. In the following sections, we define the two main systems we study, infinite nuclear matter and the homogeneous electron gas, explain why the systems are important, and briefly review some of the related research.

2.1 Inifinite nuclear matter

As far as we know, there are four different fundamental types of interactions in nature. These are the strong, weak, electromagnetic, and gravitational interactions. At high energies, the weak and electromagnetic interactions are shown to converge towards the same interaction; the electroweak interaction [6, 7]. All these fundamental interactions are present in nucleonic matter, which we define as matter with nucleons as building blocks. As predicted initially by Gell-Mann and Zweig and verified later experimentally [7, 8], nucleons have internal structure. Hadrons, including nucleons, consist of quarks and gluons, where the latter mediate the strong interaction between the quarks. According to the successful standard model of elementary particles, strong interactions are described by a theory called Quantum

Chromodynamics (QCD) [7, 9]. In addition to being the building blocks of atomic nuclei, nucleons are important basic constituents in stellar matter.

Similarly as described in, for example, the review article by Day [10], we define infinite nuclear matter as an infinitely large system of homogeneously distributed nucleons. In particular, we study two different nuclear-matter systems: symmetric nuclear matter, which consists of an equal amount of protons and neutrons, and neutron matter, which contains only neutrons. In symmetric nuclear matter, the electrical charge is by definition switched off. In finite nuclei, the gravitational force is vanishingly small [11] compared to the other fundamental interactions, whereas in macroscopic nuclear objects, such as supernovae [3] and neutron stars [12,13], the gravitational force plays an important role. However, the gravitational interaction only affects the density of the system. When studying infinite nuclear matter, we neglect the weak interaction, which is responsible for β decays [7], and concentrate only on residual effects of the strong interaction.

2.1.1 Connection to astrophysics

To understand more about the origin of the chemical elements, the evolution of stars, and the inner mechanisms of the building blocks of matter, we need more knowledge about the structure of nucleons and how they interact. In this thesis, we are particularly interested in the nuclear-matter equation of state. This equation of state describes strongly interacting matter containing only protons and neutrons. As is reviewed in, for example, Ref. [9], strongly interacting matter is predicted to appear in several different phases depending on the temperature and the baryochemical potential [1]. For example, at sufficiently high temperature and baryochemical potential, quarks and gluons become much less confined and form a so-called quark-gluon plasma. [2] In our work, we assume that the temperature and baryochemical potential (or density) are sufficiently low such that the quarks and gluons are confined as hadrons. According to Ref. [12], phases containing deconfined quarks occur at densities around two to three times the saturation density of nuclear matter, which is approximately $2.8 \cdot 10^{14}$ g $\cdot$ cm^{-3}. In this thesis, we study infinite nuclear matter at densities up to at most 10^{15} g $\cdot$ cm^{-3}. One should keep

[1] The chemical potential is defined as the derivative of the total energy density with respect to the particle density related to a given particle type [12]. The baryochemical potential therefore tells how much energy is required to add one baryon, such as for example a nucleon, to the medium.

[2] At the European Organization for Nuclear Research (CERN) [14] and at Brookhaven National Laboratory [15], formation of quark-gluon plasma is studied using heavy-ion collisions.

in mind that at the highest densities we study, hadrons may be mixed with deconfined quark-gluon plasma. At densities above the saturation point, other hadrons, such as pions, kaons, and hyperons may also coexist with nucleons [12, 16].

It is still an open question how a large part of the heavy elements beyond iron have been formed. One of the currently best explanations for the formation of heavy neutron-rich elements is a mechanism called the rapid-neutron-capture process (r-process) [1, 17]. Presently, there is no agreement of where in the universe the necessary conditions for r-prosesses are fulfilled, but core-collapse supernovae and merging neutron stars are among the suggested locations. According to Arnould [1], accurate r-prosess simulations require very precise data for a large number of stable and unstable nuclei. It is costly and difficult to measure all the required nuclei experimentally, and therefore predictive theoretical methods will be essential to understand the r-prosess [1]. Ideally, a predictive microscopic model for many-nucleon systems should reproduce the experimental saturation point of nuclear matter. In that way, nuclear-matter calculations is a good test-bed for microsopic theories. As part of the larger effort, such calculations are necessary to accurately model r-prosesses. The nuclear-matter equation of state, as well as the closely related symmetry energy, are also important components, for example, when predicting theoretically how much energy is released in a supernova type II explosion [18]. Likewise, the same equation of state is an essential input to neutron-star models [12, 13].

We define a Type II supernova following Boyd [17]: Consider a heavy star with a mass larger than ten times the solar mass. When the star has burnt up its fuel, the core contains elements lighter than or equal to iron. When no more energy is released from fusion processes, the core of this big star may start to collapse due to the strong gravitational field. The stellar matter of the core gets compressed until the density is a few times the saturation value. The mechanisms of the following stages are still poorly understood, but the result is a giant explosion where matter is thrown out and eventually the core is left. In this so-called Type II supernova, the dense core may become a neutron star or even a black hole.

There are several reasons why neutron stars are scientifically interesting objects. Firstly, neutron stars are part of several different hypotheses for where the r-prosess could occur [1, 2]. Secondly, we can learn more about how strongly interacting matter behaves at high densities by comparing different theoretical neutron-star models with astrophysical observations [16]. According to current observational data and theory [13], neutron stars have masses between one and three times the solar mass inside a radius that is roughly 12 kilometers. This makes neutron stars to be among the densest

Layer	Density ($\mathrm{g} \cdot \mathrm{cm}^{-3}$)	Composition
Inner core	$\approx 10^{15}$	Nucleons and possibly hyperons, Bose condensate of kaons and pions, and deconfined quark matter
Outer core	$2 \cdot 10^{14} - 10^{15}$	Superfluid neutrons, superconducting protons, electrons and muons
Inner crust	$4 \cdot 10^{11} - 2 \cdot 10^{14}$	Neutron-rich nuclei, superfluid neutrons, and electrons
Outer crust	$10^{6} - 4 \cdot 10^{11}$	Heavy nuclei and electrons

Table 2.1: The composition of a neutron star, as described in Refs. [12, 16]. For comparison, the saturation density of nuclear matter is approximately $2.8 \cdot 10^{14}$ g $\cdot$ cm^{-3}.

known objects in the universe. General relativity, causality, and rotational arguments give upper and lower limits for the mass, as well as maximum radii corresponding to different masses [16]. In addition, different theoretical approaches predict different relationships between the the neutron-star radius and mass [12, 16, 19].

Neutron stars contain strongly interacting matter in a number of different phases. In our description of the composition of neutron stars, we follow Refs. [12, 16]. The phases are belived to exist in layers, forming an onion-shell-like structure. The main body of the star contains inner and outer cores, constituting around 99 % of the total mass, as well as inner and outer crusts. Outside the crust, there is an envelope, and the neutron star is surrounded by an athmosphere. The neutron-star composition is illustrated, for example, in Fig. 3 of Ref. [16]. In Table 2.1, we list the compositions and estimated densities of the core and crust. It is still uncertain exactly what kind of phases exist in the inner core, but possibly there is a mix of nucleons, hyperons, Bose condensates of kaons and pions, and maybe deconfined quark matter. The outer core contains mostly superfluid neutrons, but also a fraction of superconducting protons. This layer is neutralized by electrons and muons. In the crust, neutron-rich and heavy nuclei appear in lattice structures. The crust also contains electrons and superfluid neutrons.

As described in, for example, Refs. [12,20], the nuclear-matter equation of state is a central ingredient in the equation of state of the neutron-star core. Even if different microscopic many-body methods give similar neutron-star equations of state [12], there is still much uncertainty considering the equation of state for symmetric nuclear matter [12, 20–30]. In the next section, we will come back to the symmetric-nuclear-matter problem. The symmetry energy is defined as the difference between the energy per nucleon of pure neutron matter and symmetric nuclear matter. Because of the uncertainties related to the nuclear-matter equation of state, there are large differences in theoretical predictions of the symmetry energy [22, 31–35].

Let us give a few examples that illustrate the importance of the symmetry energy. There has been suggested two important mechanisms for cooling of neutron stars by neutrino emission: the modified Urca process, which is slow, and the fast so-called direct Urca process. It is still and open question whether neutron stars may cool by the direct Urca process or not [16]. The behaviour of the symmetry energy determines if Urca processes are possible in a neutron star [16]. More reliable predictions of the symmetry energy would therefore help us to understand more about the cooling mechanisms of neutron stars. Also other neutron-star observables, such as, for example, the radius-mass relation, are strongly dependent on the symmetry energy [36]. It is well-known that the composition of both neutron stars [16] and supernova cores [37] are sensitive to the symmetry energy.

The nuclear-matter equation of state has been studied experimentally using heavy-ion collisions, giving constraints to the equation of state at densities above the saturation point [38, 39]. According to Lattimer [13], observational, theoretical, and experimental results of neutron-star studies have come to closer agreement during the last years. In future, researchers hope that graviational waves can give more information about the neutron-star equation of state [40].

- Phase diagram of nuclear matter?

Zero temperature is a good approximation if the temperature is much smaller than the Fermi temperature. The Fermi temperature for nuclear matter is very high.

Find latest litterature!

- Ref. [**?**, 41]

- Temperature, relativity, electrons, muons, hyperons, quarks, crust, etc.

2.1.2 The infinite-nuclear-matter problem

Infinite nuclear matter is, as we define it, a relativistic quantum system with an infinite number of interacting nucleons. Given the homogeneous structure, naively one may assume inifite nuclear matter to be a very simple system to study. In fact, many theoretical many-body methods can be formulated easier for a homogeneous system than for, for example, finite nuclei. In particular, the single-particle basis, which for infinite nuclear matter is the plane-wave basis, is much simpler than for finite nuclei. Nevertheless, infinite nuclear matter has been studied using microscopic approaches in more than half a century [42, 43], and still there are large deviations [44, 45] between predictions of different theoretical methods for this system.

Commonly, infinite nuclear matter is modelled using either an *ab initio* many-body method [44, 46] or a kind of mean-field approach [47, 48]. The *ab initio* methods use a Hamiltonian operator containing two- and many-body interactions. Normally, the only adjustable parameters in an *ab initio* calculation are in the Hamiltonian. In the two-body interaction, optimal parameter values are obtained by fitting phase shifts to experimental nucleon-nucleon scattering data [49]. The three-body interaction may have additional parameters which are adjusted to, for example, observables of triton or helium [50], or to the saturation density and/or energy of symmetric nuclear matter [20, 24, 51, 52]. In principle, *ab initio* methods provide a systematic way of improving the result towards the exact solution, given a Hamiltonian operator. However, the results are truly based on first principles only if that is also the case for the Hamiltonian operator.

Self-consistent mean-field approaches [47], such as the Skyrme-Hartree-Fock method, the Gogny model, and relativistic mean-field theory, are methods closely related to density functional theory [53], which is very popular in quantum chemistry and condensed-matter physics, but here tailored to nuclear-physics applications. In these methods [47], an effective density-dependent interaction is used in self-consistent calculations. The effective interaction contains several free parameters, which are typically fitted to optimally reproduce observables of many different nuclei, and possibly also saturation properties of symmetric nuclear matter [45]. In self-consistent mean-field methods, the many-body problem is reduced to an effective one-body problem, which makes these methods computationally considerably simpler than *ab initio* approaches. As a result, self-consistent mean-field approximations can be used to study nuclei from the lightest to superheavy elements.

Because self-consistent mean-field methods cannot be systematically improved, for example as function of a converegence parameter, as is common in *ab initio* methods, the mean-field approaches are believed to have less predictive power than *ab initio* approximations. *Ab initio* calculations provide therefore important tests for mean-field parametrisations. In this context, *ab initio* predictions for the nuclear-matter equation of state play an important role [45]. *Ab initio* methods, such as the non-relativistic Brueckener-Hartree-Fock and the relativistic Dirac-Brueckner-Hartree-Fock approach, have been used [45, 48, 54, 55] to extract density functionals based on the local density approximation. Even if the local density approximation has a microscopic foundation, in particular for systems where the density varies slowly, the quality of these functionals are currently not as good as more common mean-field approaches [45]. The quality of local density approximations for nuclear systems would probably improve if we had more realistic nuclear-matter equations of state [26, 56].

As is pointed out by van Dalen and Müther [25], because the saturation energy per particle in nuclear matter is much smaller than the nucleon mass in energy units, one might assume that relativistic effects are small in nucelonic systems. On the contrary, calculations show [25] that relativistic effects give important contributions for infinite nuclear matter, in particular as compared to nonrelativistic approaches with only a two-body interaction. Non-negligible relativistic effects are also found in finite nuclei [25]. According to Ref. [25], relativistic *ab initio* calculations for finite nuclei are complicated, and have therefore not yet been done. Instead, nonrelativistic approaches for finite nuclei have been widely used [57–60], giving results in good agreement with experiments, in particular when three-body forces are included [57, 61–64]. Relativistic and nonrelativistic mean-field methods are used for finite nuclei and nuclear matter side by side, and in the best calculations both approaches give approximately the same accuracy [45]. As we see, nonrelativistic and relativistic microscopic methods have a complementary role in describing low-energy nuclear systems. Because this thesis considers nonrelativistic *ab initio* methods, we concentrate on this group of methods in the rest of the present section.

When studying infinite nuclear matter, an important test for the microscopic method is to compare the theoretical saturation properties with experimental data. Inside a heavy nucleus, the density is approximately constant and similar for different nuclei [65]. The density in the center of nuclei can be obtained from electron scattering experiments, and different estimates around 0.16–0.17 fm^{-3} are used in the litterature [66, 67]. This is believed to be the saturation density of nuclear matter, also in the infinite-matter limit. In the special case of symmetric nuclear matter, the semiempirical mass for-

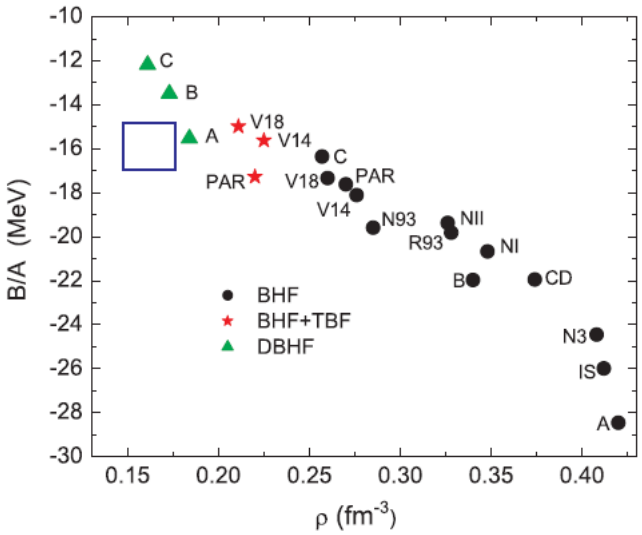

Figure 2.1: Even if different two-body interactions are optimized to reproduce the same nucleon-nucleon phase shifts, they give very different predictions for the symmetric-nuclear-matter saturation point. The figure shows results [22] obtained with the non-relativistic Brueckner-Hartree-Fock method (BHF) and only two-body interactions, with the Brueckner-Hartree-Fock method including three-body forces (BHF+TBF), and relativistic results obtained with the Dirac-Brueckner-Hartree-Fock (DBHF) method. The saturation points are given as the energy per particle B/A at a density ρ. Different points with the same color represent calculations with different two-body interactions. The unfilled square represents the uncertainty region of the experimental saturation point. The figure is courtesy of Ref. [22]. Reprinted by permission from ....

mula [65] for nuclei contains only the volume term. The parameters in the semiempirical mass formula can be determined by simultaneously optimizing with respect to many different finite nuclei [66]. Such an optimization gives an estimate for the volume term, and thus also for the experimental binding energy of symmetric nuclear matter. According to Chabanat *et al.* [66], the experimental bindining energy of nuclear matter is $-(16 \pm 0.2)$ MeV.

Figure 2.1 shows a typical set of saturation points for symmetric nuclear matter, as obtained with different *ab initio* many-body methods and different interaction models. The results are taken from Ref. [22]. The figure presents saturation points obtained with the nonrelativistic Brueckner-Hartree-Fock (BHF) method [42,43,68–72] and the Dirac-Brueckner-Hartree-Fock (DBHF) method [73–78], which is a relativistic counterpart of the BHF approximation. The uncertainty region of the experimental saturation point is marked by a blue unfilled square. As can be seen from the figure, saturation points obtained with the nonrelativistic BHF method and different two-body interaction models (black circles) occur approximately on a line that does not cross the experimental uncertainty region. The phenomenon of saturation points obtained with the same many-body method and different interaction models aligning so that a higher saturation density means more binding is well-known for both nonrelativistic [79] and relativistic calculations [44]. When including only a two-body interaction, nonrelativistic calculations typically give a so-called Coester band much farther from the experimental saturation region than relativistic calculations do [44]. Figure 2.1 also shows another commonly observed feature: When including three-body forces in nonrelativistic calculations, the saturation point is normally closer to the experimental value than in calculations neglecting three-body interactions. It is a prevailing understanding [44, 63] that either three-body interactions are needed in nonrelativistic calculations or a relativistic many-body method is necessary to obtain saturation properties in agreement with experimental data.

In many-body perturbation theory, the energy can be expressed in terms of Goldsone diagrams [80]. The hole line approximation [10, 69] builds on the assumption that the total contribution from all Goldstone diagrams with n independent hole lines is larger than the contribution from all diagrams containing $n+1$ hole lines. Given a truncation level n, all diagrams containing more than n hole lines are therefore neglected from the perturbational expansion. As Day explains [10], the truncation in the number of hole-lines is justified only at sufficiently low densities. According to Song *et al.* [81], the approximation breaks down above $3\rho_0$, where ρ_0 is the experimental nuclear-matter saturation density. The above-mentioned BHF method is equivalent to the lowest-order approximation of the hole-line expansion, including di-

agrams with maximally two independent hole lines. The BHF approach is one of the standard methods for infinite nuclear matter, and has been used and developed in a large number of studies, starting in the 1950s with the publications of Brueckner and co-workers [42, 43, 82, 83] and continuing in a steady stream until the present [10, 22, 32, 68–72, 81, 84–95]. Mahaux *et al.* introduced continuous single-particle energies [71, 72] in the G matrix, giving a faster convergence [81, 86] in terms of hole lines than the traditional gap choise [70]. The BHF approximation has been extended to finite temperatures [85, 92], asymmetric nuclear matter [87, 96, 97], and hyperonic matter [89, 98], among other. In Chapter 4, we review the theory and give details for the implementation of the BHF method.

In addition to the many BHF calculations, there have been done a few studies of nuclear matter using higher-order hole-line approximations [81, 99, 100]. By definition, Bethe-Brueckner-Goldstone (BBG) theory [10, 69, 101] does not determine the exact form of the energy denominator. A necessary condition for convergence in the number of hole lines is that the calculation does not depend on the choise of single-particle potentials in the energy denominator. Song *et al.* have compared [81] a three-hole-line approximation using the traditional gap choise with a calculation using continuous single-particle energies. In this study, the two approaches gave approximately the same binding energy, differing by less than 1 MeV around the saturation density. The weak dependence on the choise of single-particle potentials may indicate that a three-hole-line approximation is sufficient to obtain converged results [81]. In agreement with studies using other methods, the results of Song *et al.* show that it is necessary to take account of three-body forces to reproduce the experimental saturation point.

A method that is related to the hole-line approximation is coupled-cluster theory [102–106]. The first coupled-cluster calculations for nuclear matter were done using the so-called Bochum truncation scheme [107, 108]. Day and Zabolitzky did calculations [108] containing three-body equations, and included also an estimate of the four-body amplitudes. Whereas the inclusion of three-body terms gave a significant contribution to the binding energy, their estimate including a subset of the four-body terms gave results very similar to the three-body approximation. Provided that the approximation of the four-body equations was reasonable, the results showed convergence for the Bochum coupled-cluster method. Day and Zabolitzky also compared their coupled-cluster calculations with the hole-line approximation. For Fermi momenta between 1.4 and 1.8 fm^{-1}, the four-hole line approximation gave binding energies differing at most about 2–3 MeV from their most accurate coupled-cluster results [108]. In Paper II [109], we explain the differences between our coupled-cluster implementation and the Bochum scheme. In

Chapter 5, we give an introduction to coupled-cluster theory.

Symmetric nuclear matter, pure neutron matter, and asymmetric neutron-star matter have been studied using many other nonrelativistic *ab initio* methods, and we will mention some of these only briefly. There exist a large number of different methods derived from perturbation theory, some of which are obtained by partial summation of certain diagrammatic classes to infinte order [110]. When using a bare interaction, nuclear matter is commonly known to be a nonperturbative system [111]. The G matrix, which is used in BBG theory, was introduced to deal with this problem [10]. Renormalization group (RG) theory provides an alternative, modern approach to obtain softer interactions that give the same phase shifts as bare nuclear interaction models. Nuclear-matter calculations have been done [26, 111–114] using two- and three-body interactions evolved to low momenta by using either the so-called $V_{\mathrm{low}k}$ or the similarity renormalization group (SRG) method. When using a low-momentum interaction in symmetric nuclear matter, the third-order particle-particle and hole-hole diagrams give only a small additional contribution compared to second-order perturbation theory [26]. This perturbative behaviour in calculations with low-momentum potentials is potentially a great advantage. On the other hand, in these calculations the RG interactions have a cutoff dependency that is non-negligible and increasing for larger densities. Lately, Tews *et al.* have done [41] perturbation-theory calculations for neutron matter with nuclear interactions derived from chiral perturbation theory including the full next-to-next-to-next-to-leading order ($\mathrm{N^3LO}$) contribution, with three- and four-body forces. Compared to calculations with three-body interactions defined only to next-to-next-to-leading order (NNLO), the inclusion of all $\mathrm{N^3LO}$ diagrams was found to be important.

The nonrelativistic particle-hole ring approximation has been implemented for nuclear matter to fourth order [115]. Other methods derived from many-body perturbation theory are for example the model-space BHF [116–118] and the model-space particle-particle ring [118–121] approximations. In the particle-particle ring diagram approximation, particle-particle and hole-hole diagrams are summed to infinite order, and this method is therefore similar to our coupled-cluster ladder approximation presented in Paper II [109].

In the self-consistent Green's function (SCGF) method [46,58,122], single-particle and two-particle propagators are used to evaluate expectation values of different operators. The standard SCGF approximation for extended nuclear matter includes particle-particle and hole-hole ladder diagrams to infinite order [58]. In contrast to for example the BHF and coupled-cluster methods, in the SCGF approach the Fermi sea is correlated and the propagators are said to be 'dressed'. According to Dickhoff and Müther [122], per-

turbations of the Fermi surface can become important in systems with strong correlations. Due to the symmetry between particle and hole states, one can show that the number of particles is a conserved quantity in SCGF calculations [122]. Calculations in SCGF theory also have the advantage that they can be conveniently compared to experiments through spectral functions, which are evaluated using propagators. As reviewed by Dickhoff and Barbieri [58], there have been introduced several different approaches to deal with pairing instability, which occurs in the SCGF method. In Paper II [109], we explain why the pairing instability problem is not present in coupled-cluster equations. The developments of the SCGF method for nuclear matter until 2004 are reviewed in, for example, Ref. [58]. The SCGF method is still actively used and developed, and during the last decade there have been done many new studies of infinite nuclear and neutron matter [24, 29, 35, 123–131].

Beside BBG, CC, and SCGF theory, different variational and Monte Carlo methods have been important in the study of infinite nuclear matter. Let us first consider two variational methods: the Fermi hypernetted chain (FHNC) [132] and the variational Monte Carlo (VMC) [133] approximations. In both the VMC and FHNC methods, the variational energy is written using a Jastrow-type wave-function ansatz. The Jastrow-type ansatz of a nuclear system is often expanded as a sum of different operators [132, 133]. In the VMC method, the variational energy is calculated using a Monte Carlo algorithm [133]. In contrast, the FHNC approach results in a set of integral equations [132]. The so-called variational chain summation (VCS) technique, in which the Fermi-hypernetted-chain-single-operator (FHNC-SOC) equations are solved, has been used in several studies of nuclear and neutron star matter [20, 134–137]. The VMC method has likewise been applied to model infinite nuclear systems [137]. Whereas FHNC approximations can be formulated with integral equations at the thermodynamic limit, Monte Carlo methods are restricted to finite systems [132]. Infinite nuclear or neutron matter has therefore typically been approximated by a box with a finite number of particles [23, 137, 138]. In some studies, there have been used techniques such as twist-averaged boundary conditions to approximate the thermodynamic limit [138].

The variational energy estimate of the VMC method is restricted by the chosen Jastrow-type ansatz. The Green's function Monte Carlo (GFMC) method [133] provides a recipe to improve the VMC energy to almost the exact value. After rewriting the Schrödinger equation as a diffusion equation in imaginary time, the wave function is propagated towards a GFMC solution. Beacause of the fermion sign problem [139], GFMC calculations cannot be systematically improved to the exact solution. Carlson *et al.* have used the GFMC method to study pure neutron matter in both the normal [137] and su-

perfluid phases [140]. The GFMC method is computationally very expensive, and is therefore restricted to very small systems. As suggested by Schmidt and Fantoni [141], the computational scaling of the GFMC approach can be significantly improved by using a Hubbard-Stratonovich transformation, which makes it possible to sample both position and spin randomly. This approach, which is called the auxiliary field diffusion Monte Carlo (AFDMC) method, has been used by Gandolfi *et al.* in calculations of symmetric nuclear matter [23], neutron matter [138], and neutron star matter [52]. The AFDMC method has also been applied with a Jastrow-BCS wave-function ansatz to model neutron matter in the superfluid phase [142]. In Refs. [143, 144], another Monte Carlo projection method using lattice discretization has been applied to neutron matter at low densities.

Examples of other recent developments for infinite nuclear matter are, for example, the chiral-perturbation-theory approaches of Holt, Kaiser, and Weise [145], and the study of Inoue *et al.* [95], in which a nuclear interaction model derived from lattice QCD is used. In the latter calculations, the lattice-QCD two-body force still has unphysically large quark masses.

A brief historical review + current challenges

- K. Oyamatsu: Prog. Theor. Phys., Vol. 109, No. 4, 631, April 2003 [146]
- Y. Dewulf: Saturation of nuclear matter and short-range correlations
- State of the art. Results of other methods for infinite nuclear matter: resonant Fermi gas (Schwenk) [147], including relativistic effects in the interaction + V_{lowk} (Dalen and Müther) [25], Lattice ChPT (auxiliary-field MC in real space and time) [144] etc.
- Selfconsistent Green's function method: PPHH ladders and the pairing instability [148–150], thermodynamic consistency [**?**, 151]
- N. Bassan, K. E. Schmidt: PRC 84, 035807, 2011
- Virial expansion [152]
- Strongly interacting atomic fermion systems and neutron matter, which both are superfluid systems with large superfluidity gaps, behave in similar ways when the former system is suitably tuned [153]

2.2 The homogeneous electron gas

Another important physical model system with homogeneous particle distribtution and infinite extension is the electron gas [154]. The homogeneous electron gas is defined as a system of interacting electrons with a constant, neutralizing background charge.

A brief historical review + current challenges

- Why is the electron gas interesting:
  Connection to condensed matter physics and DFT
- State of the art
- Challenges
- What is the electron gas and why do we want to study it?

Chapter 3

Microscopic models of fermionic matter

3.1 A quantum many-particle system

- Nucleons appropriate degree of freedom (citations etc.)
  $\Rightarrow$ many-fermion system of interacting nucleons
- Many-body forces: Why truncation
- Why nonrelativistic theory

3.1.1 The Hamiltonian equation

In this thesis, we define infinite nuclear matter as a system in which the d-dimensional real space $\mathbb{R}^d$ is filled by homogeneous nuclear matter. We assume that nucleons are an appropriate degree of freedom in the density domains we are going to study. As is well known, nucleons have spin 1/2 and behave statistically as fermions. Infinite nuclear matter is therefore, as we define it, a system containing an infinite number of interacting fermions. On the many-particle level, we neglect relativistic effects. We can therefore use nonrelativistic many-fermion theory [80, 110, 154] for describing the system.

The physics of a general, nonrelativistic, and time-independent quantum mechanical system is described by the Hamiltonian eigenvalue equation

$$\hat{H}|\Psi\rangle = E|\Psi\rangle, \tag{3.1}$$

where $\hat{H}$ is the Hamiltonian operator, $|\Psi\rangle$ is the quantum state vector, and the eigenvalue E is the energy. In infinite nuclear matter, the Hamiltonian operator can be written as

$$\hat{H} = \hat{T} + \hat{V}, \tag{3.2}$$

where $\hat{T}$ is the kinetic energy operator and $\hat{V}$ is the interaction operator. Nucleons have an underlying quark-gluon structure, and are not point particles (citation). Interactions between three or more nucleons are therefore generally nonzero, and should be included in microscopic calculations on nuclear matter (check litterature for references). The total nuclear interaction operator is of the form

$$\hat{V} = \hat{V}_{NN} + \hat{V}_{NNN} + \hat{V}_{NNNN} + \dots \tag{3.3}$$

where $\hat{V}_{NN}$, $\hat{V}_{NNN}$, and $\hat{V}_{NNNN}$ are the two-, three-, and four-body interaction operators, respectively. (Something about evidence that higher-order terms become increasingly smaller.) In our calculations, we include only the two-body interaction (why?).

In coordinate space, the Hamiltonian operator for infinite nuclear matter has the form

$$\begin{aligned}\hat{H} = &- \frac{\hbar^2}{2m} \sum_{i=1}^{A} \nabla_i^2 + \sum_{i<j}^{A} \hat{v}_{NN}(\mathbf{r}_i, \mathbf{r}_j) \\ &+ \sum_{i<j<k}^{A} \hat{v}_{NNN}(\mathbf{r}_i, \mathbf{r}_j, \mathbf{r}_k) + \dots,\end{aligned} \tag{3.4}$$

where A is the total number of nucleons, m is the nucleon mass, $\hbar$ is the Planck constant, and $\mathbf{r}_i$ is the coordinate of nucleon i. The projection of the state vector $|\Psi\rangle$ to the position space depends on A position vectors, i.e.

$$\langle \mathbf{r}_1 \dots \mathbf{r}_A | \Psi \rangle = \Psi(\mathbf{r}_1, \dots, \mathbf{r}_A), \tag{3.5}$$

where $\mathbf{r}_i$ is particle i's position vector.

In the many-body methods we are going to consider – the hole-line expansion and the coupled-cluster method – the A-particle wave function $\Psi(\mathbf{r}_1, \dots, \mathbf{r}_A)$ is expanded in a basis, i.e.,

$$\Psi(\mathbf{r}_1, \mathbf{r}_2, \dots, \mathbf{r}_A) = \sum_m c_m \Phi_m(\mathbf{r}_1, \mathbf{r}_2, \dots, \mathbf{r}_A), \tag{3.6}$$

where the basis functions Φ_m are Slater determinants

$$\Phi_m(\mathbf{r}_1, \mathbf{r}_2, \dots, \mathbf{r}_A) = \frac{1}{\sqrt{A!}} \begin{vmatrix} \phi_{\alpha_1^{(m)}}(\mathbf{r}_1) & \phi_{\alpha_2^{(m)}}(\mathbf{r}_1) & \dots & \phi_{\alpha_A^{(m)}}(\mathbf{r}_1) \\ \phi_{\alpha_1^{(m)}}(\mathbf{r}_2) & \phi_{\alpha_2^{(m)}}(\mathbf{r}_2) & \dots & \phi_{\alpha_A^{(m)}}(\mathbf{r}_2) \\ \vdots & \vdots & \ddots & \vdots \\ \phi_{\alpha_1^{(m)}}(\mathbf{r}_A) & \phi_{\alpha_2^{(m)}}(\mathbf{r}_A) & \dots & \phi_{\alpha_A^{(m)}}(\mathbf{r}_A) \end{vmatrix} \tag{3.7}$$

constructed from a chosen single-particle basis $\{\phi_\alpha(\mathbf{r})\}_\alpha$. The structure of the Slater determinants ensures that the total wave function is antisymmtric, which is a requirement for a fermion system.

3.1.2 Second quantization

When working with many-particle quantum systems, it is convenient to utilize the power of the second quantization formalism [80, 154, 155]. In second quantization, the quantum states belong to the Fock space [155], which is the direct sum of the Hilbert spaces [**?**] with zero, one, two, and up to arbitrarily many particles. The states are given in occupation representation, in which $|n_1 n_2 \dots\rangle$ is a state with n_1 particles in the single-particle state 1, n_2 particles in single-particle state 2 and so on. The single-particle states are elements of a chosen basis, and because the system is fermionic, the occupation numbers can only take the values 0 or 1.

Let us define the fermion creation and annihilation operators $a_\alpha^\dagger$ and a_α, respectively, such that $a_\alpha^\dagger$ creates a fermion in the state $|\alpha\rangle$ and a_α annihilates a fermion in the same state. When operating on single-particle states, the operators have the properites

$$a_\alpha^\dagger|0\rangle = |\alpha\rangle, \qquad a_\alpha^\dagger|\alpha\rangle = 0 \tag{3.8}$$

and

$$a_\alpha|0\rangle = 0, \qquad a_\alpha|\alpha\rangle = |0\rangle. \tag{3.9}$$

Above, $|0\rangle$ is the physical vacuum state. The fermion creation and annihilation operators obey the anticommutator relations

$$\begin{aligned} &\{a_\alpha^\dagger, a_\beta^\dagger\} = 0, \qquad \{a_\alpha, a_\beta\} = 0, \\ &\{a_\alpha, a_\beta^\dagger\} = \delta_{\alpha,\beta}, \end{aligned} \tag{3.10}$$

where the curly brackets denote anticommutation operators and $\delta_{\alpha,\beta}$ is the Kronecker delta function. The anticommutator relations are necessary for getting antisymmetric many-particle states, as required for Fermion systems.

In second quantization, a vector with the single-particle states $\alpha_1, \alpha_2, \dots,$ α_A occupied is written in terms of creation operators as

$$|\alpha_1 \alpha_2 \dots \alpha_A\rangle = a_{\alpha_1}^\dagger \dots a_{\alpha_A}^\dagger |0\rangle, \tag{3.11}$$

where $|0\rangle$ is the vacuum state. Because the occupation number for fermions is always zero or one, one can label a vector by only those single-particle states that are occupied. A general one-body operator is written as

$$\hat{U} = \sum_{p,q} \langle p|\hat{u}|q\rangle a_p^\dagger a_q \tag{3.12}$$

and a two-body operator as

$$\hat{W} = \frac{1}{4} \sum_{p,q,r,s} \langle pq|\hat{w}|rs\rangle_{AS} a_p^\dagger a_q^\dagger a_s a_r, \tag{3.13}$$

where the brackets are inner products and the summations are taken over all single-particle states. In Eq. (3.13) we have used the definition

$$\langle pq|\hat{w}|rs\rangle_{AS} \equiv \langle pq|\hat{w}|rs\rangle - \langle pq|\hat{w}|sr\rangle \tag{3.14}$$

to denote an antisymmetrized interaction matrix element.

Let the reference state $|\Phi_0\rangle$ be constructed of A single-particle states chosen from a given basis. Here and in the following, we denote states occupied in the reference state by $i, j, k, \ldots$, states not occupied in $|\Phi_0\rangle$ by $a, b, c, \ldots$, whereas indices $p, q, r, \ldots$ are used for arbitrary single-particle states in the given basis. Using creation operators, the reference state is

$$|\Phi_0\rangle = a_{i_1}^\dagger a_{i_2}^\dagger \ldots a_{i_A}^\dagger |0\rangle, \tag{3.15}$$

where $|0\rangle$ is the physical vacuum state. Let us further define states of the form

$$|\Phi_{ij\ldots}^{ab\ldots}\rangle = a_a^\dagger a_b^\dagger \ldots a_j a_i |\Phi_0\rangle \tag{3.16}$$

as particle-hole excitations of the reference state. In a space spanned by the given single-particle basis, the total state vector $|\Psi\rangle$ may be approximated as

$$|\tilde{\Psi}\rangle = |\Phi_0\rangle + \sum_{ia} c_i^a |\Phi_i^a\rangle + \sum_{ijab} c_{ij}^{ab} |\Phi_{ij}^{ab}\rangle + \ldots. \tag{3.17}$$

This expansion can be truncated after a finite number of terms, and the coefficients are typically found using a numerical method.

3.1.3 Momentum single-particle basis

Later, we study infinite-matter systems in two and three dimensions. Similarly as explained by, for example, Fetter and Walecka [154] in three dimensions, we use d-dimensional hypercubic potential wells for modelling infinite-nuclear-matter systems. Fig. 3.1 illustrates hypercubes in one, two, and three dimensions. The external potential is assumed to be zero inside the hypercube, and infinitely large outside the box. In coordinate representation, the Hamiltonian equation of a single-nucleon system is

$$-\frac{\hbar^2}{2m}\nabla^2\phi(\mathbf{x}) = \varepsilon\phi(\mathbf{x}) \tag{3.18}$$

inside the hypercube. Here ϕ and ε are the single-particle wave function and energy, respectively, $\mathbf{x}$ is a d-dimensional position vector $\mathbf{x} \equiv (x_1, \ldots, x_d)$,

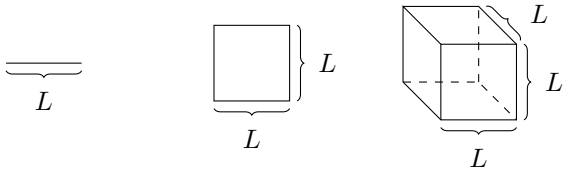

Figure 3.1: Infinite-nuclear-matter systems are modelled using hypercubes in one, two and three dimensions. (Illustration by the author.)

m is the nucleon mass, and $\hbar$ is the Planck constant. The single-particle Hamiltonian equation has solutions of the form

$$\phi_{\mathbf{k}}(\mathbf{x}) = \frac{1}{L^{d/2}} e^{i\mathbf{k}\cdot\mathbf{x}}, \tag{3.19}$$

where $|\mathbf{k}| = \sqrt{2m\varepsilon/\hbar^2}$. Continuing the approach outlined by Fetter and Walecka, we use periodic boundary conditions

$$\begin{aligned} \phi_{\mathbf{k}}(x_1 + L, \ldots, x_d) &= \phi_{\mathbf{k}}(x_1, \ldots, x_d), \\ &\vdots \\ \phi_{\mathbf{k}}(x_1, \ldots, x_d + L) &= \phi_{\mathbf{k}}(x_1, \ldots, x_d + L), \end{aligned} \tag{3.20}$$

which give the conditions

$$k_i = \frac{2\pi}{L} n_i, \qquad n_i = 0, \pm 1, \pm 2, \ldots \tag{3.21}$$

for the component i of the wave vector $\mathbf{k}$. A general single-particle state represents a set of quantum numbers $(n_1, \ldots, n_d)$. [110, 154, 156]

Single-particle states in fermionic matter have a spin projection m_s, and for nuclear matter also an isospin projection m_t. In nuclear matter, we write a single-particle state vector as

$$|\mathbf{k}_n m_s m_t\rangle = |n_1 \ldots n_d m_s m_t\rangle, \tag{3.22}$$

where the quantum numbers n_i are as defined in Eq. (3.21). We choose to label neutrons by $m_t = +\frac{1}{2}$ and protons by $m_t = -\frac{1}{2}$. In the electron gas there is no isospin dependency, but otherwise the single-particle states are equal to those in nuclear matter.

We construct infinite-matter systems by filling hypercubes with interacting nucleons, as shown for two dimensions at left in Fig. 3.2. Inifinite matter is obtained in the limit when the box length $L = L_x = L_y$ and the number of particles A approach infinity, whereas the particle density $\rho \equiv A/L^2$ is

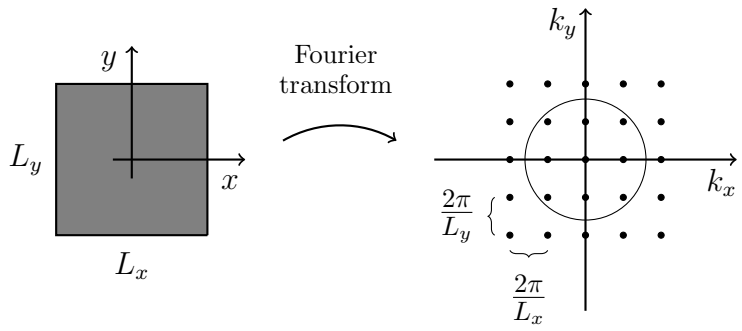

Figure 3.2: Fourier transform in two dimensions. The finite, countinuous, and rectangular region in coordinate space is mapped to a set of infinitely many discrete points in momentum space (Fourier space). The finite size of the coordinate space domain gives a finite distance between points in momentum space. The number of Fourier grid points inside the Fermi sea, denoted by a circle, is by definition the same as the number of particles in the physical box. (Illustration by the author.)

kept constant. Expressions in momentum basis may be considered as Fourier transforms of corresponding coordinate-space equations. Fig. 3.2 shows how a finite number of particles in the contiuous coordinate space is transformed to an infinite number of discrete points in the Fourier space. The spacing between points in Fourier space is inversely related to the hypercube side. In Fourier space, the physical particles are represented by all momentum points inside the Fermi sphere.

Let us neglect spin and isospin degrees of freedom and write the reference state as

$$|\Phi_0\rangle = a^\dagger_{\mathbf{k}_1} a^\dagger_{\mathbf{k}_2} \dots a^\dagger_{\mathbf{k}_A} |0\rangle, \tag{3.23}$$

where each particle $i \in \{1, 2, \dots, A\}$ has a unique momentum vector $\mathbf{k}_i$. Assume that the reference state is occupied by the A single-particle states with the lowest single-particle energies

$$\varepsilon_{\mathbf{k}} = \frac{\hbar^2 k^2}{2m}, \tag{3.24}$$

where $k \equiv |\mathbf{k}|$ is the length of the momentum vector. Then the Fermi momentum k_F is defined as the momentum $|\mathbf{k}|$ of the highest-lying occupied state. As illustrated in Fig. 3.3, in nuclear matter the Fermi momentum is defined separately for protons and neutrons. In a calculation, the proton-neutron ratio can be controlled by adjusting the neutron and proton Fermi momenta k_{F_n} and k_{F_p}. Symmetric nuclear matter is obtained by choosing

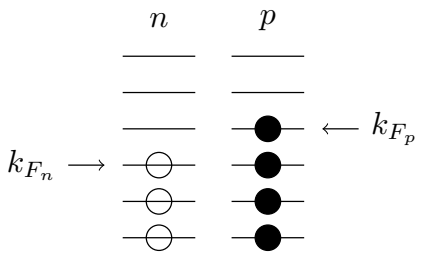

Figure 3.3: The Fermi momentum for neutrons, k_{F_n}, is defined as the momentum of the highest-lying occupied neutron state. Similarly, the Fermi momentum for protons, k_{F_p} is defined as the momentum of the highest-lying occupied proton state. In other words, the proton and neutron Fermi levels, k_{F_n} and k_{F_p}, determine together the ratio of the two nucleon types in the considered system. (Illustration by the author.)

the same Fermi level for both protons and neutrons, whereas in pure neutron matter the proton Fermi momentum k_{F_p} is set to zero.

Assuming that the d-dimensional hypercube with side length L is filled by A fermions, the particle density becomes

$$\rho \equiv \frac{A}{L^d} = \frac{1}{L^d} \sum_{m_s m_t} \sum_{|\mathbf{k}| \leq k_F(m_t)}, \tag{3.25}$$

where the Fermi momentum may be dependent on the isospin. The summation is taken over all occupied single-particle states, restricted by Eq. (3.21) and a Fermi momentum.

3.1.4 Other single-particle bases

In the expressions arising in many-body perturbation theory and coupled-cluster theory, there are summations over single-particle momenta $\mathbf{k}_p$. At the limit when the box side of the hypercube L approaches infinity, a sum over discrete Fourier states $\mathbf{k}_p$ can be approximated by an integral according to

$$\sum_{\mathbf{k}_p} \longrightarrow \left(\frac{L}{2\pi}\right)^d \int d\mathbf{k}_p, \tag{3.26}$$

where the integration is over the d-dimensional space spanned by the Fourier states. In the energy expressions, the summations are often taken over only particle or hole states. At the thermodynamic limit, a sum over two different hole states, i and j, is replaced with two integrals, as in Eq. (3.26). The

restriction to only occupied states is ensured by a hole-hole Pauli exclusion operator

$$Q_{hh}(|\mathbf{k}_i|, |\mathbf{k}_j|, k_F) \equiv \theta(k_F - |\mathbf{k}_i|)\theta(k_F - |\mathbf{k}_j|), \tag{3.27}$$

where $\theta(x)$ is the Heaviside step function. Similarly, a sum over two particle states, a and b, is transformed to two d-dimensional integrals with a particle-particle Pauli exlusion operator

$$Q_{pp}(|\mathbf{k}_a|, |\mathbf{k}_b|, k_F) \equiv \theta(|\mathbf{k}_a| - k_F)\theta(|\mathbf{k}_b| - k_F), \tag{3.28}$$

which ensures that the integration is taken over only unoccupied states. As before, k_F denotes the Fermi momentum.

The coordinates of two particles, $\mathbf{x}_p$ and $\mathbf{x}_q$, may be expressed in terms of a relative vector, $\mathbf{x}$, and a centre-of-mass (CM) vector, $\mathbf{X}$, such that

$$\mathbf{x} = \mathbf{x}_p - \mathbf{x}_q, \qquad \mathbf{X} = (\mathbf{x}_p + \mathbf{x}_q)/2. \tag{3.29}$$

Assuming that the Planck constant $\hbar$ is one, the momentum $\mathbf{p} \equiv \hbar\mathbf{k}$ is equal to the wave vector $\mathbf{k}$. Provided that the two particles have equal mass m, the reduced mass is $m_r = \frac{1}{2}m$ and the total mass $M = 2m$. Using the definitions in Eq. (3.29), the relative and CM momentum vectors, $\mathbf{k}$ and $\mathbf{K}$, become

$$\mathbf{k} = (\mathbf{k}_p - \mathbf{k}_q)/2, \qquad \mathbf{K} = \mathbf{k}_p + \mathbf{k}_q, \tag{3.30}$$

where $\mathbf{k}_p$ and $\mathbf{k}_q$ are the momenta of particles p and q in laboratory coordinates.

In relative and centre-of-mass (RCM) coordinates, the hole-hole Pauli exclusion operator becomes

$$Q_{hh}(\mathbf{k}, \mathbf{K}, k_F) = \theta(k_F - |\mathbf{k} + \mathbf{K}/2|)\theta(k_F - |-\mathbf{k} + \mathbf{K}/2|) \tag{3.31}$$

and the particle-particle Pauli exclusion operator

$$Q_{pp}(\mathbf{k}, \mathbf{K}, k_F) = \theta(|\mathbf{k} + \mathbf{K}/2| - k_F)\theta(|-\mathbf{k} + \mathbf{K}/2| - k_F). \tag{3.32}$$

Observe that in RCM coordinates, the Pauli operators are dependent on the radial coordinates of both the relative and the CM momentum vectors, as well as on the angle between these two vectors.

Methods derived from MBPT are often implemented in a partial-wave basis with relative momenta [70, 157]. The basis commonly used is of the form

$$|k\mathcal{J}m_{\mathcal{J}}(lS)m_{t_1}m_{t_2}\rangle, \tag{3.33}$$

where $k \equiv |\mathbf{k}|$ is the length of a relative momentum vector $\mathbf{k}$, l is the relative orbital angular momentum related to $\mathbf{k}$, S is the total two-particle spin, $\mathcal{J}$ is equal to the total relative angular momentum $l + S$, $m_{\mathcal{J}}$ is the z projection of $\mathcal{J}$, and m_{t_1} and m_{t_2} label the nucleon types of particles 1 and 2, respectively. If charge independence breaking and charge symmetry breaking are negelcted, m_{t_1} and m_{t_2} can be replaced with a coupled isospin T with the projection M_T. Charge symmetry and charge independence are defined in for example Refs. [50, 158].

When doing transformations from a RCM basis $|\mathbf{k}\mathbf{K}m_{s_1}m_{t_1}m_{s_2}m_{t_2}\rangle$ to the basis of Eq. (3.33), we need the completeness relations

$$\sum_{lm_l} |lm_l\rangle\langle lm_l| = \hat{\mathbb{1}}, \tag{3.34}$$

$$\sum_{SM_S} |SM_S\rangle\langle SM_S| = \hat{\mathbb{1}}, \tag{3.35}$$

where m_l and M_S are z projections of l and S, respectively, and $\hat{\mathbb{1}}$ is the unity operator. Furthermore, we need the equalities

$$\langle\hat{\mathbf{k}}|lm_l\rangle \equiv Y_{lm_l}(\hat{\mathbf{k}}), \tag{3.36}$$

$$\int d\hat{\mathbf{k}} Y^*_{lm_l}(\hat{\mathbf{k}}) Y_{l'm_{l'}}(\hat{\mathbf{k}}) = \delta_{ll'}\delta_{m_l m_{l'}}, \tag{3.37}$$

$$Y_{lm_l}(\pi - \theta_{\mathbf{k}}, \phi_{\mathbf{k}} + \pi) = (-1)^l Y_{lm_l}(\theta_{\mathbf{k}}, \phi_{\mathbf{k}}), \tag{3.38}$$

where $\hat{\mathbf{k}} = (\theta_{\mathbf{k}}, \phi_{\mathbf{k}})$ is the angular vector of the relative momentum $\mathbf{k}$, $Y_{lm_l}(\hat{\mathbf{k}})$ is the spherical harmonics function, and δ_{pq} is the Kronecker delta function. The angular momenta are coupled according to

$$|lm_l SM_S\rangle = \sum_{\mathcal{J}m_{\mathcal{J}}} \langle lm_l SM_S|\mathcal{J}m_{\mathcal{J}}lS\rangle|\mathcal{J}m_{\mathcal{J}}lS\rangle, \tag{3.39}$$

where the bracket denotes the Clebsch-Gordan coefficient. We also need the property

$$\langle j_p m_p j_q m_q|JM_J\rangle = (-1)^{j_p+j_q-J}\langle j_q m_q j_p m_p|JM_J\rangle \tag{3.40}$$

of Clebsch-Gordan coefficients. The relations (3.37) – (3.40) and other useful angular momentum relations are given in for example the text of Varshalovich *et al.* [159].

Sometimes we denote coupling of angular momenta using square brackets, for example

$$\Big[Y_{l_p m_{l_p}}(\hat{\mathbf{k}}_p) Y_{l_q m_{l_q}}(\hat{\mathbf{k}}_q)\Big]_{\lambda m_\lambda} \equiv \sum_{m_{l_p} m_{l_q}} \langle l_p m_{l_p} l_q m_{l_q}|\lambda m_\lambda\rangle Y_{l_p m_{l_p}}(\hat{\mathbf{k}}_p) Y_{l_q m_{l_q}}(\hat{\mathbf{k}}_q), \tag{3.41}$$

where a Clebsch-Gordan coefficient is used to couple two different orbital angular momenta.

3.1.5 Interaction matrix elements

Next we derive a transformation between relative and centre-of-mass (RCM) and laboratory coordinates for the two-body interaction, generalizing the approach of Fetter and Walecka [154] to d dimensions. Interaction matrix elements are defined as

$$\langle pq|\hat{v}|rs\rangle = \int d\mathbf{x}_1 \int d\mathbf{x}_2 \phi_p^*(\mathbf{x}_1)\phi_q^*(\mathbf{x}_2)v(\mathbf{x}_1,\mathbf{x}_2)\phi_r(\mathbf{x}_1)\phi_s(\mathbf{x}_2), \tag{3.42}$$

where $\phi_m(\mathbf{x})$ is the coordinate space projection of the single-particle state $|m\rangle$ and a star denotes the complex conjugate. If we take the single-particle states to be eigenfunctions of a finite hypercube with side length L, i.e. plane waves as in Eq. 3.19, the matrix elements become

$$\begin{aligned}\langle \mathbf{k}_p\mathbf{k}_q|\hat{v}|\mathbf{k}_r\mathbf{k}_s\rangle &= \int d\mathbf{x}_1 \int d\mathbf{x}_2 \phi_{\mathbf{k}_p}^*(\mathbf{x}_1)\phi_{\mathbf{k}_q}^*(\mathbf{x}_2)v(\mathbf{x}_1,\mathbf{x}_2)\phi_{\mathbf{k}_r}(\mathbf{x}_1)\phi_{\mathbf{k}_s}(\mathbf{x}_2) \\ &= \frac{1}{L^{2d}} \int d\mathbf{x}_1 \int d\mathbf{x}_2 e^{-i\mathbf{k}_p\cdot\mathbf{x}_1} e^{-i\mathbf{k}_q\cdot\mathbf{x}_2} v(\mathbf{x}_1,\mathbf{x}_2) e^{i\mathbf{k}_r\cdot\mathbf{x}_1} e^{i\mathbf{k}_s\cdot\mathbf{x}_2}.\end{aligned} \tag{3.43}$$

If we use the definitions (3.30), and do the change of integration variables

$$\mathbf{r} = \mathbf{x}_1 - \mathbf{x}_2, \qquad \mathbf{R} = (\mathbf{x}_1 + \mathbf{x}_2)/2, \tag{3.44}$$

where $\mathbf{r}$ and $\mathbf{R}$ are relative and centre-of-mass coordinates, respectively, we get the matrix element into the form

$$\langle \mathbf{k}_p\mathbf{k}_q|\hat{v}|\mathbf{k}_r\mathbf{k}_s\rangle = \underbrace{\left[\frac{1}{L^d}\int d\mathbf{r} e^{-i(\mathbf{k}-\mathbf{k}')\cdot\mathbf{r}} v(\mathbf{r})\right]}_{\equiv\langle \mathbf{k}|\hat{v}|\mathbf{k}'\rangle} \delta_{\mathbf{K},\mathbf{K}'} \tag{3.45}$$

Here we have assumed that the interaction is invariant under translations, which means that the interaction depends only on the distance $\mathbf{r} = \mathbf{x}_1 - \mathbf{x}_2$, and not on the specific positions of the two particles. We have also used the definition

$$\delta_{\mathbf{K},\mathbf{K}'} = \frac{1}{L^d}\int_{\mathbb{R}^d} d\mathbf{R} e^{i(\mathbf{K}-\mathbf{K}')\cdot\mathbf{R}} \tag{3.46}$$

of the d-dimensional Kronecker delta function, where the integration is over the entire d-dimensional real space. [154]

3.2 The nuclear interaction

- A very short historical review

3.2.1 Chiral perturbation theory

- Basic principles of ChPT: an effective field theory with a systematic expansion derived from QCD
- The most important terms and heuristic explanations

3.2.2 Optimized interaction model

- About optimization of NNLO: free parameters
- Connection between experiments and model: phase shifts etc.
- The POUNDERS optimization algorithm

3.2.3 n-body interactions

- Evidence that three-body forces are important
- Examples from the litterature
- Current problems

3.2.4 The Minnesota potential

Chapter 4

The Brueckner-Hartree-Fock approximation for nuclear matter

Rayleigh–Schrödinger perturbation theory (RSPT) [80] is one of the standard many-body methods for non-relativistic quantum systems. RSPT has the advantage that it is size-extensive [80], which roughly means that the theory scales correctly with the number of particles in the system. Unfortunately, the strong short-range interaction between nucleons makes nuclear systems non-perturbative, and generally it is necessary to renormalize the interaction before doing perturbative many-body calculations. Brueckner-Goldstone theory and the hole-line approximation [10, 69] are approaches related to RSPT in which the interaction has been replaced with a so-called G matrix. The G matrix is obtained by summing to infinite order in perturbation theory certain correlation contributions that are important for short-range correlations.

Being the lowest-order approximation of both Brueckner-Goldstone theory and the hole-line approximation [10, 69], the Brueckner-Hartree-Fock (BHF) approximation [10, 22, 27, 42, 43, 68, 69, 81–84, 86] is one of the standard many-body methods for infinite-nuclear-matter studies. In Ref. [109] we have derived a coupled-cluster ladder approximation in a partial-wave basis using exact Pauli exclusion operators. As we show in the paper, the coupled-cluster ladder approximation is closely related to the BHF method. In the work with Ref. [109], we have used the BHF method to verify important parts of our coupled-cluster ladder implementations. We have also compared the coupled-cluster results with BHF calculations. In this chapter, we discuss the basic principles of RSPT and the BHF approximation. Furthermore, we show how we have implemented the BHF method and the

lowest orders of perturbation theory for nuclear-matter systems. Apart from minor details related to the practical implementations, most of the material presented in this chapter is based on well-known theory.

4.1 Many-body perturbation theory

We follow Shavitt and Bartlett [80] when introducing many-body perturbation theory (MBPT). For the interested reader, the textbook of Harris, Monkhorst, and Freeman [110] also gives a thorough introduction to MBPT. If there is no external potential, the physics of a time-independent nuclear system is determined by a Hamiltonian operator

$$\hat{H} = \hat{T} + \hat{V}, \tag{4.1}$$

where $\hat{T}$ is the kinetic energy operator and $\hat{V}$ is the interaction operator. The Hamiltonian operator $\hat{H}$ can be regrouped into a noninteracting part $\hat{H}_0$ and a perturbation operator $\hat{H}_I$, i.e.

$$\hat{H} = \hat{H}_0 + \hat{H}_I, \tag{4.2}$$

where

$$\hat{H}_0 = \hat{T} + \hat{U}, \tag{4.3}$$

$$\hat{H}_I = \hat{V} - \hat{U}. \tag{4.4}$$

Here $\hat{U}$ is an arbitrary single-particle potential operator that preferably is chosen such that the contribution of the perturbation $\hat{H}_I$ is as small as possible.

Let the state $|\Psi\rangle$ be the eigenvector of the total Hamiltonian $\hat{H}$ corresponding to the lowest eigenvalue, i.e.

$$\hat{H}|\Psi\rangle = E|\Psi\rangle, \tag{4.5}$$

and let $|\Phi_0\rangle$ be the eigenvector of the noninteracting part $\hat{H}_0$ corresponding to the lowest eigenvalue, i.e.

$$\hat{H}_0|\Phi_0\rangle = E_0|\Phi_0\rangle. \tag{4.6}$$

Here E and E_0 are the ground state total and non-interacting energy, respectively. In the following, we assume that the ground state is nondegenerate. We define further the operators $\hat{P}$ and $\hat{Q}$ such that

$$\hat{P}|\Psi\rangle = |\Phi_0\rangle \tag{4.7}$$

and $\hat{P} + \hat{Q} = \hat{I}$, where $\hat{I}$ is the unity operator.

As shown by Shavitt and Bartlett [80], the total energy can be written as

$$E = E_0 + \Delta E, \tag{4.8}$$

where the energy perturbation

$$\Delta E = \sum_{n=1}^{\infty} \Delta E^{(n)} \tag{4.9}$$

is expanded in powers of the perturbation $\hat{H}_I$. The energy contribution to the n:th power of $\hat{H}_I$ is

$$\Delta E^{(n)} = \langle \Phi_0 | \hat{H}_I \left(\hat{R} \left(E - \mu - \hat{H}_I \right) \right)^{n-1} | \Phi_0 \rangle, \tag{4.10}$$

where $\hat{R}$ is the resolvent operator, defined as

$$\hat{R} \equiv \left(\hat{Q} \left(\hat{H}_0 - \mu \right) \hat{Q} \right)^{-1}, \tag{4.11}$$

and μ is an arbitrary constant. The Rayeligh-Schrödinger perturbation theory (RSPT) is defined such that $\mu = E_0$. It can be shown that RSPT is a size-extensive method, which roughly means that the energy scales correctly with the number of particles. Shavitt and Bartlett [80] explain the concept of size-extensivity, and show that RSPT is size-extensive for a special system with equal, noninteracting atoms. In this thesis, we consider only perturbative methods derived from RSPT.

Expressed in second quantization, the single-particle operators can be written as

$$\hat{T} = \sum_{p,q} \langle p | \hat{t} | q \rangle a_p^\dagger a_q, \tag{4.12}$$

$$\hat{U} = \sum_{p,q} \langle p | \hat{u} | q \rangle a_p^\dagger a_q, \tag{4.13}$$

and the two-particle operator becomes

$$\hat{V} = \sum_{p,q,r,s} \langle pq | v | rs \rangle_{AS} a_p^\dagger a_q^\dagger a_s a_r. \tag{4.14}$$

Let us define the Fock operator as

$$\hat{F} = \sum_{p,q} \langle p | \hat{f} | q \rangle a_p^\dagger a_q, \tag{4.15}$$

where

$$\langle p|\hat{f}|q\rangle = \langle p|\hat{t}|q\rangle + \langle p|\hat{u}|q\rangle. \tag{4.16}$$

In the laboratory coordinate momentum basis, the matrix elements of the kinetic energy operator are diagonal.

Observe that the explicit expressions of $\Delta E^{(n)}$ in Eq. (4.10) depend on which operator $\hat{U}$ is used. Let us first choose the single-particle potential

$$\langle p|\hat{u}|q\rangle = \sum_i \langle pi|\hat{v}|qi\rangle_{AS}, \tag{4.17}$$

where i denotes a state that is occupied in the Fermi vacuum. Provided the Fock operator contains the single-particle potential (4.17), the Hartree-Fock equations [110] are

$$\begin{aligned} \langle p|\hat{f}|q\rangle &= \varepsilon_q \langle p|q\rangle, \\ \langle p|q\rangle &= \delta_{pq}, \end{aligned} \tag{4.18}$$

where the single-particle states are restricted to be orthonormal. A Hartree-Fock single-particle basis is a basis that fulfills Eq. (4.18). If the interaction $\hat{v}$ conserves the total momentum, the Fock matrix becomes diagonal in the plane wave basis. Consequently, the Hartree-Fock equations (4.18) are fulfilled in this basis, and the momentum basis is a Hartree-Fock single-particle basis for infinite nuclear matter.

From now on, we use a notation with explicit momentum states. For brevity, we do not write out the spin and isospin degrees of freedom explicitly. The state vectors and sums

$$|\mathbf{k}\rangle \quad \text{and} \quad \sum_{\mathbf{k}} \tag{4.19}$$

should therefore be read as

$$|\mathbf{k}\rangle|m_s m_t\rangle \quad \text{and} \quad \sum_{m_s m_t} \sum_{\mathbf{k}}, \tag{4.20}$$

where m_s and m_t are the z projections of the single-particle spin and isospin, respectively. Let us define the reference energy as

$$E_{REF} \equiv \langle \Phi_0|\hat{H}|\Phi_0\rangle = E_0 + \Delta E^{(1)}. \tag{4.21}$$

As shown by Shavitt and Bartlett [80], the explicit expression for the reference energy is

$$E_{REF} = \sum_{\mathbf{k}_i} \langle \mathbf{k}_i|\hat{t}|\mathbf{k}_i\rangle + \frac{1}{2} \sum_{\mathbf{k}_i,\mathbf{k}_j} \langle \mathbf{k}_i\mathbf{k}_j|\hat{v}|\mathbf{k}_i\mathbf{k}_j\rangle_{AS}. \tag{4.22}$$

By definition, the Hartree-Fock energy is the reference energy of a system calculated in a Hartree-Fock basis [110]. For infinite nuclear matter, the plane wave basis is a Hartree-Fock basis and the reference energy (4.22) is therefore also the Hartree-Fock energy. The reference energy is by definition independent of the potential $\hat{U}$. With the chosen operator $\hat{U}$, the second-order contribution is

$$\Delta E^{(2)} = \frac{1}{4} \sum_{\mathbf{k}_i,\mathbf{k}_j} \sum_{\mathbf{k}_a,\mathbf{k}_b} \frac{\langle \mathbf{k}_i\mathbf{k}_j|\hat{v}|\mathbf{k}_a\mathbf{k}_b\rangle_{AS}\langle \mathbf{k}_a\mathbf{k}_b|\hat{v}|\mathbf{k}_i\mathbf{k}_j\rangle_{AS}}{\varepsilon_{\mathbf{k}_i} + \varepsilon_{\mathbf{k}_j} - \varepsilon_{\mathbf{k}_a} - \varepsilon_{\mathbf{k}_b}}, \tag{4.23}$$

where we have used the definition

$$\varepsilon_{\mathbf{k}} \equiv \langle \mathbf{k}|\hat{f}|\mathbf{k}\rangle. \tag{4.24}$$

In this special case, the contribution to the third order is

$$\Delta E^{(3)} = \Delta E^{(3)}_{pp} + \Delta E^{(3)}_{hh} + \Delta E^{(3)}_{ph}. \tag{4.25}$$

Here the third-order energy consists of the so-called particle-particle term

$$\begin{aligned}\Delta E^{(3)}_{pp} = \frac{1}{8} \sum_{\mathbf{k}_a,\mathbf{k}_b} \sum_{\mathbf{k}_c,\mathbf{k}_d} \sum_{\mathbf{k}_i,\mathbf{k}_j} & \frac{\langle \mathbf{k}_i\mathbf{k}_j|\hat{v}|\mathbf{k}_a\mathbf{k}_b\rangle_{AS}\langle \mathbf{k}_a\mathbf{k}_b|\hat{v}|\mathbf{k}_c\mathbf{k}_d\rangle_{AS}}{\left(\varepsilon_{\mathbf{k}_i} - \varepsilon_{\mathbf{k}_j} - \varepsilon_{\mathbf{k}_a} - \varepsilon_{\mathbf{k}_b}\right)} \\ \times & \frac{\langle \mathbf{k}_c\mathbf{k}_d|\hat{v}|\mathbf{k}_i\mathbf{k}_j\rangle_{AS}}{\left(\varepsilon_{\mathbf{k}_i} - \varepsilon_{\mathbf{k}_j} + \varepsilon_{\mathbf{k}_c} - \varepsilon_{\mathbf{k}_d}\right)},\end{aligned} \tag{4.26}$$

the hole-hole term

$$\begin{aligned}\Delta E^{(3)}_{hh} = \frac{1}{8} \sum_{\mathbf{k}_a,\mathbf{k}_b} \sum_{\mathbf{k}_i,\mathbf{k}_j} \sum_{\mathbf{k}_k,\mathbf{k}_l} & \frac{\langle \mathbf{k}_i\mathbf{k}_j|\hat{v}|\mathbf{k}_a\mathbf{k}_b\rangle_{AS}\langle \mathbf{k}_a\mathbf{k}_b|\hat{v}|\mathbf{k}_k\mathbf{k}_l\rangle_{AS}}{\left(\varepsilon_{\mathbf{k}_i} + \varepsilon_{\mathbf{k}_j} - \varepsilon_{\mathbf{k}_a} - \varepsilon_{\mathbf{k}_b}\right)} \\ \times & \frac{\langle \mathbf{k}_k\mathbf{k}_l|\hat{v}|\mathbf{k}_i\mathbf{k}_j\rangle_{AS}}{\left(\varepsilon_{\mathbf{k}_k} + \varepsilon_{\mathbf{k}_l} - \varepsilon_{\mathbf{k}_a} - \varepsilon_{\mathbf{k}_b}\right)},\end{aligned} \tag{4.27}$$

and the particle-hole term

$$\begin{aligned}\Delta E^{(3)}_{ph} = -\sum_{\mathbf{k}_a,\mathbf{k}_b} \sum_{\mathbf{k}_c,\mathbf{k}_i} \sum_{\mathbf{k}_j,\mathbf{k}_k} & \frac{\langle \mathbf{k}_i\mathbf{k}_j|\hat{v}|\mathbf{k}_a\mathbf{k}_b\rangle_{AS}\langle \mathbf{k}_k\mathbf{k}_b|\hat{v}|\mathbf{k}_i\mathbf{k}_c\rangle_{AS}}{\left(\varepsilon_{\mathbf{k}_i} + \varepsilon_{\mathbf{k}_j} - \varepsilon_{\mathbf{k}_a} - \varepsilon_{\mathbf{k}_b}\right)} \\ \times & \frac{\langle \mathbf{k}_a\mathbf{k}_c|\hat{v}|\mathbf{k}_i\mathbf{k}_j\rangle_{AS}}{\left(\varepsilon_{\mathbf{k}_k} + \varepsilon_{\mathbf{k}_j} - \varepsilon_{\mathbf{k}_a} - \varepsilon_{\mathbf{k}_c}\right)}.\end{aligned} \tag{4.28}$$

The reference and second-order energy terms of Eqs. (4.22) and (4.23) are given diagrammatically in Fig. 4.1. We use the diagrammatic rules defined in Ref. [80]. A vertical line with an arrow pointing up (down) represents

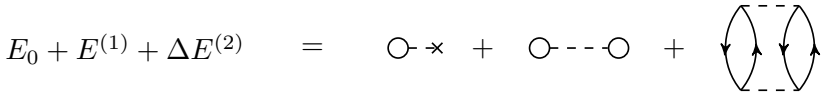

Figure 4.1: Diagrammatic representation of the energy to second order in perturbation theory, as obtained when assuming a Hartree-Fock single-particle potential $\hat{U}$. (Illustration by the author.)

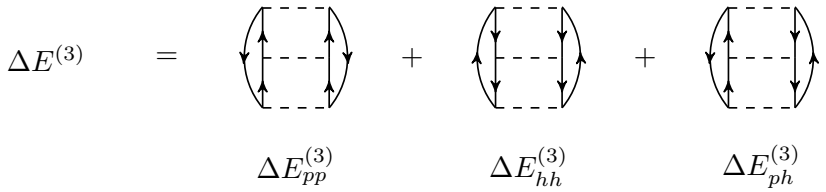

Figure 4.2: MBPT diagrams for the third-order energy correction, when the operator $\hat{U}$ is as in Eq. 4.17. For a more general operator $\hat{U}$, there are additional third-order diagrams containing the Fock operator. (Illustration by the author.)

the summation over a particle (hole) state, whereas a ring without an arrow represents a summation over a hole state. The kinetic energy operator is denoted by a horisontal dashed line with a cross in one of the ends, and the antisymmetrized two-body operator is represented by a horisontal dashed line that is connected to four vertical lines. Between every pair of interaction lines, there is an energy denominator. For an introduction to the diagrammatic rules, the reader is referred to Refs. [80, 110, 160]. The third-order diagrams for this special case are given in Fig. 4.2. Shavitt and Bartlett [80] show all MBPT diagrams up to fourth order for the general case.

A diagram is said to be *closed* if both ends of all particle/hole lines are connected to an operator, and the diagram is *connected* if it cannot be divided into two topologically unconnected parts without breaking lines. The linked-diagram theorem theorem [161] states that the RSPT energy correction ΔE is the sum of all closed and connected diagrams which give different correlation contributions. As explained in for example Refs. [80, 110], inclusion of only connected diagrams ensures that the energy is *size-consistent*. Size-consistency is defined as the property that the total energy of two subsystems, calculated independently, must be equal to the energy of a system where both parts are present, but so far from each other that they do not interact [80]. It follows therefore from the linked-diagram theorem that RSPT is a size-consistent method. Size-consistency becomes increasingly important for larger systems, and is a critical property when studying infinite matter.

As Harris *et al.* show in their textbook [110], the configuration interaction doubles approximation, which is not size-consistent, gives zero correlation energy per particle for the electron gas.

4.2 Brueckner-Hartree-Fock approximation

The perturbation series contains diagrams similar to the particle-particle diagram $\Delta E^{(3)}_{pp}$, given in Fig. 4.2, with one, two, three, and up to infinitely many interaction matrix elements. That class of terms are commonly called particle-particle ladder diagrams, and a few of them are shown in Fig. 4.3. In a similar way, the RSPT contains hole-hole ladder diagrams to infinite order. The hole-hole ladder diagrams are obtained from the particle-particle ladders by exchanging all particle and hole lines with each other. The complete set of particle-particle ladder diagrams can be constructed using the so-called G matrix [82], which is defined by the implicit equation

$$\begin{aligned}\langle \mathbf{k}_p\mathbf{k}_q|\hat{g}|\mathbf{k}_r\mathbf{k}_s\rangle &= \langle \mathbf{k}_p\mathbf{k}_q|\hat{v}|\mathbf{k}_r\mathbf{k}_s\rangle \\ &+ \sum_{\mathbf{k}_c\mathbf{k}_d} \frac{\langle \mathbf{k}_p\mathbf{k}_q|\hat{v}|\mathbf{k}_c\mathbf{k}_d\rangle\langle \mathbf{k}_c\mathbf{k}_d|\hat{g}|\mathbf{k}_r\mathbf{k}_s\rangle}{\varepsilon_{\mathbf{k}_p}+\varepsilon_{\mathbf{k}_q}-\varepsilon_{\mathbf{k}_c}-\varepsilon_{\mathbf{k}_d}},\end{aligned} \tag{4.29}$$

where the single-particle energies are defined as in Eq. (4.24) and the summation is over only particle states. Observe that the G matrix is on both sides of the equation and the single-particle eneriges are dependent on the auxiliary potential $\hat{U}$. In terms of antisymmetric matrix elements, the same equation can be written as

$$\begin{aligned}\langle \mathbf{k}_p\mathbf{k}_q|\hat{g}|\mathbf{k}_r\mathbf{k}_s\rangle_{AS} &= \langle \mathbf{k}_p\mathbf{k}_q|\hat{v}|\mathbf{k}_r\mathbf{k}_s\rangle_{AS} \\ &+ \frac{1}{2}\sum_{\mathbf{k}_c\mathbf{k}_d} \frac{\langle \mathbf{k}_p\mathbf{k}_q|\hat{v}|\mathbf{k}_c\mathbf{k}_d\rangle_{AS}\langle \mathbf{k}_c\mathbf{k}_d|\hat{g}|\mathbf{k}_r\mathbf{k}_s\rangle_{AS}}{\varepsilon_{\mathbf{k}_p}+\varepsilon_{\mathbf{k}_q}-\varepsilon_{\mathbf{k}_c}-\varepsilon_{\mathbf{k}_d}},\end{aligned} \tag{4.30}$$

where the sum is now multiplied by a factor of one half. The G-matrix equation is shown diagrammatically in Fig. 4.4.

The strong short-range forces of the nuclear interaction induce correlations that cannot be accounted for in a mean-field theory. By replacing the bare interaction with a G matrix, important parts of the correlations are included already at the lowest order of perturbation theory. The Brueckner-Goldstone (BG) expansion [10] is obtained by replacing all interaction matrix elements in the RSPT with G matrices. In BG theory, the diagonal matrix elements of the auxiliary potential $\hat{U}$ are commonly chosen to be

$$\langle \mathbf{k}_p|\hat{u}|\mathbf{k}_p\rangle = \sum_{\mathbf{k}_i}\langle \mathbf{k}_p\mathbf{k}_i|\hat{g}|\mathbf{k}_p\mathbf{k}_i\rangle_{AS} \tag{4.31}$$

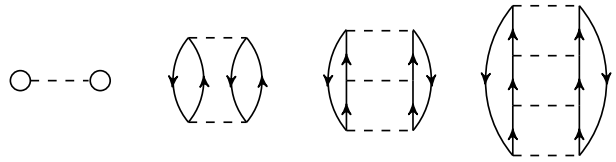

Figure 4.3: Particle-particle ladder diagrams up to fourth order, as they occur in the MBPT energy expansion. (Illustration by the author.)

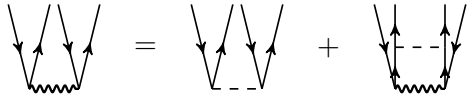

Figure 4.4: Diagrammatic representation of the G-matrix equation, which is used in Brueckner theory [43, 161] (Figure 4 in Paper II). The wave-shaped line represents the G matrix, which is an effective interaction obtained by resummation of short-range correlation contributions. Reprinted by permission from ... The figure is also used in Ref. [109].

for single-particle states that are occupied in the uncorrelated Fermi vacuum. In the first-order approximation, which corresponds to the reference energy in RSPT, the energy becomes

$$E_{BHF} = \sum_{\mathbf{k}_i} \langle \mathbf{k}_i | \hat{t} | \mathbf{k}_i \rangle + \frac{1}{2} \sum_{\mathbf{k}_i, \mathbf{k}_j} \langle \mathbf{k}_i \mathbf{k}_j | \hat{g} | \mathbf{k}_i \mathbf{k}_j \rangle_{AS}. \tag{4.32}$$

This approximation is commonly called the Brueckner-Hartree-Fock (BHF) method [162], because the interaction in the Hartree-Fock energy has been replaced with a self-consistently solved Brueckner G matrix. Observe that the matrix elements of the auxiliary potential is not yet defined for single-particle states above the Fermi level. There have been different approaches to handling the single-particle potential for particle states, such as the conventional gap option [162], in which the single-particle potential is set to zero above the Fermi level, and the continuous option [71, 72], in which the potential in Eq. (4.31) is used for both particle and hole single-particle states. In our calculations, we use the latter approach. Day has written a pedagogical introduction [10] to Brueckner-Goldstone theory and its application to infinite nuclear matter.

According to Rajaraman and Bethe [101], the Brueckner-Goldstone expansion does not converge when using the G matrix as a convergence parameter. Instead, they argue that the number of independent hole lines is a more appropriate cutoff parameter in the perturbation series. The first-order energy in the Brueckner-Goldstone theory, the BHF approximation, is equal

to the Brueckner-Bethe approximation including up to two hole lines [69].

- Give a short heuristic argumentation for the hole-line expansion
- The hole-line approximation is a good assumption only at sufficiently low densities

4.3 Transformation to partial-wave expansion

The nuclear interaction is often given explicitly in the partial-wave basis (3.33). Next, we rewrite some of the previously defined expressions derived from RSPT and the BHF approximation in the partial-wave basis. In this basis, the equations can be considerably simplified by approximating the Pauli exclusion operators (3.31) and (3.32) by averages over the angle between the relative and CM momentum vectors. In this section, we consider only three-dimensional nuclear matter.

4.3.1 The first orders of perturbation theory

Infinite nuclear matter contains in theory an infinite number of particles, and one is therefore normally interested in the energy per nucleon. The kinetic energy per particle can be calculated analytically, and is for both PNM and SNM simply

$$\begin{aligned}\frac{E_{kin}}{A} &= \frac{\Omega}{A}\frac{1}{(2\pi)^3}\sum_{m_s,m_t}\int_{|\mathbf{k}|\leq k_F} d\mathbf{k}\frac{\hbar^2 k^2}{2m} \\ &= \frac{3\hbar^2 k_F^2}{10m},\end{aligned} \tag{4.33}$$

where $\Omega \equiv L^3$ is the volume, A is the number of nucleons, k_F is the Fermi momentum, m is the nucleon mass, and $\hbar$ is the Planck constant. To obtain the final expression in Eq. (4.33), the number of particles A is calculated as

$$A = \frac{\Omega}{(2\pi)^3}\sum_{m_s,m_t}\int_{|\mathbf{k}|\leq k_F} d\mathbf{k}, \tag{4.34}$$

that is, by counting all nucleons under the Fermi surface. In PNM calculations, we use the neutron mass m_n, and in SNM calculations we use the average of the proton and neutron masses $\overline{m} = (m_n + m_p)/2$.

- Give an estimate of the error coming from using the average nucleon mass

The expressions for the potential energy are obtained by first writing the equations in terms of relative momenta, and then transforming to a partial-wave basis. When transforming the potential energy expressions to the desired form, we first rewrite the sums as integrals using the transformation (3.26). Next, the equations are written in a RCM basis, as defined in Eq. (3.30), and the identity operators (3.34) and (3.35) are used to to introduce angular momenta. A coupled angular momentum basis is obtained by using the relation (3.39). In this chapter, we approximate all Pauli exclusion operators (3.31) and (3.32) by averages over the angle between the relative and CM momentum vectors, $\theta_{\mathbf{kK}}$. That is, the exact Pauli operators are replaced with the angular-averaged hole-hole operator

$$\begin{aligned}\overline{Q}_{hh}(k,K,k_F) = \frac{1}{2}\int_{-1}^{1} d\cos\theta_{\mathbf{kK}} \\ \times \theta(k_F - |\mathbf{k}+\mathbf{K}/2|)\theta(k_F - |-\mathbf{k}+\mathbf{K}/2|),\end{aligned} \tag{4.35}$$

and the angular-averaged particle-particle operator

$$\begin{aligned}\overline{Q}_{pp}(k',K,k_F) = \frac{1}{2}\int_{-1}^{1} d\cos\theta_{\mathbf{k'K}} \\ \times \theta(|\mathbf{k}'+\mathbf{K}/2| - k_F)\theta(|-\mathbf{k}'+\mathbf{K}/2| - k_F).\end{aligned} \tag{4.36}$$

Explicit expressions of the angular-averaged Pauli exclusion operators are given in for example Ref. [163]. Finally, the dependency on the angular coordinates of the relative momentum vectors are integrated out using Eq. (3.37).

With a transformation as described above, the first-order correction to the energy per nucleon becomes

$$\begin{aligned}\frac{\Delta E^{(1)}}{A} = C\sum_{\mathcal{J}Sl}\sum_{M_T}(2\mathcal{J}+1) \\ \times \int_0^{k_F} dk k^2 \left(1 - \frac{3}{2}\frac{k}{k_F} + \frac{1}{2}\left(\frac{k}{k_F}\right)^3\right) \\ \times \langle k\mathcal{J}lSM_T|\hat{v}|k\mathcal{J}lSM_T\rangle,\end{aligned} \tag{4.37}$$

where the constant C is 1 for symmetric nuclear matter and 2 for pure neutron matter. The summation over M_T takes the values -1, 0, 1 for symmetric nuclear matter and only 0 for pure neutron matter. Here and in the following, all interaction matrix elements are assumed to be multiplied by the operator (A.5), which ensures proper antisymmetry and conservation of parity. A similar expression as Eq. (4.37) is given for symmetric nuclear matter by

MacKenzie [157] using coupled isospin T. The differing factor $4/\pi$ comes from a different definition of the Fourier-Bessel transform in the interaction matrix elements.

Similarly, the second-order perturbation correction (4.23) can be written as

$$\begin{aligned}\frac{\Delta E^{(2)}}{A} = C\frac{3}{16k_F^3}\sum_{\mathcal{J}S}\sum_{ll'}\sum_{M_T}(2\mathcal{J}+1)\int_0^{2k_F} dKK^2 \\ \times \int_0^{\sqrt{k_F^2-K^2/4)}} dkk^2 \int_{\sqrt{k_F^2-K^2/4}}^{\infty} dk'k'^2 \\ \times |\langle k\mathcal{J}lSM_T|\hat{v}|k'\mathcal{J}l'SM_T\rangle|^2 \\ \times \frac{\overline{Q}_{hh}(k,K,k_F)\overline{Q}_{pp}(k',K,k_F)}{\Delta\varepsilon_{ave}(k,k',K,M_T)},\end{aligned} \tag{4.38}$$

where we have used angular-averaged Pauli exclusion operators and the constant C is as defined for the Hartree-Fock term. In Eq. (4.38), the energy denominator has been approximated by the expression

$$\begin{aligned}\Delta\varepsilon_{ave}(k,k',K) = \varepsilon(\overline{|\mathbf{k}+\mathbf{K}/2|}) + \varepsilon(\overline{|-\mathbf{k}+\mathbf{K}/2|}) \\ - \varepsilon(\overline{|\mathbf{k}'+\mathbf{K}/2|}) - \varepsilon(\overline{|-\mathbf{k}'+\mathbf{K}/2|}),\end{aligned} \tag{4.39}$$

where angular-averaged arguments are marked with an overline. Above, the isospin dependence in the energy denominator has been neglected for brevity. A similar expression as Eq. (4.38) is given in Ref. [157], in which they assume that the interaction is a function of the total isospin only.

The exact energy denominator contains the single-particle energy terms

$$\varepsilon(k_i) + \varepsilon(k_j) = \varepsilon(|\mathbf{k}+\mathbf{K}/2|) + \varepsilon(|-\mathbf{k}+\mathbf{K}/2|), \tag{4.40}$$

where the laboratory frame momenta k_i and k_j have been written using RCM momenta on the right-hand side of the equation. When approximating the arguments of the single-particle energies, we use a technique first suggested by Brueckner and Gammel [43] and explained in the PhD thesis of Ramos [163,164]. In this method, the single-particle energy is first approximated by a polynomial expansion. Because nuclear matter is an isotropic medium, the single-particle energy must be a symmetric function, and therefore only even powers in the polynomial have a non-zero contribution. The single-particle energy is approximated by a polynomial

$$\varepsilon(k) = \alpha + \beta k^2 + \gamma k^4 + \ldots, \tag{4.41}$$

where α, β, and γ are constants, and consequently

$$\begin{aligned}\varepsilon(k_i) + \varepsilon(k_j) &= 2\alpha + \beta(k_i^2 + k_j^2) + \gamma(k_i^4 + k_j^4) + \dots \\ &= \dots \\ &= 2\alpha + 2\beta(k^2 + K^2/4) \\ &+ 2\gamma\left((k^2 + K^2/4)^2 + (\mathbf{k}\cdot\mathbf{K})^2\right) + \dots . \end{aligned} \tag{4.42}$$

As Ramos points out, the first dependence on the angle between $\mathbf{k}$ and $\mathbf{K}$ comes at second order. [164]

Following Ramos, we do the angular-average approximation

$$(\mathbf{k}\cdot\mathbf{K})^2 \approx K^2 k^2 \overline{\cos^2\theta_{\mathbf{kK}}}, \tag{4.43}$$

where

$$\begin{aligned}\overline{\cos^2\theta_{\mathbf{kK}}} &= \frac{1}{2}\int_{-1}^{1} d\cos\theta_{\mathbf{kK}} \cos^2\theta_{\mathbf{kK}} \\ &\times \theta(k_F - |\mathbf{k} + \mathbf{K}/2|)\theta(k_F - |-\mathbf{k} + \mathbf{K}/2|) \end{aligned} \tag{4.44}$$

for hole states and

$$\begin{aligned}\overline{\cos^2\theta_{\mathbf{kK}}} &= \frac{1}{2}\int_{-1}^{1} d\cos\theta_{\mathbf{kK}} \cos^2\theta_{\mathbf{kK}} \\ &\times \theta(|\mathbf{k} + \mathbf{K}/2| - k_F)\theta(|-\mathbf{k} + \mathbf{K}/2| - k_F) \end{aligned} \tag{4.45}$$

for particle states. The angular-averaged value can be shown to be

$$\overline{\cos^2\theta_{\mathbf{kK}}} = \frac{1}{3}\overline{Q}^3(k, K, k_F), \tag{4.46}$$

where $\overline{Q}$ is replaced with the angular-averaged Pauli exclusion operator $\overline{Q}_{hh}$ for two-hole states, and by $\overline{Q}_{pp}$ for two-particle states. Now we get the angular-averaged input momenta

$$\begin{aligned}k_i^2 &= \overline{|\mathbf{k} + \mathbf{K}/2|^2} \\ &= k^2 + K^2/4 + \frac{1}{\sqrt{3}} kK Q_{hh}^{3/2}(k, K, k_F) \end{aligned} \tag{4.47}$$

and

$$\begin{aligned}k_j^2 &= \overline{|-\mathbf{k} + \mathbf{K}/2|^2} \\ &= k^2 + K^2/4 - \frac{1}{\sqrt{3}} kK Q_{hh}^{3/2}(k, K, k_F). \end{aligned} \tag{4.48}$$

Angular-averaged input momenta for particle states k_a and k_b are defined in a similar way. [164] Explicit expressions for the sinlge-particle energies are obtained from Eqs. (4.60) and (4.61) by replacing the G matrix with a bare interaction.

The particle-particle term in third-order perturbation theory, Eq. (4.26), can be written as

$$\begin{aligned}\frac{\Delta E_{pp}^{(3)}}{A} &= C\frac{3}{32k_F^3}\sum_{\mathcal{J}S}\sum_{ll'l''}\sum_{M_T}(2\mathcal{J}+1)\int_0^{2k_F} dKK^2 \\ &\times \int_0^{\sqrt{k_F^2-K^2/4}} dkk^2 \int_{\sqrt{k_F^2-K^2/4}}^{\infty} dpp^2 \int_{\sqrt{k_F^2-K^2/4}}^{\infty} dp'p'^2 \\ &\times \frac{\langle k\mathcal{J}(lS)M_T|\hat{v}|p\mathcal{J}(l'S)M_T\rangle\langle p\mathcal{J}(l'S)M_T|\hat{v}|p'\mathcal{J}(l''S)M_T\rangle}{\Delta\varepsilon_{ave}(k,p,K)\Delta\varepsilon_{ave}(k,p',K)} \\ &\times \langle p'\mathcal{J}(l''S)M_T|\hat{v}|k\mathcal{J}(lS)M_T\rangle \\ &\times \overline{Q}_{hh}(k,K,k_F)\overline{Q}_{pp}(p,K,k_F)\overline{Q}_{pp}(p',K,k_F), \end{aligned} \tag{4.49}$$

where C is 1 for symmetric nuclear matter and 2 for pure neutron matter. In Eq. (4.49), the Pauli exclusion operators in the nominator have been approximated by angular-averaged operators. A similar expression for the particle-particle term is given by MacKenzie [157] for symmetric nuclear matter with total two-particle isospin as a good quantum number. In Ref. [157], there is an additional factor $(4/\pi)^3$ owing to a different definition of the interaction matrix elements.

4.3.2 The BHF approximation

The Brueckner-Hartree-Fock approximation is a standard approach for calculating the binding energy of infinite nuclear matter. Implementations of the G-matrix equation have therefore been discussed many places in the litterature [70,71,162,164]. In addition to being an essential part of the Brueckner-Goldstone theory [10], the G matrix is encountered also in for example the self-consistent Greens function method [163]. We have solved the G-matrix equation using the matrix inversion technique of Haftel and Tabakin [70], but using continuous single-particle energy spectra [71, 72]. Using continuous single-particle spectra means that the operator $\hat{U}$ is chosen such that the definition (4.31) is used for both hole and particle single-particle states.

Our implementation of the BHF approximation follows to a large degree Haftel and Tabakin [70], using angular-averaged Pauli exclusion operators. As given in Ref. [70], the G-matrix equation (4.30) can be written in a partial-

wave expansion basis as

$$\begin{aligned}
&\langle k\mathcal{J}(lS)M_T|\hat{g}(K)|k'\mathcal{J}(l'S)M_T\rangle \\
&= \langle k\mathcal{J}(lS)M_T|\hat{v}|k'\mathcal{J}(l'S)M_T\rangle \\
&+ \frac{1}{2}\sum_{l''}\int_0^\infty dpp^2 Q_{pp}(p,K,k_F) \\
&\times \frac{\langle k\mathcal{J}(lS)M_T|\hat{v}|p\mathcal{J}(l''S)M_T\rangle\langle p\mathcal{J}(l''S)M_T|\hat{g}(K)|k'\mathcal{J}(l'S)M_T\rangle}{\Delta\varepsilon_{ave}(k',p,K,M_T)},
\end{aligned} \tag{4.50}$$

where we notice that the G matrix depends on the radial part of the CM momentum. The energy denominator is defined as in Eq. (4.39).

Next, let us consider the energy denominator. The single-particle energy of a state $|\mathbf{k}_p, m_s, m_t\rangle$ is

$$\begin{aligned}
\varepsilon(\mathbf{k}_p, m_s, m_t) = \frac{\hbar^2 k_p^2}{2m} + \sum_{m_{s'}}\sum_{m_{t'}}\int d\mathbf{k}_j \theta(k_F - |\mathbf{k}_j|) \\
\times \langle \mathbf{k}_p m_s m_t \mathbf{k}_j m_{s'} m_{t'}|\hat{g}|\mathbf{k}_p m_s m_t \mathbf{k}_j m_{s'} m_{t'}\rangle_{AS},
\end{aligned} \tag{4.51}$$

where m_s and m_t are the z projections of spin and isospin, respectively, and a factor $\Omega/(2\pi)^3$ is included in the two-body interaction. If the integration variable is changed to relative coordinates, i.e.,

$$\mathbf{k} = (\mathbf{k}_p - \mathbf{k}_j)/2, \qquad \mathbf{K} = \mathbf{k}_p + \mathbf{k}_j, \tag{4.52}$$

where $\mathbf{k}$ and $\mathbf{K}$ are relative and CM coordinates, respectively, the single-particle potential becomes

$$\begin{aligned}
U(\mathbf{k}_p, m_s, m_t) = 8\sum_{m_{s'}}\sum_{m_{t'}}\int_{\min\{0,(k_p-k_F)/2\}}^{(k_p+k_F)/2} dk k^2 \int_0^{2\pi} d\phi_{\mathbf{k}} \int_{-1}^{1} d(\cos\theta_{\mathbf{k}}) \\
\times \langle \mathbf{k} m_s m_t m_{s'} m_{t'}|\hat{g}(\mathbf{K})|\mathbf{k} m_s m_t m_{s'} m_{t'}\rangle_{AS} \\
\times \theta(k_F - |-2\mathbf{k} + \mathbf{k}_p|).
\end{aligned} \tag{4.53}$$

Because infinite nuclear matter is an isotropic medium, the single-particle energy should not depend on the direction of $\mathbf{k}_p$. The input momentum vector is chosen to be directed along the positive z axis.

In our calculations we have replaced the CM momentum with $\overline{K^2}$, defined as the average of $|\mathbf{K}|^2$ when integrating with respect to the vector $\mathbf{k}$. If $\mathbf{k}_p$ is directed along the z axis, the average of the squared CM momentum becomes

$$\overline{K^2} \equiv \frac{1}{2}\int_{-1}^{1} d\cos\theta_{\mathbf{k}} \, |2(\mathbf{k}_p - \mathbf{k})|^2 \, \theta(k_F - |-2\mathbf{k} + \mathbf{k}_p|). \tag{4.54}$$

By evaluating this expression, we got the explicit formula

$$\overline{K^2} = \begin{cases} 4(k_p^2 + k^2), & \text{if } 0 \le 2k \le k_F - k_p \\ & \text{and } k_p \le k_F, \\ 4(k_p^2 + k^2) + \frac{1}{8kk_p}\left[-16k_p k^3\right. & \\ -4(7k_p^2 + k_F^2)k^2 - 16k_p^3 k & \\ \left. + k_F^4 + 2k_F^2 k_p^2 - 3k_p^4\right], & \text{if } |k_F - k_p| \le 2k \le k_F + k_p. \end{cases} \tag{4.55}$$

Haftel and Tabakin [70] have given a similar averaged CM momentum that is defined only when $k_p \le k_F$. Our expression differs from Haftel and Tabakin's in the second interval, but the limits of the intervals are the same. In Fig. 4.5, our formula for $\overline{K^2}$ is compared with that of Ref. [70]. Observe that our definition of the CM momentum vector $\mathbf{K}$ is different than the definition

$$\mathbf{P} = (\mathbf{k}_i - \mathbf{k}_j)/2 \tag{4.56}$$

used by Haftel and Tabakin. In Fig. 4.5, both expressions were calculated using the definition (4.56). In contrast to the expression given by Haftel and Tabakin, our average CM momentum vanishes at $k = (k_p + k_F)/2$, as is required by the definition (4.54). It seems therefore that the formula for $\overline{K^2}$ given in Ref. [70] is wrong.

In addition to using the averaged CM momentum (4.54), we replace the Pauli exclusion operator in Eq. (4.53) with the angular-averaged operator

$$Q(k, k_p, k_F) = \frac{1}{2}\int_{-1}^{1} d\cos\theta_{\mathbf{k}}\,\theta(k_F - |-2\mathbf{k} + \mathbf{k}_p|), \tag{4.57}$$

similarly as done in Ref. [70]. Applying angular momentum algebra, we got the expression

$$\begin{aligned} U(k_p, m_t) =& 16\sum_{m_{t'}}\sum_{\mathcal{J}lS}(2\mathcal{J}+1)\left[\theta(k_F - |k_p|)\int_0^{|k_F-k_p|/2} dk k^2\right. \\ &\left. + \int_{|k_F-k_p|/2}^{(k_F+k_p)/2} dk k^2\left(\frac{-4k^2 + 4kk_p - k_p^2 + k_F^2}{8kk_p}\right)\right] \\ &\times\left[\langle k\mathcal{J}(lS)m_t m_{t'}|g(K_{av})|k\mathcal{J}(lS)m_t m_{t'}\rangle\right. \\ &\left. -(-1)^{1+S+l}\langle k\mathcal{J}(lS)m_t m_{t'}|g(K_{av})|k\mathcal{J}(lS)m_{t'} m_t\rangle\right]. \end{aligned} \tag{4.58}$$

Above, the single-particle potential is given as a function of a single-particle isospin projection m_t. In the energy denominator, the single-particle potential always occurs in pairs

$$W(k_p, m_{t_p}, k_q, m_{t_q}) \equiv U(k_p, m_{t_p}) + U(k_q, m_{t_q}). \tag{4.59}$$

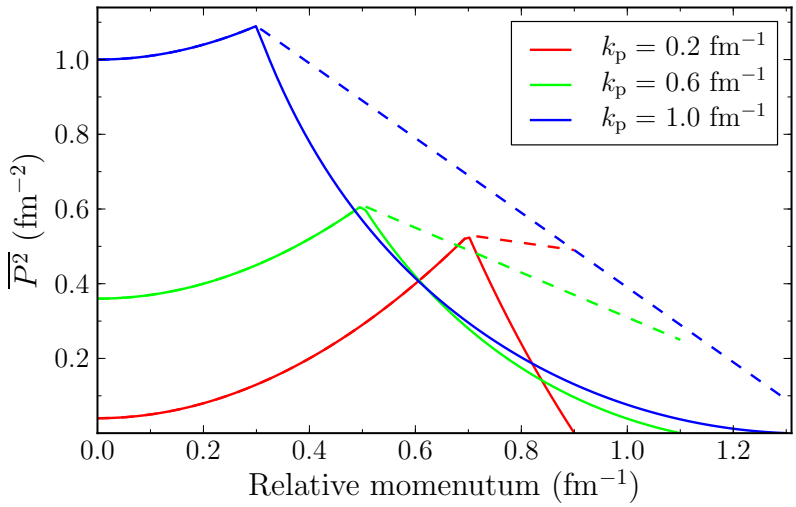

Figure 4.5: Average of the squared CM momentum, $\overline{P^2} = \overline{K^2}/4$, plotted as a function of the relative momentum for given lab momenta k_p. The Fermi momentum k_F was fixed to 1.6 fm^{-1}. The dashed lines represent results calculated with the formula for $\overline{P^2}$ given in Eq. (3.19) of Ref. [70]. In contrast to the formula given in Ref. [70], our formula for $\overline{K^2}$ gives the correct values at the end points of the relative momentum interval.

The function W is a function of the two-particle isospin projection $M_T = m_{t_p} + m_{t_q}$, i.e.

$$W^{M_T}(k_p, k_q) \equiv U^{M_T,+}(k_p) + U^{M_T,-}(k_q), \tag{4.60}$$

where the explicit expressions of the single-particle potentials are

$$\begin{aligned} U^{M_T,\pm}(k_p) =& 16 \sum_{\mathcal{J}lS} (2\mathcal{J}+1) \left[\theta(k_F - |k_p|) \int_0^{|k_F - k_p|/2} dk k^2 \right. \\ & \left. + \int_{|k_F-k_p|/2}^{(k_F+k_p)/2} dk k^2 \left(\frac{-4k^2 + 4kk_p - k_p^2 + k_F^2}{8kk_p} \right) \right] \\ & \times \mathcal{B}^{M_T,\pm} \langle k\mathcal{J}(lS)|g(K_{av})|k\mathcal{J}(lS)\rangle, \end{aligned} \tag{4.61}$$

and the antisymmetrization operator $\mathcal{B}^{M_T,\pm}$ is defined in Eqs. (A.6) and (A.7).

Finally, let us write the BHF energy (4.32) in the partial-wave basis. If the angular-average approxmation (4.35) is used for the hole-hole Pauli exclusion operator, the BHF energy per nucleon is

$$\begin{aligned} \frac{\Delta E_{BHF}}{A} =& \frac{3\pi}{2k_F^3} \sum_{\mathcal{J}lS} \sum_{M_T} (2\mathcal{J}+1) \int_0^{k_F} dk k^2 \\ & \times \left\{ \int_0^{2(k_F-k)} dK K^2 - \int_{2(k_F-k)}^{2\sqrt{k_F^2-k^2}} dK K^2 \frac{k^2 - k_F^2 + K^2/4}{kK} \right\} \\ & \times \langle k\mathcal{J}lSM_T|g(K)|k\mathcal{J}lSM_T\rangle, \end{aligned} \tag{4.62}$$

where the G-matrix elements are assumed to be multiplied by the antisymmetrization and parity conservation operator $\mathcal{A}^{llSM_T}$, defined in Eq. (A.5). Haftel and Tabakin [70] have given a similar expression for a system in which the interaction depends only on the total two-particle isospin.

- A figure with results: HF, MBPT(2), MBPT(3) with only pp ladders, and BHF with NNLO_{opt} and AV18

4.4 Implementations

4.4.1 The first orders of perturbation theory

The energy expressions for the lowest orders of perturbation theory, given in Eqs. (4.37), (4.38), and (4.49), were straightforwardly implemented using

numerical integration with Gauss-Legendre quadratures [165]. The expressions for the angular-averaged Pauli exclusion operators are discontinuous with respect to the first derivative. In our implementation, we split the integration intervals at the discontinuity points of the Pauli operators to avoid convergency problems in the numerical integrations.

4.4.2 The BHF approximation

We solve the G-matrix equation using a matrix inversion technique introduced by Haftel and Tabakin [70]. As outlined in Ref. [70], the G-matrix equation (4.50) may be written as

$$\mathbf{V} = \mathbf{U}\mathbf{G}, \tag{4.63}$$

where, for coupled channels, $\mathbf{G}$ is a $2(N+1) \times 2(N+1)$ matrix

$$\mathbf{G} = \begin{bmatrix} \mathbf{G}_{l_{\min},l_{\min}} & \mathbf{G}_{l_{\min},l_{\max}} \\ \mathbf{G}_{l_{\max},l_{\min}} & \mathbf{G}_{l_{\max},l_{\max}} \end{bmatrix}, \tag{4.64}$$

where $l_{\min} = \mathcal{J} - 1$ and $l_{\max} = \mathcal{J} + 1$. The matrices $\mathbf{V}$ and $\mathbf{U}$ are set up similarly for coupled channels. For uncoupled channels, the matrices $\mathbf{V}$, $\mathbf{U}$, and $\mathbf{G}$ contain only one submatrix. In Eq. (4.64), the submatrices have matrix elements

$$[\mathbf{G}_{l,l'}]_{i,j} \equiv \langle k_i \mathcal{J}(lS) M_T | \hat{g}(K) | k_j \mathcal{J}(l'S) M_T \rangle, \tag{4.65}$$

for $i, j \in \{1, \ldots, N+1\}$. Similarly, the matrix $\mathbf{V}$ is defined by the interaction matrix elements

$$[\mathbf{V}_{l,l'}]_{i,j} \equiv \langle k_i \mathcal{J}(lS) M_T | \hat{v} | k_j \mathcal{J}(l'S) M_T \rangle \tag{4.66}$$

and $\mathbf{U}$ by the elements

$$[\mathbf{U}_{l,l'}]_{i,j} \equiv \delta_{ij} + u_j \left[\mathbf{V}_{l,l'}\right]_{i,j}, \tag{4.67}$$

where

$$u_j = \begin{cases} -\frac{\omega_{k_j} k_j^2 Q_{pp}(k_j,K,k_F)}{\Delta\varepsilon_{av}(k_j,k_0,K)}, & \text{if } j \leq N, \\ \sum_{p=1}^{N} \frac{\omega_{k_p} k_0^2 Q_{pp}(k_0,K,k_F)}{\Delta\varepsilon_{av}(k_p,k_0,K)}, & \text{if } j = N+1, \end{cases} \tag{4.68}$$

and $u_{j+N+1} = u_j$ for $j = 1, 2, \ldots, N+1$. The coefficients ω_{k_j} are the quadrature weights corresponding to the grid points k_j, and k_0 is the relative momentum point we want to evaluate the G matrix at. Following Haftel and

Tabakin, we calculate only the principal value of the integral in the G-matrix equation (4.50). As shown in Ref. [70], the singlarity in the integrand is removed by adding a term that integrates to zero. A more proper way of dealing with the singularity is to solve a complex G-matrix equation, as is explained, for example, in the PhD thesis of Engvik [166]. In the submatrices (4.65), (4.66), and (4.67), the momentum mesh points are $[k_1, k_2, \ldots, k_N, k_0]$, where the elements $k_1, k_2, \ldots, k_N$ are integration points used to integrate from zero to infinity and k_0 is the chosen evaluation point.

When solving the G-matrix equation, the grid points must be set up carefully to get good convergence in the numerical integrations. The angular-averaged Pauli exclusion operator $Q_{pp}(k, K, k_F)$ has a discontinuous first derivative at certain momenta k that depend on the CM momentum K and the Fermi momentum k_F. Therefore, we split the integration interval in relative momentum k at the discontinuity points of the Pauli operator. Even if the singularity point of the G-matrix equation is removed by calculating only the principal value, the region where the energy denominator is small still may cause convergence problems in a numerical integration. According to Engvik [166], better numerical accuracy can be obtained by choosing integration points symmetrically around the singluarity point where the denominator vanishes. Using this technique, the setup of the integration points $[k_1, \ldots, k_N]$ becomes therefore dependent on both K, which is the CM momentum, and k_0, which is the singularity point of the integrand. We set up the relative momentum grid points using the algorithm given in Fig. 4.6. In her PhD thesis [164], Ramos has set up the momentum grid points in a similar way. However, we have written an algorithm to find a grid with ceratain conditions.

Selfconsistency loop for the BHF approximation.
while not converged **do**
    Set up a vector of the single-particle potential.
    Loop over input laboratory frame momenta
    Get average CM momentum given k_{lab} and k_{rel}
end while

ALGORITHM – SETUP OF MOMENTUM GRID POINTS

Assume a CM momentum K and a pole k_0 are given.

1. Get the discontinuity points of the Pauli exclusion operator. Label these points by $L_1(K)$ and $L_2(K)$.

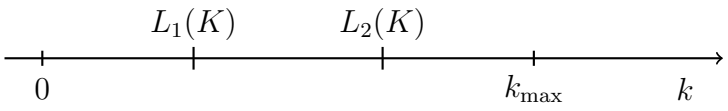

2. Locate in which subinterval the given pole k_0 is.

3. Determine whether k_0 is closer to the lower or upper limit in the subinterval it is in. Label the limit which is closest to k_0 by L_C.

4. Get the mirror point of L_C with respect to k_0 and label it by the symbol $L_3(k_0)$.

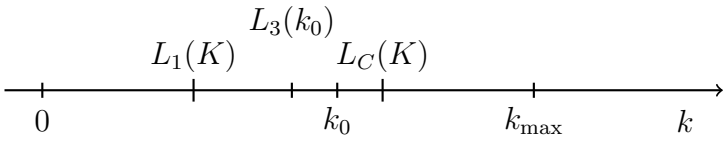

5. Set up Gauss-Legendre quadratures in all the intervals obtained by splitting the total interval at L_1, L_2, and L_3.

Figure 4.6: We use this algorithm to set up the momentum grid points for the G matrix. The principles of this setup are similar as in Refs. [164, 166], but here we automatically find a suitable grid.

Chapter 5

Coupled-cluster approximations for infinite matter

The coupled-cluster (CC) method is one of the most popular *ab initio* many-body approaches in quantum chemistry [106]. A major advantage of the CC approach is that it combines high accuracy with moderate computational cost. The method scales polynomially with the number of occupied and unoccupied orbitals, and is currently the most accurate many-body method for medium-size molecules [106]. Since the late 1990s, CC theory has been used to calculate the binding energy of light and medium-mass nuclei [167–171], nuclei around the neutron drip line [61,172], calculations of spectroscopic factors [173], and a study of time-dependent behaviour of simple nuclear models [174], among other. In contrast, there have been very few applications of CC theory for infinite nuclear and neutron star matter. To our knowledge, there has been no coupled-cluster studies of nuclear matter since Day and Zabolitzky did their calculations in the early 1980s [108]. In Refs. [109] and [] we present new applications of CC theory for nuclear matter, using interaction models derived from chiral perturbation theory.

5.1 Coupled-cluster theory

- Why CC theory?

As mentioned in Chapter 4, the hole-line expansion [10,101,175,176] provides a physically motivated convergence parameter in the number of independent hole lines. Unfortunately, the hole-line expansion requires a rapidly increasing number of diagrams for higher-order approximations. In addition, the assumption that the number of hole lines is a good convergence parameter is only valid at sufficiently low densities, when the average distance between

the nucleons is large compared to the range of the interaction [10, 46]. A method that is related to the perturbative techniques is coupled-cluster theory [102, 103, 106]. Coupled-cluster theory has some of the same properties as many-body methods derived from Rayleigh-Schrödinger perturbation theory, such as size consistency and a non-variational energy, but it suggests a convenient scheme for obtaining a physically justified truncation. Already in the lowest-order coupled-cluster approximations, large sets of diagrams are included to infinite order. The theory gives a system of nonlinear equations, which describe all possible correlations in a model where arbitrary many one-, two-, and up to n-particle clusters can be formed [110, 160].

- The SUB2 approximation (= CCSD ?) contains among others RPA ring diagrams, the Bethe-Goldstone approximation, and the Brueckner-Bethe-Goldstone theory [177, 178]

We here follow Refs. [110, 160] when introducing the general concepts of CC theory. CC theory starts from the assumption that the total wave function can be written in the exponential form

$$|\Psi_{CC}\rangle = e^{\hat{T}}|\Phi_0\rangle, \tag{5.1}$$

where $|\Phi_0\rangle$ is the Fermi vacuum state, the total cluster operator $\hat{T}$ is defined as the sum of cluster operators

$$\hat{T} = \sum_{m=1}^{A} \hat{T}_m, \tag{5.2}$$

and a single m-particle-m-hole cluster operator is defined as

$$\hat{T}_m = \left(\frac{1}{m!}\right)^2 \sum_{\substack{i_1,\ldots,i_m \\ a_1,\ldots,a_m}} t_{i_1,\ldots,i_m}^{a_1,\ldots,a_m} a_{a_1}^\dagger \ldots a_{a_m}^\dagger a_{i_m} \ldots a_{i_1}. \tag{5.3}$$

Here the labels $i_1, \ldots, i_m$ and $a_1, \ldots, a_m$ denote states occupied and unoccupied in $|\Phi_0\rangle$, respectively, $a_p^\dagger$ and a_p are creation and annihilation operators, respectively, and the CC amplitudes $t_{i_1,\ldots,i_m}^{a_1,\ldots,a_m}$ are unknowns that can be obtained by solving a set of nonlinear equations. As is shown in Refs. [110, 160], the exponential form arises naturally if the wave function ansatz is required to include all possible correlations of arbitrary many one-particle, two-particle and up to A-particle clusters.

The CC equations are obtained by projecting the Schrödinger equation

$$\hat{H}e^{\hat{T}}|\Phi_0\rangle = Ee^{\hat{T}}|\Phi_0\rangle \tag{5.4}$$

onto the bra vectors

$$\langle\Phi_0|e^{-\hat{T}}, \qquad \langle\Phi_{i_1,\ldots,i_m}^{a_1,\ldots,a_m}|e^{-\hat{T}}, \tag{5.5}$$

where $m = 1, 2, \ldots, A$ in the latter vector. In other words, the Hamiltonian operator $\hat{H}$ is replaced with a similarity-transformed operator $\overline{H}$, defined as

$$\overline{H} = e^{-\hat{T}}\hat{H}e^{\hat{T}}, \tag{5.6}$$

and the Hamiltonian equation of $\overline{H}$ is projected against the bra vectors $\langle\Phi_0|$ and $\langle\Phi_{i_1,\ldots,i_m}^{a_1,\ldots,a_m}|$. The CC equations consist of the energy equation

$$\langle\Phi_0|\overline{H}|\Phi_0\rangle = E \tag{5.7}$$

and the amplitude equations

$$\langle\Phi_{i_1,\ldots,i_m}^{a_1,\ldots,a_m}|\overline{H}|\Phi_0\rangle = 0, \qquad m = 1, 2, \ldots A. \tag{5.8}$$

In practical calculations, the CC amplitudes $t_{i_1,\ldots,i_m}^{a_1,\ldots,a_m}$ are first obtained by solving Eq. (5.8). Thereafter the CC amplitudes are used for calculating the energy from Eq. (5.7).

The coupled-cluster equations as presented above is an exact reformulation of the Schrödinger energy eigenvalue problem. Except for very simple model systems, few- or many-body problems cannot be solved exactly. In quantum chemistry, the most common approach for approximating the coupled-cluster equations is to truncate the cluster operator (5.2) after $m = n$, where n is smaller than the number of particles [106, 160]. Approximations including $\hat{T}_1$, $\hat{T}_2$, $\hat{T}_3$, etc., are in the CC litterature commonly denoted by singles (S), doubles (D), triples (T), etc., respectively [160]. For example, the CCSD approximation includes only $\hat{T}_1$ and $\hat{T}_2$, whereas in the CCD approximation only $\hat{T}_2$ is nonzero. The same approximations are sometimes called SUBn truncations [177], where for example the SUB2 approximation is equal to CCSD. An alternative family of approximations is the so-called Bochum truncation scheme [107], which is tailored for systems with hard-core interaction models. In this work, we consider only the SUBn truncation scheme of CC theory.

In the following, we give the explicit CC equations in the CCD approximation, as has been derived in for example Ref. [160]. The same equations have been given in Ref. [109], but we repeat the basic equations to make it easier to follow the discussions. In addition, these equations are also used in our studies of the homogeneous electron gas, which are presented in Sec. 5.3. As was explained in Ref. [109], conservation of momentum and symmetry

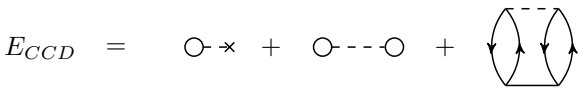

Figure 5.1: A diagrammatic expression for the CCD energy (Figure 2 in Paper II). Reprinted by permission from ... as given in Ref. [109].

makes the $\hat{T}_1$ amplitude to vanish for infinite homogeneous matter. For homogeneous matter, the CCD approximation is therefore equal to CCSD. The general equations are given in a momentum basis. For brevity, we neglect the spin and isospin degrees of freedom in the equations.

The total CCD energy is split into two terms, i.e.

$$E_{CCD} = E_{REF} + \Delta E_{CCD}, \tag{5.9}$$

where E_{REF} is the reference energy, defined as the Fermi vacuum expectation value

$$E_{REF} = \langle \Phi_0 | \hat{H} | \Phi_0 \rangle, \tag{5.10}$$

and ΔE_{CCD} is the remaining correction in the given approximation. In the momentum single-particle basis, the reference energy is

$$E_{REF} = \sum_{\mathbf{k}_i} \langle \mathbf{k}_i | \hat{t} | \mathbf{k}_i \rangle + \frac{1}{2} \sum_{\mathbf{k}_i, \mathbf{k}_j} \langle \mathbf{k}_i \mathbf{k}_j | \hat{v} | \mathbf{k}_i \mathbf{k}_j \rangle_{AS}, \tag{5.11}$$

and the CCD correction

$$\Delta E_{CCD} = \frac{1}{4} \sum_{\mathbf{k}_i, \mathbf{k}_j} \sum_{\mathbf{k}_a, \mathbf{k}_b} \langle \mathbf{k}_i \mathbf{k}_j | \hat{v} | \mathbf{k}_a \mathbf{k}_b \rangle_{AS} \langle \mathbf{k}_a \mathbf{k}_b | \hat{t} | \mathbf{k}_i \mathbf{k}_j \rangle, \tag{5.12}$$

where in the latter equation the CC amplitude is written using a bracket notation. In the following, we always use the bracket notation for the CC amplitudes. Fig. 5.1 shows the CCD energy diagrammatically. In a Hartree-Fock single-particle basis, as is the plane wave basis in infinite nuclear matter, the reference energy E_0 equals the Hartree-Fock energy and the rest is by definition the correlation energy.

Let us define the Fock operator as

$$\hat{F} = \sum_{p,q} \langle p | \hat{f} | q \rangle a_p^\dagger a_q, \tag{5.13}$$

where

$$\langle p | \hat{f} | q \rangle = \langle p | \hat{t}_0 | q \rangle + \sum_i \langle pi | \hat{v} | qi \rangle_{AS}. \tag{5.14}$$

The explicit expression of the CC $\hat{T}_2$ amplitude equation is given in for example Ref. [160]. Restricting ourself to the CCD approximation and writing the equations in a momentum basis, we get the $\hat{T}_2$ amplitude equation

$$
\begin{aligned}
&\left\{\langle \mathbf{k}_i|\hat{f}|\mathbf{k}_i\rangle + \langle \mathbf{k}_j|\hat{f}|\mathbf{k}_j\rangle - \langle \mathbf{k}_a|\hat{f}|\mathbf{k}_a\rangle - \langle \mathbf{k}_b|\hat{f}|\mathbf{k}_b\rangle\right\}\langle \mathbf{k}_a\mathbf{k}_c|\hat{t}|\mathbf{k}_i\mathbf{k}_j\rangle \\
&= \langle \mathbf{k}_a\mathbf{k}_b|\hat{v}|\mathbf{k}_i\mathbf{k}_j\rangle_{AS} \\
&+ \frac{1}{2}\sum_{\mathbf{k}_c,\mathbf{k}_d}\langle \mathbf{k}_a\mathbf{k}_b|\hat{v}|\mathbf{k}_c\mathbf{k}_d\rangle_{AS}\langle \mathbf{k}_c\mathbf{k}_d|\hat{t}|\mathbf{k}_i\mathbf{k}_j\rangle \\
&+ \frac{1}{2}\sum_{\mathbf{k}_k,\mathbf{k}_l}\langle \mathbf{k}_a\mathbf{k}_b|\hat{t}|\mathbf{k}_k\mathbf{k}_l\rangle\left\{\langle \mathbf{k}_k\mathbf{k}_l|\hat{v}|\mathbf{k}_i\mathbf{k}_j\rangle_{AS} + \frac{1}{2}\sum_{\mathbf{k}_c,\mathbf{k}_d}\langle \mathbf{k}_k\mathbf{k}_l|\hat{v}|\mathbf{k}_c\mathbf{k}_d\rangle_{AS}\langle \mathbf{k}_c\mathbf{k}_d|\hat{t}|\mathbf{k}_i\mathbf{k}_j\rangle\right\} \\
&+ \hat{P}(\mathbf{k}_i\mathbf{k}_j)\hat{P}(\mathbf{k}_a\mathbf{k}_b)\sum_{\mathbf{k}_k,\mathbf{k}_c}\langle \mathbf{k}_a\mathbf{k}_c|\hat{t}|\mathbf{k}_i\mathbf{k}_k\rangle \\
&\times\left\{\langle \mathbf{k}_k\mathbf{k}_b|\hat{v}|\mathbf{k}_c\mathbf{k}_j\rangle_{AS} + \frac{1}{2}\sum_{\mathbf{k}_l,\mathbf{k}_d}\langle \mathbf{k}_k\mathbf{k}_l|\hat{v}|\mathbf{k}_c\mathbf{k}_d\rangle_{AS}\langle \mathbf{k}_d\mathbf{k}_b|\hat{t}|\mathbf{k}_l\mathbf{k}_j\rangle\right\} \\
&- \frac{1}{2}\hat{P}(\mathbf{k}_i\mathbf{k}_j)\sum_{\mathbf{k}_k}\langle \mathbf{k}_a\mathbf{k}_b|\hat{t}|\mathbf{k}_i\mathbf{k}_k\rangle\left\{\sum_{\mathbf{k}_l}\sum_{\mathbf{k}_c,\mathbf{k}_d}\langle \mathbf{k}_k\mathbf{k}_l|\hat{v}|\mathbf{k}_c\mathbf{k}_d\rangle_{AS}\langle \mathbf{k}_c\mathbf{k}_d|\hat{t}|\mathbf{k}_j\mathbf{k}_l\rangle\right\} \\
&- \frac{1}{2}\hat{P}(\mathbf{k}_a\mathbf{k}_b)\sum_{\mathbf{k}_c}\langle \mathbf{k}_a\mathbf{k}_c|\hat{t}|\mathbf{k}_i\mathbf{k}_j\rangle\left\{\sum_{\mathbf{k}_k,\mathbf{k}_l}\sum_{\mathbf{k}_d}\langle \mathbf{k}_k\mathbf{k}_l|\hat{v}|\mathbf{k}_c\mathbf{k}_d\rangle_{AS}\langle \mathbf{k}_b\mathbf{k}_d|\hat{t}|\mathbf{k}_k\mathbf{k}_l\rangle\right\},
\end{aligned}
\tag{5.15}
$$

where the permutation operator $\hat{P}$ is defined such that

$$
\hat{P}(x,y)\eta(x,y) = \eta(x,y) - \eta(y,x), \tag{5.16}
$$

given an arbitrary function $\eta(x,y)$. In Eq. (5.15) we have assumed that the Fock operator is diagonal, as it is in homogeneous matter when the interaction conserves total momentum. The CC amplitude equations are commonly factorized to reduce the computational cost [160]. Let us denote the expressions in brackets on right-hand side of Eq. (5.15) by

$$
\langle \mathbf{k}_k\mathbf{k}_l|I_1|\mathbf{k}_i\mathbf{k}_j\rangle, \langle \mathbf{k}_k\mathbf{k}_b|I_2|\mathbf{k}_c\mathbf{k}_j\rangle, \langle \mathbf{k}_k|I_3|\mathbf{k}_j\rangle, \langle \mathbf{k}_b|I_4|\mathbf{k}_c\rangle,
$$

where the intermediate terms are given in the same order as in the amplitude equation above. As Crawford explains it [160], the computational cost is significantly reduced by computing the intermediates separately before substituting them into the amplitude equation. For example, the computational

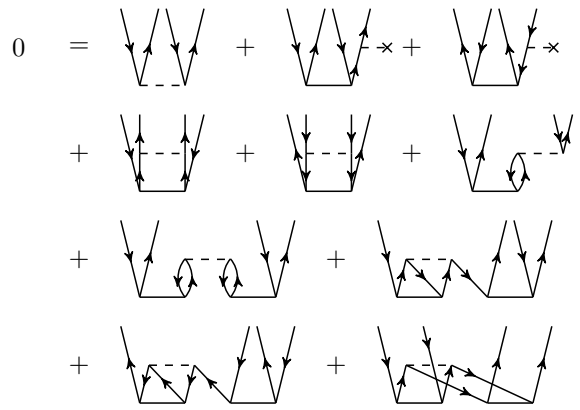

Figure 5.2: The CCD $\hat{T}_2$ amplitude equation (Figure 1 in Paper II). Reprinted by permission from ... given in a diagrammatic representation [109].

cost of evaluating the last term may be reduced from the order $\sim n_h^4 n_p^4$ to $\sim n_h^3 n_p^2$, where n_h and n_p are the number of occupied and unoccupied orbitals, respectively. Typically, n_p is much larger than n_h, and the scaling in terms of n_p is therefore the dominant contribution to the computational cost. The CCD $\hat{T}_2$ amplitude equation is given diagrammatically in Fig. 5.2.

Let us for a moment consider only the terms that are linear in the t amplitude on right-hand side of Eq. (5.15). The terms on the second, third and fifth to sixth row on right-hand side have summations over two particle states, two hole states and one hole and one particle state, respectively. We call the term with summation over two particle states the particle-particle ladder contribution. Similarly, the linear term with summation over two hole states is called the hole-hole ladder contribution. The term with summation over one particle and one hole state gives particle-hole ring contributions. The particle-particle and hole-hole ladder approximation (PPHH-LAD) is obtianed from the CCD equations by setting the second term of I_1, as well as I_2, I_3, and I_4 to zero. The particle-particle ladder approximation (PP-LAD) is otherwise like PPHH-LAD, but in PP-LAD the entire intermediate I_1 is neglected. Explicit CC ladder equations are given in for example Ref. [109].

As explained in Refs. [109, 177], the PP-LAD approximation generates short-range correlation contributions in a similar way as in the Brueckner G-matrix equation. In the PPHH-LAD approximation, particle-particle and hole-hole ladder diagrams are summed to infinite order, similarly as for example in the ladder approximation of the self-consistent Green's function (SCGF) method [58]. The CC ladder approximations differ from the BHF and SCGF methods in that the single-particle potentials are not solved self-consistently, but instead include only the Hartree-Fock contribution. As

shown in Refs. [177, 179], the linear particle-hole term together with the interaction term generate the direct and exchange parts of ring diagrams with forward time-order. Bishop and Lührmann [177] explain thoroughly how the full CCD approximation contains ladder diagrams, the random phase approximation (RPA), and a large number of other diagrams to infinite order. Observe that in CC theory, the different contributions also couple to each other, thereby generating additional diagrams.

In the following sections, we discuss applications of the CC method for nuclear matter and the electron gas.

5.2 Applications for nuclear matter

A long-standing problem in nuclear physics [10, 20, 23, 26, 27, 48, 58, 84] has been to properly model the nuclear-matter equation of state, starting from a realistic nuclear interaction model. In this context, an important quantity is the energy per nucleon as a function of the particle density. In this thesis, we assume that the temperature is much smaller than the Fermi temperature, and model the interactions between nucleons using nonrelativistic quantum mechanics. In most many-body quantum approaches, including the CC method, the energy at zero temperature is obtained from the basic formulation of the theory. In principle, it should therefore be possible to calculate the energy per particles using the CC approach, and thereby get essential input to the nuclear-matter equation of state.

More than thirty years ago, Day and Zabolitzky studied the nuclear-matter equation of state [108] using the Bochum truncation [107] of CC theory. Day and Zabolitzky did calculations including reduced two- and three-particle subsystem amplitudes, as well as an estimate of the four-particle amplitude. One aim of this thesis has been to take up again the work on coupled-cluster theory for nuclear matter, now using the n-particle-n-hole truncation scheme explained in Sec. 5.1 together with modern nuclear interaction models. The latter truncation scheme has been successfully applied to finite nuclei, and it is therefore of interest to extend the method to the limit of infinitely many nucleons. In the next subsection, we give an introduction to Ref. [109], where we have done CC calculations for nuclear matter at the thermodynamic limit. The results of Ref. [109] have also been used to validate the CC method used in Ref. [], where the infinite system was modelled using finite-size boxes with twisted-angle boundary conditions.

5.2.1 Coupled-cluster ladder approximation in three dimensions

As a first step towards new and improved CC calculations for nuclear matter, we have approximated the CCD amplitude equations (5.15) by including only particle-particle ladder diagrams, which are necessary to properly treat the short-range correlations between nucleons [42, 58], and hole-hole ladder diagrams, which constitute the symmetric counterpart for hole states. Our work has been described in detail in Ref. [109], and we here only give a brief introduction.

In Chapter 4, we explained how the BHF equations are commonly simplified using an angular-average approximation of the Pauli exclusion operators (3.31) and (3.32). The angular-average approximation, defined by Eqs. (4.35) and (4.36), is obtained by replacing the exact Pauli operators with averages integrated over the angle between the relative and CM momentum vectors. This approximation makes the BHF equations considerably simpler, as the G matrix becomes diagonal in the total angular momentum $\mathcal{J}$ and its projection $m_{\mathcal{J}}$ [90]. As shown in Refs. [88, 90], the error in the BHF binding energy introduced by using angular-averaged Pauli exclusion operators is of the order $0.2 - 0.5$ MeV.

Suzuki *et al.* [90] have suggested an approach to expand the exact Pauli operators of the BHF equations in partial waves. In Ref. [109], we derive explicit expressions for the CC ladder equations using the same technique. When using exact Pauli operators, the CC ladder equations become complex, and storage of the amplitude matrix requires a huge amount of memory. To make the computations manageable, we simplify the amplitude matrix by inferring an angular-average approximation of the momentum arguments in the single-particle energies, as shown in Eqs. (4.39), (4.47) and (4.48). When using these approximated single-particle energies, the amplitude matrix gets a symmetry that makes it possible to evaluate the matrix elements for only one direction of the CM momentum vector, and then use a rotation matrix to obtain matrix elements for other CM momentum directions [90, 109]. Using the rotation matrix, we are therfore able to decrease the size of the amplitude matrix further. The angular-average approximation in the single-particle energies also opens the possibility to use simplified formulae for the exact Pauli operators, as introduced by Suzuki *et al.* [90].

Taken that convergence is obtained in the number of momentum grid points, the only approximations of the CC ladder equations in Ref. [109] are the angular-average approximation in the single-particle potential and a finite cutoff in angular momentum. As seen from Fig. 6 of Ref. [109], the error owing to the cutoff in angular momentum is smaller than approximately

$0.2-0.3$ MeV. We have not been able to directly quantify the error related to the angular-average approximation in the single-particle potentials. However, in Ref. [] we show that a CC ladder approximation with a finite number of particles in a box and twisted-averaged boundary conitions gives energies within $0.1-0.2$ MeV from the ladder approximation described above. The good agreement between these two quite different approches indicates that the error owing to the angular-averaged single-particle potentials is small.

In Ref. [109] we also compare CC ladder approximations with exact and angular-averaged Pauli exclusion operators. Using exact Pauli operators, we get energies that are at most about 0.2 MeV from the energies obtained using angular-averaged Pauli operators. Similarly as observed in the BHF method [88, 90], exact treatment of the Pauli exclusion operators gives more binding for symmetric nuclear matter. In pure neutron matter, we find that the angular-average approximation of Pauli operators has a much smaller effect on the binding energy.

- Figure: MBPT(2) with exact and angular-averaged Pauli operators

5.2.2 Problems with particle-hole diagrams

In three-dimensional nuclear matter, the CC $\hat{T}_2$ amplitude is a function of four three-dimensional momentum vectors. One vector can be removed owing to momentum conservation, but still the size of the $\hat{T}_2$ amplitude matrix may become very large. The realistic two-particle nuclear interactions we use are given in a coupled angluar-momentum basis with relative momentum coordinates. We have therefore chosen to transform the CC equations to the coupled angular-momentum and relative momentum basis, given in Eq. (3.33). As discussed in the previous subsection, the partial-wave expanded CC ladder equations may be considerably simplified using angular-averaged single-particle potentials. In this approximation, the size of the amplitude matrix decreases by two dimensions. Unfortunately, as we show in the following, the complete CCD equations become considerably more complicated in the partial-wave basis.

In the following, we repeat parts of the theory explained in Ref. [109], but we extend the discussion to include terms that are negelcted in the article. For simplicity, let us for a moment consider only those terms in the the CCD $\hat{T}_2$ amplitude equation (5.15) that are linear in the CC amplitude. Using integrals at the limit when the box size approaches infinity, as in Eq. (3.26),

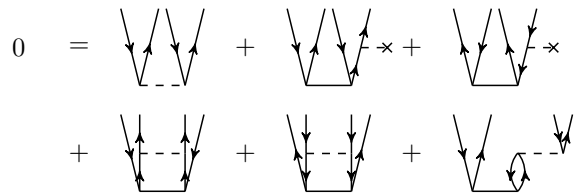

Figure 5.3: Diagrams of the CCD $\hat{T}_2$ amplitude equation that are linear in the CC amplitude (Illustration by the author). The complete figure with all diagrams is given in Ref. [109].

the linear part of the amplitude equation becomes

$$
\begin{aligned}
0 &= \langle \mathbf{k}_a \mathbf{k}_b | \hat{v} | \mathbf{k}_i \mathbf{k}_j \rangle_{AS} \\
&+ \left(\varepsilon(\mathbf{k}_a) + \varepsilon(\mathbf{k}_b) - \varepsilon(\mathbf{k}_i) - \varepsilon(\mathbf{k}_j) \right) \langle \mathbf{k}_a \mathbf{k}_b | \hat{t} | \mathbf{k}_i \mathbf{k}_j \rangle \\
&+ \frac{1}{2} \left(\frac{L}{2\pi} \right)^6 \int d\mathbf{k}_k \int d\mathbf{k}_l \langle \mathbf{k}_a \mathbf{k}_b | \hat{t} | \mathbf{k}_k \mathbf{k}_l \rangle \langle \mathbf{k}_k \mathbf{k}_l | \hat{v} | \mathbf{k}_i \mathbf{k}_j \rangle_{AS} \\
&\times \theta(k_F - |\mathbf{k}_k|) \theta(k_F - |\mathbf{k}_l|) \\
&+ \frac{1}{2} \left(\frac{L}{2\pi} \right)^6 \int d\mathbf{k}_c \int d\mathbf{k}_d \langle \mathbf{k}_a \mathbf{k}_b | \hat{v} | \mathbf{k}_c \mathbf{k}_d \rangle_{AS} \langle \mathbf{k}_c \mathbf{k}_d | \hat{t} | \mathbf{k}_i \mathbf{k}_j \rangle \\
&\times \theta(|\mathbf{k}_c| - k_F) \theta(|\mathbf{k}_d| - k_F) \\
&+ \hat{P}(\mathbf{k}_i, \mathbf{k}_j) \hat{P}(\mathbf{k}_a, \mathbf{k}_b) \left(\frac{L}{2\pi} \right)^6 \int d\mathbf{k}_k \int d\mathbf{k}_c \langle \mathbf{k}_a \mathbf{k}_c | \hat{t} | \mathbf{k}_i \mathbf{k}_k \rangle \\
&\times \langle \mathbf{k}_k \mathbf{k}_b | \hat{v} | \mathbf{k}_c \mathbf{k}_j \rangle_{AS} \theta(k_F - |\mathbf{k}_k|) \theta(|\mathbf{k}_c| - k_F),
\end{aligned}
\tag{5.17}
$$

where $\theta(x)$ is the Heaviside step function. In Eq. (5.17) we have used the definition $\varepsilon(\mathbf{k}) \equiv \langle \mathbf{k} | f | \mathbf{k} \rangle$. The term on the third and fourth lines of Eq. (5.17) has summation over two hole states. The correponding diagram is the one in the middle on the second row of Fig. 5.3. Let us call this term the hole-hole ladder (HHLAD) diagram, because the term generates diagrams similar to the hole-hole ladders in many-body perturbation theory [110]. In the same way, there is a summation over two particle states in the term on the fifth and sixth lines of Eq. (5.17). The corresponding diagram is given on the second row at left of Fig. 5.3. This term generates diagrams similar to the particle-particle ladders encountered in many-body perturbation theory [110], and therefore we call the term the particle-particle ladder (PPLAD) diagram. In the last term of Eq. (5.17), there is a summation over one hole and one particle state. The corresponding diagram is the last one in Fig. 5.3. Let us call this term the particle-hole (PH) diagram.

Similarly as in Ref. [109], we write the linear part of the CCD amplitude

equation in RCM coordinates, but including here also the PH term. The amplitude equation becomes

$$
\begin{aligned}
0 &= \langle \mathbf{k}'|\hat{v}|\mathbf{k}\rangle_{AS} + (\varepsilon(|\mathbf{k}'+\mathbf{K}/2|) + \varepsilon(|-\mathbf{k}'+\mathbf{K}/2|) \\
&\quad -\varepsilon(|\mathbf{k}+\mathbf{K}/2|) - \varepsilon(|-\mathbf{k}+\mathbf{K}/2|))\,\langle \mathbf{k}'|\hat{t}|\mathbf{k}\rangle \\
&\quad + \frac{1}{2}\int d\mathbf{h}\langle \mathbf{k}'|t(\mathbf{K})|\mathbf{h}\rangle\langle \mathbf{h}|\hat{v}|\mathbf{k}\rangle_{AS} \\
&\quad \times \theta(k_F - |\mathbf{h}+\mathbf{K}/2|)\theta(k_F - |-\mathbf{h}+\mathbf{K}/2|) \\
&\quad + \frac{1}{2}\int d\mathbf{p}\langle \mathbf{k}'|\hat{v}|\mathbf{p}\rangle_{AS}\langle \mathbf{p}|\hat{t}|\mathbf{k}\rangle \\
&\quad \times \theta(|\mathbf{p}+\mathbf{K}/2| - k_F)\theta(|-\mathbf{p}+\mathbf{K}/2| - k_F) \\
&\quad + \int d\mathbf{B}\langle \mathbf{B}/4 + 3\mathbf{k}'/4 - \mathbf{k}/4 - \mathbf{K}/4|\hat{v}|\mathbf{B}/4 - \mathbf{k}'/4 + 3\mathbf{k}/4 - \mathbf{K}/4\rangle_{AS} \\
&\quad \times \langle -\mathbf{B}/4 + 3\mathbf{k}'/4 - \mathbf{k}/4 + \mathbf{K}/4|\hat{t}|\mathbf{B}/4 + 3\mathbf{k}/4 - \mathbf{k}'/4 + \mathbf{K}/4\rangle \\
&\quad \times \theta(k_F - |\mathbf{B}/2 + (\mathbf{k}'-\mathbf{k})/2|)\theta(|\mathbf{B}/2 - (\mathbf{k}'-\mathbf{k})/2| - k_F) \\
&\quad + \ldots,
\end{aligned}
\tag{5.18}
$$

where the last term is the unpermuted particle-hole part. Here we have used the definitions

$$
\mathbf{h} = (\mathbf{k}_k - \mathbf{k}_l)/2, \qquad \mathbf{p} = (\mathbf{k}_c - \mathbf{k}_d)/2, \tag{5.19}
$$

and the relative momentum vectors $\mathbf{k}$, $\mathbf{k}'$ and CM momentum vector $\mathbf{K}$ are defined in Eq. (3.30).

In Ref. [109] we wrote the amplitude equation into such a form that both the interaction and the CC amplitude were given in a coupled angular momentum and relative momentum basis

$$
|k\mathcal{J}m_{\mathcal{J}}(lS)M_T\rangle, \tag{5.20}
$$

where $k \equiv |\mathbf{k}|$ is the length of a relative momentum vector $\mathbf{k}$, l is the orbital angular momentum related to $\mathbf{k}$, S is the total two-particle spin, $\mathcal{J}$ is equal to the total angular momentum $l+S$, $m_{\mathcal{J}}$ is the z projection of $\mathcal{J}$, and M_T is the projection of the total two-particle isospin.

Let us now consider the simpler linear equation in which the PH diagrams are negelcted, as was done in Ref. [109]. When using an angular-average approximation for the inputs in the single-particle potentials $\varepsilon(|\mathbf{p}|)$ of the amplitude equation, all the vectors $|\mathbf{k}\rangle$, $|\mathbf{k}'\rangle$, and their conjugates can simply be replaced with vectors as in Eq. (5.20). The resulting CC amplitude

equation is of the form

$$\begin{aligned}
&\Delta\tilde{\varepsilon}(k,k',K)\langle k'\mathcal{J}'m_{\mathcal{J}'}(l'S)M_T|\hat{t}(K)|k\mathcal{J}m_{\mathcal{J}}(lS)M_T\rangle \\
&= \langle k'\mathcal{J}'m_{\mathcal{J}'}(l'S)M_T|\hat{v}|k\mathcal{J}m_{\mathcal{J}}(lS)M_T\rangle\delta_{\mathcal{J}\mathcal{J}'}\delta_{m_{\mathcal{J}}m_{\mathcal{J}'}} \\
&+ \frac{1}{2}\sum_{\mathcal{J}''m_{\mathcal{J}''}}\sum_{l''l'''}\int_0^{k_F} h^2dh \\
&\times \langle k'\mathcal{J}'m_{\mathcal{J}'}(l'S)M_T|\hat{t}(K)|h\mathcal{J}''m_{\mathcal{J}''}(l''S)M_T\rangle \\
&\times \langle h\mathcal{J}m_{\mathcal{J}}(l'''S)M_T|\hat{v}|k\mathcal{J}m_{\mathcal{J}}(lS)M_T\rangle \\
&\times Q_{hh}(l''\mathcal{J}''m_{\mathcal{J}''},l'''\mathcal{J}m_{\mathcal{J}};SM_ThK\theta_K\phi_K) \\
&+ \frac{1}{2}\sum_{\mathcal{J}''m_{\mathcal{J}''}}\sum_{l''l'''}\int_0^{\infty} p^2dp \\
&\times \langle k'\mathcal{J}'m_{\mathcal{J}'}(l'S)M_T|\hat{v}|p\mathcal{J}'m_{\mathcal{J}'}(l''S)M_T\rangle \\
&\times \langle p\mathcal{J}''m_{\mathcal{J}''}(l'''S)M_T|\hat{t}(K)|k\mathcal{J}m_{\mathcal{J}}(lS)M_T\rangle \\
&\times Q_{pp}(l''\mathcal{J}'m_{\mathcal{J}'},l'''\mathcal{J}''m_{\mathcal{J}''};SM_TpK\theta_K\phi_K), \qquad (5.21)
\end{aligned}$$

where the Pauli operators Q_{hh} and Q_{pp} and the function $\tilde{\varepsilon}(k,k',K)$ are defined in Ref. [109]. In the expression above, we have used a technique introduced by Suzuki *et al* [90]. Unfortunately, the PH terms in Eq. 5.18 have complicated dependencies on the angular parts of $\mathbf{k}$ and $\mathbf{k}'$. When including the PH term, the angular parts of $\mathbf{k}$ and $\mathbf{k}'$ can therefore no longer be separated out in a simple way. Because of this problem, we have omitted the PH diagrams from our CC amplitude equation in Ref. [109].

An advantage with using partial waves is that the CC amplitude matrix can be calculated for only one direction of the CM momentum vector $\mathbf{K}$, for example only vectors $\mathbf{K} = (0,0,K)$, and then the matrix elements for other directions can be obtained by using rotation matrices. In Ref. [109], the CC $\hat{T}_2$ amplitude matrix was rotated as

$$\begin{aligned}
&\langle k'\mathcal{J}'m_{\mathcal{J}'}(l'S)|\hat{t}(\mathbf{K})|k\mathcal{J}m_{\mathcal{J}}(lS)\rangle \\
&= \sum_{m_{\mathcal{J}'''}m_{\mathcal{J}''}} D^{\mathcal{J}'}_{m_{\mathcal{J}'}m_{\mathcal{J}'''}}(\phi_K,\theta_K,0)D^{\mathcal{J}^*}_{m_{\mathcal{J}}m_{\mathcal{J}''}}(\phi_K,\theta_K,0) \\
&\times \langle k'\mathcal{J}'m_{\mathcal{J}'''}(l'S)|\hat{t}(K)|k\mathcal{J}m_{\mathcal{J}''}(lS)\rangle, \qquad (5.22)
\end{aligned}$$

where $D^{\mathcal{J}}_{m_{\mathcal{J}}m_{\mathcal{J}'}}(\phi,\theta,\sigma)$ is a rotation matrix defined by Varshalovich *et al* [159]. It is possible to solve the amplitude equation using three-dimensional momentum vectors, but then we loose the rotational symmetry of the CC amplitude matrix. Consequently, the CC amplitude matrix needs two degrees more of freedom, which increases the demand for computer memory.

- How recoupling can be done. What problems arise?

5.2.3 Implementations

Let us discuss the implementation of the CC ladder equations with exact Pauli operators, given as Eqs. (18) and (23) in Paper II. The ladder equations using angular-averaged Pauli operators may be implemented in a similar way. As stated above, the nuclear interaction is diagonal in the total two-particle spin S, in the isospin projection M_T, and in the total relative angular momentum $\mathcal{J}$. Because of this symmetry, we store the interaction matrices in blocks of the conserved quantum numbers. Utilization of block diagonality decreases the memory consumption significantly, and it can also reduce the number of floating-point operations greatly. However, as shown in Paper II, the Pauli exclusion operators and the t-amplitude matrix are not diagonal in $\mathcal{J}$ and its projection $m_{\mathcal{J}}$. Furthermore, these matrices depend on the radial CM momentum K, and the Pauli operators are also functions of the angle θ_K related to the CM momentum.

The CC energy equation (18) of Paper II may be written as

$$\begin{aligned}\Delta E_{CCD}/A = \text{Constant} \times & \sum_{SM_T} \sum_{\mathcal{J}m_{\mathcal{J}}} \sum_{\mathcal{J}''m_{\mathcal{J}''}} \sum_{\mathcal{J}'''m_{\mathcal{J}'''}} \sum_{m_{\mathcal{J}'}} \\ \times \sum_{K_i} K_i^2 \omega_{K_i} & \sum_{\theta_j} \sin\theta_j \omega_{\theta_j} d^{\mathcal{J}''}_{m_{\mathcal{J}''}m_{\mathcal{J}'}}(\theta_j) d^{\mathcal{J}'''}_{m_{\mathcal{J}'''}m_{\mathcal{J}'}}(\theta_j) \\ \times \text{Tr}\left[\mathbf{V}^{SM_T\mathcal{J}} \mathbf{Q}_{pp}^{SM_TK_i\mathcal{J}m_{\mathcal{J}}\mathcal{J}''m_{\mathcal{J}''}\theta_j} \mathbf{T}^{SM_TK_i\mathcal{J}''m_{\mathcal{J}'}\mathcal{J}'''} \mathbf{Q}_{hh}^{SM_TK_i\mathcal{J}'''m_{\mathcal{J}'''}\mathcal{J}m_{\mathcal{J}}\theta_j}\right],\end{aligned} \tag{5.23}$$

where the two-body interaction, the Pauli operators and the t amplitude are expressed as matrices. Here K_i and θ_j are radial and angular coordinates of the CM momentum, ω_{K_i} and ω_{θ_j} are the corresponding quadrature weights, and the function d is part of the Wigner D function, as defined in Refs. [109, 159]. Using the relation

$$\text{Tr}\left[\mathbf{AB}\right] = \text{Tr}\left[\mathbf{BA}\right] \tag{5.24}$$

for the trace of a matrix-matrix product, we can replace the trace in Eq. (5.23) by

$$\text{Tr}\left[\mathbf{M}^{SM_TK_i\mathcal{J}m_{\mathcal{J}}\mathcal{J}''m_{\mathcal{J}''}\mathcal{J}'''m_{\mathcal{J}'''}\theta_j} \mathbf{T}^{SM_TK_i\mathcal{J}''m_{\mathcal{J}'}\mathcal{J}'''}\right], \tag{5.25}$$

where

$$\mathbf{M}^{SM_TK_i\mathcal{J}m_{\mathcal{J}}\mathcal{J}''m_{\mathcal{J}''}\mathcal{J}'''m_{\mathcal{J}'''}\theta_j} = \mathbf{Q}_{hh}^{SM_TK_i\mathcal{J}'''m_{\mathcal{J}'''}\mathcal{J}m_{\mathcal{J}}} \mathbf{V}^{SM_T\mathcal{J}} \mathbf{Q}_{pp}^{SM_TK_i\mathcal{J}m_{\mathcal{J}}\mathcal{J}''m_{\mathcal{J}''}\theta_j}. \tag{5.26}$$

The matrix $\mathbf{M}$ does not change during the CC self-consistency loop, and is therefore set up only once at the beginning of the calculations. The trace is evaluated as

$$\mathrm{Tr}\left[\mathbf{MT}\right] = \sum_{\alpha}\left(\sum_{\beta} M_{\alpha\beta}T_{\beta\alpha}\right), \tag{5.27}$$

and a matrix-matrix multiplication is therfore not necessary. If the dimension of $\mathbf{T}$ is $m \times n$, the simplification in Eq. (5.27) reduces the number of floating-point operations from m^2n^2 to mn [180].

We further simplify the CC energy equation and write it as

$$\begin{aligned}\Delta E_{CCD}/A = \text{Constant} \times & \sum_{K_i}\sum_{SM_T}\sum_{\mathcal{J}''m_{\mathcal{J}'}}\sum_{\mathcal{J}'''} \\ & \times \sum_{\alpha}\left(\sum_{\beta}\tilde{T}_{\alpha\beta}^{SM_TK_i\mathcal{J}''m_{\mathcal{J}'}\mathcal{J}'''}O_{\beta\alpha}^{SM_TK_i\mathcal{J}''m_{\mathcal{J}'}\mathcal{J}'''}\right),\end{aligned} \tag{5.28}$$

where the matrix elements $\tilde{T}_{\alpha\beta}$ are defined as

$$\tilde{T}_{\alpha\beta}^{SM_TK_i\mathcal{J}''m_{\mathcal{J}'}\mathcal{J}'''} = T_{\alpha\beta}^{SM_TK_i\mathcal{J}''m_{\mathcal{J}'}\mathcal{J}'''}/\Delta\tilde{\varepsilon}(k_\alpha, k_\beta, K_i), \tag{5.29}$$

that is, the t amplitude divided by the energy denominator. The matrix $\mathbf{O}$ is defined such that

$$\mathbf{O}^{SM_TK_i\mathcal{J}''m_{\mathcal{J}'}\mathcal{J}'''} = \sum_{\mathcal{J}m_{\mathcal{J}}}\sum_{m_{\mathcal{J}''}m_{\mathcal{J}'''}}\sum_{\theta_j}\mathbf{N}^{(SM_TK_i\mathcal{J}''m_{\mathcal{J}'}\mathcal{J}''')(\mathcal{J}m_{\mathcal{J}}m_{\mathcal{J}''}m_{\mathcal{J}'''}\theta_j)}, \tag{5.30}$$

where

$$\begin{aligned}&\mathbf{N}^{(SM_TK_i\mathcal{J}''m_{\mathcal{J}'}\mathcal{J}''')(\mathcal{J}m_{\mathcal{J}}m_{\mathcal{J}''}m_{\mathcal{J}'''}\theta_j)} \\ &= K_i^2\omega_{K_i}\sin\theta_j\omega_{\theta_j}d^{\mathcal{J}''}_{m_{\mathcal{J}''}m_{\mathcal{J}'}}(\theta_j)d^{\mathcal{J}'''}_{m_{\mathcal{J}'''}m_{\mathcal{J}'}}(\theta_j) \\ &\times \mathbf{M}^{SM_TK_i\mathcal{J}m_{\mathcal{J}}\mathcal{J}''m_{\mathcal{J}''}\mathcal{J}'''m_{\mathcal{J}'''}\theta_j}.\end{aligned} \tag{5.31}$$

Similarly as for the energy equation, we write the amplitude equation as

$$\begin{aligned}\mathbf{T}^{SM_TK_i\mathcal{J}'m_{\mathcal{J}}\mathcal{J}} &= \mathbf{V}^{SM_T\mathcal{J}}\delta_{\mathcal{J}\mathcal{J}'} \\ &+ \frac{1}{2}\sum_{\mathcal{J}''}\tilde{\mathbf{T}}^{SM_TK_i\mathcal{J}'m_{\mathcal{J}}\mathcal{J}''}\mathbf{W}^{SM_TK_i\mathcal{J}''m_{\mathcal{J}}\mathcal{J}} \\ &+ \frac{1}{2}\sum_{\mathcal{J}''}\mathbf{U}^{SM_TK_i\mathcal{J}'m_{\mathcal{J}}\mathcal{J}''}\tilde{\mathbf{T}}^{SM_TK_i\mathcal{J}''m_{\mathcal{J}}\mathcal{J}},\end{aligned} \tag{5.32}$$

where we have used the definitions

$$\mathbf{W}^{SM_TK_i\mathcal{J}''m_{\mathcal{J}}\mathcal{J}} = \mathbf{Q}_{hh}^{SM_TK_i\mathcal{J}''m_{\mathcal{J}}\mathcal{J}m_{\mathcal{J}}}\mathbf{V}^{SM_T\mathcal{J}} \tag{5.33}$$

and

$$\mathbf{U}^{SM_TK_i\mathcal{J}'m_{\mathcal{J}}\mathcal{J}''} = \mathbf{V}^{SM_T\mathcal{J}'}\mathbf{Q}_{pp}^{SM_TK_i\mathcal{J}'m_{\mathcal{J}}\mathcal{J}''m_{\mathcal{J}}}. \tag{5.34}$$

The different matrices are stored in lists of matrices, where the list index is determined by the superscript quantum numbers. For example, the matrices $\mathbf{O}^{SM_TK_i\mathcal{J}''m_{\mathcal{J}'}\mathcal{J}'''}$ are stored as elements in a list in which the quantum numbers S, M_T, K_i, $\mathcal{J}''$, $m_{\mathcal{J}'}$, and $\mathcal{J}'''$ determine the location. To obtain sufficient accuarcy, the grid in relative momentum must be set up such that the total interval is split at the points where the derivatives of the Pauli operators are discontinuous. In our numerical integrations, we use Gauss-Legendre quadratures [165].

In our calculations, we set up the matrices $\mathbf{O}$, $\mathbf{W}$, and $\mathbf{U}$ only once, and then we use Eqs. (5.28) and (5.32) to evaluate the energy in each iteration of the CC self-consistency loop. In large calculations, most of the computing time is used to set up the matrix $\mathbf{O}$. By setting up this matrix only once, the computing time of a typical symmetric-nuclear-matter calculation therefore decreases by approximately a factor of ten. To utilize the computing power of large computing clusters, we have parallelized the code using both the Message Passing Interface (MPI) Standard [181, 182] and OpenMP [183]. MPI is a standard for parallelization that is designed to work on computers with distributed memory. Therefore, we use MPI to share work load between different computing nodes on a supercomputer. We split the CC ladder equations into parts corresponding to different CM momentum values K_i, and distribute these parts to different MPI processes. As mentioned above, most of the computing time is used to set up the matrix $\mathbf{O}$. The code can therefore be further optimized by parallelizing the setup of $\mathbf{O}$ on each computing node. In our program, we use OpenMP to parallelize the setup of the matrices $\mathbf{O}^{SM_TK_i\mathcal{J}''m_{\mathcal{J}'}\mathcal{J}'''}$ on the different computing nodes.

- Other optimizations

5.2.4 Other approaches to CCSD in three dimensions

As discussed in the previous subsection, the CCSD amplitude equations become very complicated in the partial-wave expansion using RCM coordinates. In Paper III, a cartesian momentum basis was successfully applied to nuclear-mattter systems. We have studied two other approches to implementing coupled-cluster theory for infinite matter. In these approaches, the

interaction matrix elements are transformed from the relative partial-wave basis (3.33) to a single-particle basis in laboratory coordinates. Once the interaction matrix elements have been transformed to a laboratory frame basis, it is straightforward to derive and implement explicit coupled-cluster equations.

A seemingly appealing approach is to transform the interaction matrix to the laboratory frame single-particle basis

$$|k_p j_p m_{j_p} l_p s_p m_{t_p}\rangle, \tag{5.35}$$

where k_p is the laboratory momentum, l_p is the orbital angular momentum, s_p is the spin, j_p is the angular momentum, m_{j_p} is the z projection of j_p, and m_{t_p} is the isospin projection. G. Hagen *et al.* have shown [184] how more efficient coupled-cluster implementations can be obtained by coupling single-particle angular momenta j_p and j_q to a total angular momentum J. This kind of angular momentum coupling is possible because the nuclear interaction is rotationally invariant [185] and therefore conserves the total momentum. We would therefore like to write the two-nucleon states in the basis

$$|k_p j_p l_p, k_q j_q l_q; J m_{t_p} m_{t_q}\rangle, \tag{5.36}$$

where the single-particle angular momenta j_p and j_q have been coupled to a total angular momentum.

We now show how the interaction matrix elements can be transformed to the basis (5.36). Assume for a while that we have the continuous plane wave basis

$$\psi_{\mathbf{k}}(\mathbf{x}) = \frac{1}{(2\pi)^{3/2}} e^{i\mathbf{k}\cdot\mathbf{x}}, \tag{5.37}$$

instead of the discrete box potential plane wave basis of Eq. (3.19). A bra vector $\langle \mathbf{k}_p \mathbf{k}_q|$ can be expanded as [186]

$$\begin{aligned}
\langle \mathbf{k}_p \mathbf{k}_q| &= \langle \mathbf{k}_p \mathbf{k}_q| \left(\sum_{l_p m_{l_p}} \sum_{l_q m_{l_q}} |l_p m_{l_p} l_q m_{l_q}\rangle\langle l_p m_{l_p} l_q m_{l_q}| \right) \\
&= \langle \mathbf{k}_p \mathbf{k}_q| \sum_{l_p m_{l_p}} \sum_{l_q m_{l_q}} |l_p m_{l_p} l_q m_{l_q}\rangle \\
&\times \left(\sum_{\lambda\mu} \langle l_p m_{l_p} l_q m_{l_q}|\lambda\mu\rangle\langle\lambda\mu l_p l_q| \right) \\
&= \sum_{l_p l_q \lambda\mu} \langle k_p l_p k_q l_q, \lambda\mu| \left[Y_{l_p m_{l_p}}(\hat{\mathbf{k}}_p) Y_{l_q m_{l_q}}(\hat{\mathbf{k}}_q) \right]_{\lambda m_\lambda},
\end{aligned} \tag{5.38}$$

where the functions $Y_{lm_l}(\hat{\mathbf{k}}) \equiv \langle \hat{\mathbf{k}} | lm_l \rangle$ are spherical harmonics, the bracket denotes a Clebsch-Gordan coefficient [159], l_p and l_q are orbital angular momenta of the two particles, λ is the total orbital angular momentum, and m_λ its projection in the z direction. In Eq. (5.38) the square brackets represent coupling of orbital angular momenta, as in Eq. (3.41). We define the radial states with the normalization condition

$$\langle klm_l | k'l'm_{l'} \rangle = \frac{1}{kk'} \delta(k - k') \delta_{ll'} \delta_{m_l m_{l'}}, \tag{5.39}$$

and Eq. (5.38) differs therefore from the expression in Ref. [186] by a factor $(k_p k_q)^{-1}$. When projecting to the real space, we get [156]

$$\varphi_{klm_l}(\mathbf{r}) \equiv \langle \mathbf{r} | klm_l \rangle = j_l(kr) Y_{lm_l}(\theta_r, \phi_r), \tag{5.40}$$

where $j_l(x)$ is spherical Bessel function. Observe that continuous momentum variables gives a Dirac delta distribution in the normalization expression.

Radial ket vectors can be transformed between the laboratory and RCM coordinate systems using the relation [186]

$$|k_p l_p k_q l_q, \lambda m_\lambda\rangle = \int k^2 dk \int K^2 dK \sum_{lL} |klKL, \lambda m_\lambda\rangle \langle klKL, \lambda | k_p l_p k_q l_q, \lambda\rangle, \tag{5.41}$$

where k and K are radial coordinates of relative and CM momenta, respectively, l and L are corresponding orbtial angular momenta, and the coefficient denoted by a bracket is called a vector bracket [186,187]. The vector bracket can be written as

$$\langle klKL, \lambda | k_p l_p k_q l_q, \lambda\rangle = (4\pi)^2 \, \delta(u) \theta(1 - v^2) A(v), \tag{5.42}$$

where

$$\begin{aligned} A(v) = \frac{1}{(2\lambda + 1)} \frac{1}{k_p k_q k K} \sum_{m_\lambda} & \left[Y_{lm_l}(\hat{\mathbf{k}}) \times Y_{LM_L}(\hat{\mathbf{K}}) \right]^*_{\lambda m_\lambda} \\ & \times \left[Y_{l_p m_{l_p}}(\hat{\mathbf{k}}_p) \times Y_{l_q m_{l_q}}(\hat{\mathbf{k}}_q) \right]_{\lambda m_\lambda}, \end{aligned} \tag{5.43}$$

as formulated by Balian and Brezin [186,188], and

$$u = k^2 + \frac{1}{4} K^2 - \frac{1}{2}(k_p^2 + k_q^2), \tag{5.44}$$

$$v = \frac{1}{kK} \left(k_p^2 - k^2 - \frac{1}{4} K^2 \right). \tag{5.45}$$

The delta distribution ensures that kinetic energy is conserved in the transformation between coordinate systems. The variable v may also be written as

$$v = \cos(\theta_{\mathbf{kK}}),$$

where $\theta_{\mathbf{kK}}$ is the angle between the relative and CM momentum vectors $\mathbf{k}$ and $\mathbf{K}$. The step funtion $\theta(1-v^2)$ therefore gives the geometric restriction $|\cos(\theta_{\mathbf{kK}})| \leq 1$.

We want to write a vector $|(k_p l_p j_p)(k_p l_p j_p)(JM_J)\rangle$ as a linear combination of vectors $|klKL(\mathcal{J})SJM_J\rangle$. This transformation has been given in, for example, Refs. [187, 189]. In the following, we sketch a derivation of the transformation between the two bases. The derivation is done in several steps. First we do a recoupling from the j–j scheme to the L–S scheme, as in Eq. (4.13) of Ref. [190]. Further, we do the recoupling $JM_J\lambda S \longrightarrow \lambda\mu SM_S$, and get

$$|(k_p l_p j_p)(k_q l_q j_q)(JM_J)\rangle = \sum_{\lambda m_\lambda}\sum_{SM_S} \hat{j}_p\hat{j}_q\hat{\lambda}\hat{S} \begin{Bmatrix} l_p & \frac{1}{2} & j_p \\ l_q & \frac{1}{2} & j_q \\ \lambda & S & J \end{Bmatrix} \times \langle \lambda m_\lambda SM_S|JM_J\rangle |k_p l_p k_q l_q, \lambda m_\lambda\rangle |SM_S\rangle, \quad (5.46)$$

where we have used the definition $\hat{x} = \sqrt{2x+1}$. If we now use the laboratory to RCM transformation (5.41), do the recoupling $\lambda m_\lambda SM_S \longrightarrow JM_J\lambda S$, and use the $9j$ coefficient relation (A4.27) in Ref. [190], we get

$$|(k_p l_p j_p)(k_q l_q j_q)(JM_J)\rangle = \sum_{\lambda S}\sum_{lL}\int k^2dk \int K^2dK \hat{j}_p\hat{j}_q\hat{\lambda}\hat{S} \begin{Bmatrix} l_p & l_q & \lambda \\ \frac{1}{2} & \frac{1}{2} & S \\ j_p & j_q & J \end{Bmatrix} \times \langle klKL, \lambda|k_p l_p k_q l_q, \lambda\rangle |klKL(\lambda)SJM_J\rangle. \quad (5.47)$$

To get the desired basis on the right-hand side, we must further do the recoupling of three angular momenta $lL(\lambda)SJM_J \longrightarrow lL(\mathcal{J})SJM_J$, diagrammatically sketched as [190]

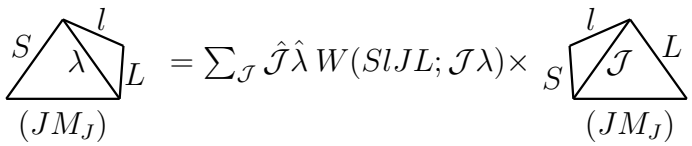

where $W(SlJL;\mathcal{J}\lambda)$ is a Racah coefficient [159, 191]. When we apply this

recoupling, we get the expression

$$|(k_p l_p j_p)(k_q l_q j_q)(JM_J)\rangle = \sum_{\lambda S}\sum_{lL}\sum_{\mathcal{J}} \int k^2 dk \int K^2 dK \hat{j}_p \hat{j}_q \hat{\lambda}^2 \hat{S}\hat{\mathcal{J}} \times \begin{Bmatrix} l_p & l_q & \lambda \\ \frac{1}{2} & \frac{1}{2} & S \\ j_p & j_q & J \end{Bmatrix} \langle klKL, \lambda | k_p l_p k_q l_q, \lambda\rangle \times W(LlJS;\lambda\mathcal{J}) |klKL(\mathcal{J})SJM_J\rangle. \quad (5.48)$$

Here we have used some symmtry relations for Racah coefficients. If we now use the relation between Racah coefficients and $6j$ symbols, and include the isospin degree of freedom, we obtain

$$|(k_p l_p j_p)(k_q l_q j_q)(JM_J m_{t_p} m_{t_q})\rangle = \sum_{\lambda S}\sum_{lL}\sum_{\mathcal{J}} \int k^2 dk \int K^2 dK \, \hat{j}_p \hat{j}_q \hat{\lambda}^2 \hat{S}\hat{\mathcal{J}} \times (-1)^{L+l+J+S} \begin{Bmatrix} l_p & l_q & \lambda \\ \frac{1}{2} & \frac{1}{2} & S \\ j_p & j_q & J \end{Bmatrix} \times \langle klKL, \lambda | k_p l_p k_q l_q, \lambda\rangle \begin{Bmatrix} L & l & \lambda \\ S & J & \mathcal{J} \end{Bmatrix} \times |klKL(\mathcal{J})SJM_J m_{t_p} m_{t_q}\rangle. \quad (5.49)$$

The corresponding antisymmetrized vector is obtained by multiplying the right-hand side of Eq. (5.49) by $\mathcal{A}^{lSM_T}$, where $M_T = m_{t_p} + m_{t_q}$ and the antisymmetrization factor is defined in Eq. (A.5). The transformation in Eq. (5.49) differs from the expressions in Refs. [187, 189] by a phase factor $(-1)^{(J-\lambda)-(\mathcal{J}-l)}$, which is one owing to triangular relations.

Using the transformation (5.49), a two-body interaction matrix element

may now be written as

$$
\begin{aligned}
&\langle k_p l_p j_p k_q l_q j_q JTM_T|V|k_r l_r j_r k_s l_s j_s JTM_T\rangle \\
&\quad = \sum_{lL\lambda S\mathcal{J}} \int_0^\infty k^2 dk \int_0^\infty K^2 dK \left\{ \begin{array}{ccc} l_p & l_q & \lambda \\ \frac{1}{2} & \frac{1}{2} & S \\ j_p & j_q & J \end{array} \right\} \\
&\quad \times (-1)^{\lambda+\mathcal{J}-L-S} \hat{\mathcal{J}}\hat{\lambda}^2 \hat{j}_p \hat{j}_q \hat{S} \left\{ \begin{array}{ccc} L & l & \lambda \\ S & J & \mathcal{J} \end{array} \right\} 4\pi^2 \delta\left(k^2 + \frac{1}{4}K^2 - \frac{1}{2}(k_p^2 + k_q^2)\right) \\
&\quad \times \theta\left(1 - \frac{(k_p^2 - k^2 - \frac{1}{4}K^2)^2}{k^2 K^2}\right) A\left(\frac{k_p^2 - k^2 - \frac{1}{4}K^2}{kK}\right) \\
&\quad \times \sum_{l'\lambda'} \int_0^\infty k'^2 dk' \int_0^\infty K'^2 dK' \left\{ \begin{array}{ccc} l_r & l_s & \lambda' \\ \frac{1}{2} & \frac{1}{2} & S \\ j_p & j_q & J \end{array} \right\} \\
&\quad \times (-1)^{\lambda'+\mathcal{J}-L-S} \hat{\mathcal{J}}\hat{\lambda}'^2 \hat{j}_r \hat{j}_s \hat{S} \left\{ \begin{array}{ccc} L & l' & \lambda' \\ S & J & \mathcal{J} \end{array} \right\} 4\pi^2 \delta\left(k'^2 + \frac{1}{4}K'^2 - \frac{1}{2}(k_r^2 + k_s^2)\right) \\
&\quad \times \theta\left(1 - \frac{(k_r^2 - k'^2 - \frac{1}{4}K'^2)^2}{k'^2 K'^2}\right) A\left(\frac{k_r^2 - k'^2 - \frac{1}{4}K'^2}{k'K'}\right) \\
&\quad \times \langle klKL(\mathcal{J})SJTM_T|V|k'l'K'L(\mathcal{J})SJTM_T\rangle, \qquad (5.50)
\end{aligned}
$$

where the vector brackets are given explicitly using Eq. (5.42). We assume that the antisymmetrization factors are incorporated implicitly in the relative coordinate two-body interaction.

The nuclear interaction is generally diagonal in $\mathcal{J}$, S, M_T, K, L, J, and T, and independent on the latter four. Let us separate the quantum numbers that the interaction is independent on, and use the normalization

$$\langle K|K'\rangle = \delta(K - K')/(KK').$$

After reorganising the different terms, the transformation becomes

$$
\begin{aligned}
&\langle k_p l_p j_p k_q l_q j_q JTM_T|V|k_r l_r j_r k_s l_s j_s JTM_T\rangle \\
&\quad = \left(4\pi^2\right)^2 \sum_{lL\lambda S\mathcal{J}} \sum_{l'\lambda'} (-1)^{\lambda+\lambda'} \hat{\mathcal{J}}^2 \hat{\lambda}^2 \hat{\lambda}'^2 \hat{S}^2 \hat{j}_p \hat{j}_q \hat{j}_r \hat{j}_s \\
&\quad \times \left\{ \begin{array}{ccc} L & l & \lambda \\ S & J & \mathcal{J} \end{array} \right\} \left\{ \begin{array}{ccc} L & l' & \lambda' \\ S & J & \mathcal{J} \end{array} \right\} \left\{ \begin{array}{ccc} l_p & l_q & \lambda \\ \frac{1}{2} & \frac{1}{2} & S \\ j_p & j_q & J \end{array} \right\} \left\{ \begin{array}{ccc} l_r & l_s & \lambda' \\ \frac{1}{2} & \frac{1}{2} & S \\ j_p & j_q & J \end{array} \right\} \\
&\quad \times \int_0^\infty dk' k'^2 \tilde{K} \tilde{k} \langle \tilde{k} l(\mathcal{J}) S M_T|V|k' l'(\mathcal{J}) S M_T\rangle \\
&\quad \times \theta\left(1 - \frac{(k_p^2 - \tilde{k}^2 - \frac{1}{4}\tilde{K}^2)^2}{\tilde{k}^2 \tilde{K}^2}\right) A\left(\frac{k_p^2 - \tilde{k}^2 - \frac{1}{4}\tilde{K}^2}{\tilde{k}\tilde{K}}\right) \\
&\quad \times \theta\left(1 - \frac{(k_r^2 - k'^2 - \frac{1}{4}\tilde{K}^2)^2}{k'^2 \tilde{K}^2}\right) A\left(\frac{k_r^2 - k'^2 - \frac{1}{4}\tilde{K}^2}{k'\tilde{K}}\right),
\end{aligned}
\tag{5.51}
$$

where we have used the definitions

$$
\begin{aligned}
\tilde{K} &= 2\left(\frac{1}{2}\left(k_c^2 + k_d^2\right) - k'^2\right)^{1/2}, \\
\tilde{k} &= \left(\frac{1}{2}\left(k_a^2 + k_b^2 - k_c^2 - k_d^2\right) + k'^2\right)^{1/2}.
\end{aligned}
\tag{5.52}
$$

To remove the Dirac delta distributions, we have defined the new integration variables

$$
\begin{aligned}
s &= \frac{1}{4}K^2 + k^2 - \frac{1}{2}\left(k_p^2 + k_q^2\right), \\
t &= k'^2 + \frac{1}{4}K^2 - \frac{1}{2}\left(k_r^2 + k_s^2\right),
\end{aligned}
\tag{5.53}
$$

and simplified the integral as explained in Appendix B.1.

The reference energy is given algebraically in Eq. (5.11). Next we want to write the reference energy in the coupled partial-wave basis (5.36). A bra vector can be transformed as

$$
\begin{aligned}
&\sum_{m_{s_p} m_{s_q}} \sum_{m_{t_p} m_{t_q}} \langle \mathbf{k}_p \mathbf{k}_q| \langle m_{s_p} m_{s_q}| \langle m_{t_p} m_{t_q}| \\
&\quad = \sum_{\substack{l_p l_q \\ m_{l_p} m_{l_q}}} \sum_{\substack{m_{s_p} m_{s_q} \\ m_{t_p} m_{t_q}}} \sum_{\substack{j_p j_q \\ m_{j_p} m_{j_q}}} \sum_{JM_J} \\
&\quad \times \langle l_p s_p m_{l_p} m_{s_p}|j_p m_{j_p}\rangle \langle l_q s_q m_{l_q} m_{s_q}|j_q m_{j_q}\rangle \langle j_p j_q m_{j_p} m_{j_q}|JM_J\rangle \\
&\quad \times \langle k_p j_p l_p, k_q j_q l_q; JM_J| \langle m_{t_p} m_{t_q}|Y_{l_p m_{l_p}}(\hat{\mathbf{k}}_p) Y_{l_q m_{l_q}}(\hat{\mathbf{k}}_q),
\end{aligned}
\tag{5.54}
$$

where we have used completeness relations similar to Eqs. (3.34) and (3.35), as well as coupling of angular momenta as in Eq. (3.39). If we use the angular momentum expansion (5.54), the orthogonality of spherical harmonics, and the relation [190]

$$\sum_{m_p m_q} (j_p j_q m_p m_q | J M_J)(j_p j_q m_p m_q | J' M'_J) = \delta_{JJ'} \delta_{M_J M'_J} \tag{5.55}$$

for Clebsch-Gordan coefficients, the reference energy per particle becomes

$$\begin{aligned} \frac{E_{REF}}{A} &= \frac{1}{5\pi^2} \frac{\hbar^2 k_F^5}{m\rho} + \frac{1}{2A} \int_0^{k_F} k_1^2 dk_1 \int_0^{k_F} k_2^2 dk_2 \\ &\times \sum_{\substack{l_1 l_2 \\ j_1 j_2}} \sum_J \sum_{m_{t_1} m_{t_2}} (2J+1) \\ &\times \langle k_1 j_1 l_1, k_2 j_2 l_2; J m_{t_1} m_{t_2} | \tilde{v} | k_1 j_1 l_1, k_2 j_2 l_2; J m_{t_1} m_{t_2} \rangle, \end{aligned} \tag{5.56}$$

where A is the number of nucleons and $\rho = A/V$ is the nucleon density. In Eq. (5.56), we need an explicit expression for the number of particles, which in principle is an infinitely large number. When evaluating Eq. (5.56), we hope that the expansion in partial waves may be truncated after a reasonably small number of angular momenta. On the other hand, above we have assumed that the momentum points are infinitely dense. The total number of particles therefore becomes infinitely large. Assuming that convergence has been obtained in the partial-wave expansion, the number of nucleons is

$$\begin{aligned} A &= \sum_{m_s} \sum_{m_t} \frac{V}{(2\pi)^3} \int_{|\mathbf{k}| \leq k_F} d\mathbf{k} \\ &= V \frac{2k_F^3}{3\pi^2} \end{aligned} \tag{5.57}$$

in the special case of symmetric nuclear matter. A practical problem arises here: The expression for the number of particles (5.57) depends on the volume of the nuclear-matter system. When deriving Eqs. (5.51) and (5.56), we have assumed that the volume is infinitely large. Unfortunately, there is no volume term in Eq. (5.51) that cancels the volume in the expression for the number of particles. Dimensional analysis of the given expressions also gives correct units for the energy per particle. We have therefore not been able to calculate the binding energy of nuclear matter using the approach described above.

The problem with infinite numbers can be avoided by discretizing the radial momentum explicitly [192]. This corresponds to using eigenstates of

a spherical well. Following the textbook of Liboff [156], a spherical well has the single-particle wave functions

$$\psi_{nlm_l}(r,\theta_r,\phi_r) \equiv \langle \mathbf{r}|nlm_l\rangle = j_l(k_{nl}r)Y_{lm_l}(\theta_r,\phi_r) \tag{5.58}$$

and single-particle energies

$$\varepsilon_{nl} = \frac{\hbar^2 k_{nl}^2}{2m}, \tag{5.59}$$

where $j_l(x)$ is the spherical Bessel function. The discrete momenta k_{nl} are obtained from the Dirichlet boundary condition

$$\psi_{nlm_l}(R,\theta_r,\phi_r) = 0, \tag{5.60}$$

where R is the radius of the spherical box. Including spin and isospin, the single-particle states may be written as

$$\psi_{njm_jlsm_t}(r,\theta_r,\phi_r) = \sum_{m_l m_s} \langle lm_l sm_s|jm_j ls\rangle j_l(k_{nl}r)Y_{lm_l}(\theta_r,\phi_r)|m_s m_t\rangle, \tag{5.61}$$

where spin and orbital angular momentum have been coupled to a total single-particle angular momentum.

Similarly as in a more general case, the uncorrelated Fermi vacuum state is constructed by choosing the A single-particle states $|njm_jlm_t\rangle$ with the lowest single-particle energies. To be able to use single-reference coupled-cluster theory, the number of particles must be chosen such that all energy shells below the Fermi level are fully occupied. Similarly, one may choose the unoccupied single-particle states such that a given number of energy shells above the Fermi level are completely filled. Given a density ρ and a number of nucleons A, the radius is

$$R = \left(\frac{3A}{4\pi\rho}\right)^{1/3}. \tag{5.62}$$

The discrete spherical Bessel single-particle basis is useful for nuclear-matter studies if the energy per particle converges fast with the number of occupied and unoccupied single-particle states.

Above we concluded that the continuous radial basis $|kjm_jlm_t\rangle$ gives problems with infinite numbers, and we therefore want to replace this basis with the discrete equivalent $|njm_jlm_t\rangle$, which corresponds to eigenstates of a spherical well. Our task is now to rewrite the transformation given in Eq. (5.49) into a discrete form. The only part that is problematic is the

vector bracket, which is defined for continuous radial states. One alternative is to derive a new discrete counterpart to the vector bracket. However, there is another well-known transformation coefficient between discrete laboratory and RCM states, which is the Moshinsky bracket [190], defined for harmonic oscillator states. If we use Moshinsky coefficients to transform the interaction matrix elements to laboratory frame harmonic oscillator states, matrix elements in the discrete radial basis $|njm_jlm_t\rangle$ can be obtained as

$$\langle pq|v|rs\rangle = \sum_{\substack{\alpha\leq\beta \\ \gamma\leq\delta}} \langle pq|\alpha\beta\rangle\langle\alpha\beta|v|\gamma\delta\rangle\langle\gamma\delta|rs\rangle, \tag{5.63}$$

where p, q, r, s represent radial single-particle states and $\alpha, \beta, \gamma, \delta$ harmonic oscillator states. Hagen *et al.* [193] have used a similar transformation from the harmonic oscillator basis to a Gamow basis. As given in Ref. [193], the two-particle overlaps are

$$\langle pq|\alpha\beta\rangle = \begin{cases} \frac{\langle p|\alpha\rangle\langle q|\beta\rangle - (-1)^{J-j_\alpha-j_\beta}\langle p|\beta\rangle\langle q|\alpha\rangle}{\sqrt{(1+\delta_{pq})(1+\delta_{\alpha\beta})}}, & \text{if } m_{t_p} = m_{t_q}, \\ \langle p|\alpha\rangle\langle q|\beta\rangle, & \text{if } m_{t_p} \neq m_{t_q}. \end{cases} \tag{5.64}$$

When doing the transformation from the harmonic oscillator basis to the discrete radial single-particle basis, the single-particle overlaps are

$$\langle p|\alpha\rangle = \delta_{j_p j_\alpha}\delta_{l_p l_\alpha}\delta_{m_{t_p} m_{t_\alpha}} \int_0^R dr r^2 j_{l_p}(k_{n_p l_p} r) R_{n_\alpha l_\alpha}(Cr), \tag{5.65}$$

where

$$C = \sqrt{m\omega/\hbar},$$

the variable ω is the harmonic oscillator strength, and $R_{n_\alpha l_\alpha}(Cr)$ is the radial part of the harmonic oscillator wave function. Numerical calculations should include sufficiently many harmonic oscillator single-particle states to get a result that is only weakly dependent on the oscillator strength. Similarly as done in Ref. [193] with the Gamow basis, we calculate the CM correction term directly in the Bessel basis (should we have a CM correction term??).

- Show results of bad convergence, explain problems with dimensionality
- Discuss the spherical Bessel basis. Show results of bad convergence

5.3 Applications for the electron gas

Another important homogeneous system beside nuclear matter is the electron gas. We have implemented CC theory for the two- and three-dimensional electron gas using finite hypercubic cells. Our studies of the electron gas is an extension of the CC calculations by Shepherd *et al.* [194] and Roggero *et al.* [195] to two-dimensional systems. Similarly as in Ref. [194], we approximate the electron gas by a finite number of electrons in a finite hypercube. The single-particle basis consists of state vectors as given in Eq. (3.22), with the momentum discretized in cartesian coordinates. Essentially the same technique, discretizing the momentum vectors in cartesian coordinates, was also used in the CC calculations for nuclear matter presented in Paper III. Finite hypercubes and discretized cartesian momentum vectors have also been used to model infinite matter with other many-body methods: For the electron gas, there has been done calculations with the full configuration interaction quantum Monte Carlo method [194, 196, 197], second-order perturbation theory and random-phase approximation [194], and the same single-particle basis has been used with the auxiliary-field diffusion Monte Carlo [23, 138, 141], Green's function Monte Carlo, and variational chain summation [137] methods to study symmetric nuclear and/or pure neutron matter.

The homogeneous electron gas is defined as an infinite system consisting of electrons distributed with a constant density thorugh the entire real space. The system is assumed to contain a constant positive background charge which cancels the negative charges of the electrons. The Hamiltonian operator of the homogeneous electron gas can be written as

$$\hat{H} = \hat{H}_0 + \hat{H}_I + \hat{H}_{eb} + \hat{H}_{bb}, \tag{5.66}$$

where

$$\hat{H}_0 = -\frac{\hbar^2}{2m} \sum_{i=1}^{N} \nabla_i^2 \tag{5.67}$$

is the kinetic energy operator,

$$\hat{H}_I = \frac{1}{2} \sum_{i<j}^{N} v\left(|\mathbf{r}_i - \mathbf{r}_j|\right) \tag{5.68}$$

is the two-body electron-electron interaction,

$$\hat{H}_{eb} = -\sum_{i=1}^{N} \int d\mathbf{r} \rho(\mathbf{r}) v\left(|\mathbf{r} - \mathbf{r}_i|\right) \tag{5.69}$$

models the interaction between the electrons and the positive background charge, and

$$\hat{H}_{bb} = \frac{1}{2} \int d\mathbf{r} \int d\mathbf{r}' \rho(\mathbf{r}) \rho(\mathbf{r}') v\left(|\mathbf{r} - \mathbf{r}'|\right) \tag{5.70}$$

represents the interaction between the background charge and itself. Above $\rho(\mathbf{r})$ is the electron density and $v(|\mathbf{r}|)$ is the Coulomb interaction. In the following, we replace the Coulomb interaction by

$$v(r) = e^2 \frac{\exp\left(-\mu r\right)}{r}, \tag{5.71}$$

where the Coulomb potential is obtained at the limit in which μ approaches zero.

Let us write the Hamiltonian operator in the discrete momentum basis (3.22). Fetter and Walecka show [154] that the total Hamiltonian for the three-dimensional system can be written as

$$\hat{H} = \hat{H}_0 + \hat{H}_I - \frac{2\pi e^2 N^2}{L^3 \mu^2}, \tag{5.72}$$

where the kinetic energy operator is

$$\hat{H}_0 = \sum_{\mathbf{k}_p} \sum_{m_{sp}} \frac{\hbar^2 k_p^2}{2m} a^\dagger_{\mathbf{k}_p m_{sp}} a_{\mathbf{k}_p m_{sp}}, \tag{5.73}$$

the two-body interaction operator is

$$\hat{H}_I = \sum_{\substack{\mathbf{k}_p \mathbf{k}_q \\ \mathbf{k}_r \mathbf{k}_s}} \sum_{\substack{m_{s_p} m_{s_q} \\ m_{s_r} m_{s_s}}} \langle \mathbf{k}_p m_{s_p} \mathbf{k}_q m_{s_q} | v | \mathbf{k}_r m_{s_r} \mathbf{k}_s m_{s_s} \rangle_{AS} a^\dagger_{\mathbf{k}_p m_{s_p}} a^\dagger_{\mathbf{k}_q m_{s_q}} a_{\mathbf{k}_s m_{s_s}} a_{\mathbf{k}_r m_{s_r}}, \tag{5.74}$$

the variable N represents the number of electrons, and L is the side length of the cube. The interaction matrix elements are obtained as Fourier transformations of the Yukawa interaction. Further, they show that the part of the two-body interaction operator with zero momentum transfer gives a constant

$$\frac{2\pi e^2}{L^3 \mu^2} \left(N^2 - N\right), \tag{5.75}$$

where the the part with N^2 exacly cancels the constant in Eq. (5.72). If we first let $L \to \infty$ and thereafter take the limit $\mu \to 0$, the part of (5.75) that

is linear in N also vanishes in the expression for the energy per particle [154]. In that case, the total Hamiltonian operator may be written as

$$\hat{H} = \hat{H}_0 + \hat{H}_I, \tag{5.76}$$

where the antisymmetrized momentum-space interaction matrix elements are

$$\begin{aligned}
&\langle \mathbf{k}_p m_{s_p} \mathbf{k}_q m_{s_q} | v | \mathbf{k}_r m_{s_r} \mathbf{k}_s m_{s_s} \rangle_{AS} \\
&= \frac{e^2}{L^3} \delta_{\mathbf{k}_p + \mathbf{k}_q, \mathbf{k}_r + \mathbf{k}_s} \left\{ \delta_{m_{s_p} m_{s_r}} \delta_{m_{s_q} m_{s_s}} \left(1 - \delta_{\mathbf{k}_p \mathbf{k}_r}\right) \frac{4\pi}{\mu^2 + |\mathbf{k}_r - \mathbf{k}_p|^2} \right. \\
&\left. - \delta_{m_{s_p} m_{s_s}} \delta_{m_{s_q} m_{s_r}} \left(1 - \delta_{\mathbf{k}_p \mathbf{k}_s}\right) \frac{4\pi}{\mu^2 + |\mathbf{k}_s - \mathbf{k}_p|^2} \right\}.
\end{aligned} \tag{5.77}$$

The Kronecker delta functions $\delta_{\mathbf{k}_p \mathbf{k}_r}$ and $\delta_{\mathbf{k}_p \mathbf{k}_s}$ ensure that the contribution with zero momentum transfer vanishes. If the side length L is finite, the latter term of Eq. (5.75) remains finite for nonzero μ values, and becomes infinite as μ approaches zero.

Following a similar approach as outlined above for the three-dimensional case, the Hamiltonian of a two-dimensional electron gas can be written as

$$\hat{H} = \hat{H}_0 + \hat{H}_I - \frac{\pi e^2 N^2}{L^2 \mu}, \tag{5.78}$$

where $\hat{H}_0$ and $\hat{H}_I$ are defined as in Eqs. (5.73) and (5.74), but with two-dimensional momentum vectors and different interaction matrix elements. Similarly as in the three-dimensional case [154], the momentum-space interaction matrix elements for the two-dimensional system are

$$\begin{aligned}
&\langle \mathbf{k}_p m_{s_p} \mathbf{k}_q m_{s_q} | v | \mathbf{k}_r m_{s_r} \mathbf{k}_s m_{s_s} \rangle_{AS} \\
&= \frac{e^2}{L^2} \delta_{m_{s_p} m_{s_r}} \delta_{m_{s_q} m_{s_s}} \int d\mathbf{r} \int d\mathbf{r}' \exp\left(-i \mathbf{k}_p \cdot \mathbf{r}\right) \exp\left(-i \mathbf{k}_q \cdot \mathbf{r}'\right) \\
&\times \frac{\exp\left(-\mu |\mathbf{r} - \mathbf{r}'|\right)}{|\mathbf{r} - \mathbf{r}'|} \exp\left(i \mathbf{k}_r \cdot \mathbf{r}\right) \exp\left(i \mathbf{k}_s \cdot \mathbf{r}'\right) \\
&= \frac{e^2}{L^2} \delta_{m_{s_p} m_{s_r}} \delta_{m_{s_q} m_{s_s}} \delta_{\mathbf{k}_p + \mathbf{k}_q, \mathbf{k}_r + \mathbf{k}_s} \int d\mathbf{r} \exp\left(i (\mathbf{k}_r - \mathbf{k}_p) \cdot \mathbf{r}\right) \frac{\exp\left(-\mu r\right)}{r},
\end{aligned} \tag{5.79}$$

where r is the radial coordinate of the position vector. Using Eqs. (9.1.21) and (9.1.10) of Ref. [198], that is,

$$\int_0^{2\pi} \exp\left(ipr \cos\phi\right) = 2\pi J_0(pr) \tag{5.80}$$

and

$$J_0(x) = J_0(-x), \tag{5.81}$$

where $J_0(x)$ is the Bessel function of the first kind, as well as the relation

$$\int_0^\infty dr \exp(-\mu r) J_0(pr) = \frac{1}{\sqrt{\mu^2 + p^2}}, \tag{5.82}$$

which is given in Eq. (6.611) of Ref. [199], the interaction matrix elements of $\hat{H}_I$ in Eq. (5.78) may be written as

$$\begin{aligned}
&\langle \mathbf{k}_p m_{s_p} \mathbf{k}_q m_{s_q} | v | \mathbf{k}_r m_{s_r} \mathbf{k}_s m_{s_s} \rangle_{AS} \\
&= \frac{e^2}{L^2} \delta_{\mathbf{k}_p + \mathbf{k}_q, \mathbf{k}_r + \mathbf{k}_s} \left\{ \delta_{m_{sp} m_{sr}} \delta_{m_{sq} m_{ss}} \left(1 - \delta_{\mathbf{k}_p \mathbf{k}_r}\right) \frac{2\pi}{\sqrt{\mu^2 + |\mathbf{k}_r - \mathbf{k}_p|^2}} \right. \\
&\left. - \delta_{m_{sp} m_{ss}} \delta_{m_{sq} m_{sr}} \left(1 - \delta_{\mathbf{k}_p \mathbf{k}_s}\right) \frac{2\pi}{\sqrt{\mu^2 + |\mathbf{k}_s - \mathbf{k}_p|^2}} \right\}.
\end{aligned} \tag{5.83}$$

Interaction matrix elements for the Coulomb interaction, with μ set to zero, have been derived in a similar way in for example the textbook by Hamaguchi [200].

In the discrete momentum basis with periodic boundary conditions, the single-particle energy is

$$\varepsilon_{n_x, n_y} = \frac{\hbar^2}{2m} \left(\frac{2\pi}{L}\right)^2 \left(n_x^2 + n_y^2\right) \tag{5.84}$$

for two-dimensional sytems and

$$\varepsilon_{n_x, n_y, n_z} = \frac{\hbar^2}{2m} \left(\frac{2\pi}{L}\right)^2 \left(n_x^2 + n_y^2 + n_z^2\right) \tag{5.85}$$

for three-dimensional systems. Similarly as in for example Refs. [30, 195, 196], we choose the single-particle basis such that both the occupied and unoccupied single-particle spaces have a closed-shell structure. This means that all single-particle states corresponding to energies below a chosen cutoff are included in the basis. We study only the unpolarized spin phase, in which all orbitals are occupied with one spin-up and one spin-down electron. Table 5.1 shows the lowest-lying spin-orbitals and the cumulated numbers of single-particle states for a two-dimensional electron box with periodic boundary conditions. The CCD energy is obtained by solving the energy equations (5.11) and (5.12) together with the $\hat{T}_2$ amplitude equation (5.15) using the discrete momentum basis.

$n_x^2 + n_y^2$	n_x	n_y	$N_{\uparrow\downarrow}$	$N_{\uparrow\uparrow}$
0	0	0	2	1
1	-1	0		
	1	0		
	0	-1		
	0	1	10	5
2	-1	-1		
	-1	1		
	1	-1		
	1	1	18	9
4	-2	0		
	2	0		
	0	-2		
	0	2	26	13
5	-2	-1		
	2	-1		
	-2	1		
	2	1		
	-1	-2		
	-1	2		
	1	-2		
	1	2	42	21

Table 5.1: Illustration of how single-particle energies fill energy shells in a two-dimensional electron box. Here n_x and n_y are the momentum quantum numbers, $n_x^2 + n_y^2$ determines the single-particle energy level, $N_{\uparrow\downarrow}$ represents the cumulated number of spin-orbitals in an unpolarized spin phase, and $N_{\uparrow\uparrow}$ stands for the cumulated number of spin-orbitals in a spin-polarized system.

- General introduction: Why and what has been done
- Discrete momentum coordinates: definition, advantages and disadvantages
- How finite-size effects could have been handled

5.3.1 Implementation

As can be seen from Eqs. (5.77) and (5.79), the Coulomb interaction is diagonal in CM momentum $\mathbf{K}$ and spin projection M_S. Because of these symmetries, we store the two-body interaction and t-amplitude matrices in blocks of $(\mathbf{K}, M_S)$. From a computational point of view, the storage in blocks saves a considerable amount of memory and processor time. In the CCD equations (5.12) and (5.15), the terms with summation over two particle states or two hole states can straightforwardly be written as matrix-matrix multiplications. Unfortunately, the terms in the CCD amplitude equation with summation over one particle and one hole state cannot be calculated directly using matrix-matrix multiplications. To circumvent this problem, we use a similar cross-coupling technique as introduced by Kuo *et al.* for coupling of angular momenta [201]. In the discretized Cartesian momentum basis, all diagrams of the CCD equations can therefore be implemented using matrix-matrix multiplications [30].

Let us explain the basic principles of the cross-coupling of matrix elements in the discrete momentum basis. Consider a matrix element

$$\langle pq|v|rs\rangle.$$

In a diagram with summation over the two ket states, for example, we set up the matrix elements as

$$V_{\alpha(p,q),\beta(r,s)} \equiv \langle pq|v|rs\rangle$$

and sum over the two-particle states labelled with β. In this case, the blocks are set up such that the conservation requirements

$$\mathbf{k}_p + \mathbf{k}_q = \mathbf{k}_r + \mathbf{k}_s$$

and

$$m_{s_p} + m_{s_q} = m_{s_r} + m_{s_s}$$

are fulfilled. This gives blocks in total momentum $\mathbf{K}$ and total spin projection M_S. On the other hand, if the original summation is over the states s and q, for example, the matrix elements can be set up as

$$V_{\gamma(p,r),\delta(s,q)} \equiv \langle pq|v|rs\rangle, \tag{5.86}$$

where the summation is taken over the two-particle states δ. To ensure conservation of total momentum and spin projection, the matrices must be stored in blocks such that

$$\mathbf{k}_p - \mathbf{k}_r = \mathbf{k}_s - \mathbf{k}_q$$

and

$$m_{s_p} - m_{s_r} = m_{s_s} - m_{s_q}.$$

The blocks are now in relative momentum $\tilde{\mathbf{k}}$ and relative spin projection $\tilde{m}_s$. We call matrix elements set up as in Eq. (5.86) cross-coupled matrix elements.

Let us show how the particle-hole diagrams are calculated with matrix-matrix multiplications using cross-coupled matrices. Consider the particle-hole term

$$\langle ab|I_{ph}|ij\rangle \equiv \sum_{kc}\langle ac|t|ik\rangle \left\{ \langle kb|v|cj\rangle + \frac{1}{2}\sum_{ld}\langle kl|v|cd\rangle\langle db|t|lj\rangle \right\}, \qquad (5.87)$$

which is part of the CCD amplitude equation. We cross-couple the matrix I_{ph} using the matrix-element transformation

$$\langle ab|I_{ph}|ij\rangle \longrightarrow \langle bj|I^*_{ph}|ia\rangle, \qquad (5.88)$$

where the star denotes that the matrix has been cross-coupled from a particle-particle-hole-hole form to a particle-hole-hole-particle form. Technically, the matrix-element transformation is a relocation of matrix elements. The cross-coupled matrix I^*_{ph} is now written as the matrix-matrix product

$$\langle bj|I^*_{ph}|ia\rangle = \sum_{kc}\langle bj|I^*_2|ck\rangle\langle ck|t^*|ia\rangle, \qquad (5.89)$$

where the matrix t^* is obtained using a similar element-transformation as in Eq. (5.88) and

$$\langle bj|I^*_2|ck\rangle = \langle bj|v^{\#}|ck\rangle + \frac{1}{2}\sum_{ld}\langle bj|t^*|ld\rangle\langle ld|v^*|ck\rangle. \qquad (5.90)$$

Again, the matrices v^* and $v^{\#}$ are obtained with an element-transformation of the type shown in Eq. (5.88). The matrix v^* has been obtained by cross-coupling a matrix with hole-hole-particle-particle configuration, whereas the matrix $v^{\#}$ has been obtained by cross-coupling a hole-particle-particle-hole matrix. The equations (5.89) and (5.90) are straightforwardly implemented

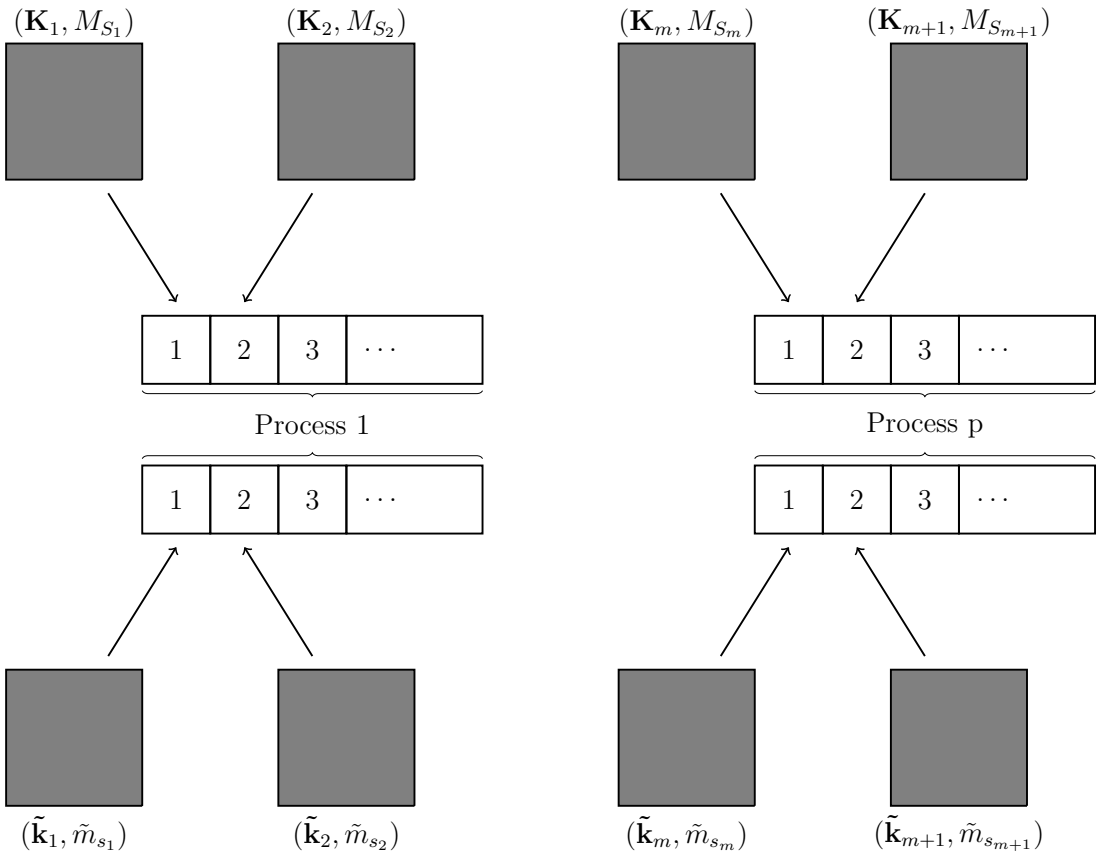

Figure 5.4: The big matrices are divided into matrix blocks, each being an element of an array. Subarrays of the different matrix lists are associated with different MPI processes. There are different matrix lists for normally coupled and cross-coupled matrices. (Illustration by the author.)

as matrix-matrix multiplications. Finally, the matrix I^*_{ph} is transformed back to the normal coupling scheme, and blocks of I_{ph} are added to the CCD amplitude equation. The implementation of matrix-matrix multiplications for all diagrams gives a significant speedup of the computer program. Figure 5.5 shows that the computing time scales quadatically with the number of unoccupied orbitals, n_{unocc}, when utilizing block diagonalization and matrix-matrix multiplications as described above.

To be able to utilize large-scale distributed computing clusters, we have parallelized the CC program in Cartesian momentum coordinates using the Message Passing Interface (MPI) Standard [181,182]. In our implementation, both the cross-coupled and normally coupled matrices are stored in arrays containing matrix blocks. Most of the matrix arrays are divided into subar-

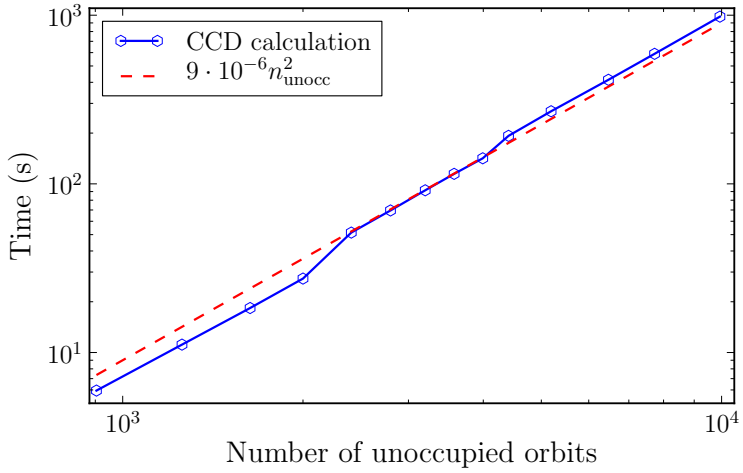

Figure 5.5: The computing time scales quadratically as a function of unoccupied single-particle orbits n_{unocc}. The CCD calculations were done for the two-dimensional electron gas with ten electrons at $r_s = 0.5$, without MPI parallelization and with a fixed number of cpus on a single computing node.

rays that are distributed to different MPI processes (see Figure 5.4). A given subarray containing matrices is then stored only locally on the computing node where the corresponding MPI process resides. In addition to parallelizing the computation operations, this arrangement reduces the memory consumption on each node. Some of the matrices, such as the cross-coupled amplitude matrix and the normally coupled matrix of the particle-hole diagrams must be communicated to all nodes. We therefore chose to store complete matrix arrays of these parts on every node. For example, different parts of the normally coupled particle-hole diagrams, I_{ph}, are calculated locally on different computing nodes, and finally all parts are summed up and the resulting matrix array is distributed to all nodes.

- Precomputation of different parts
- Other optimizations

Chapter 6

Numerical results

- Tests for the 3D electron gas: comparison with Alavi *et al.*
- Results for two-dimensional electron gas: CCD, ring and ladder approximations
- Comparisons with SRG and FCIQMC?
- Comparison with other results, discussion

Chapter 7

Conclusions

This work showed that ...

- Limitations in our methods
- The main results

What are the next steps?

- Calculation of astrophysical observables
- Finite size effects in the electron gas
- Triples in the electron gas
- Three-body forces in N3LO for neutron matter
- CC at finite temperatures in cartesian momentum coordinates? (Simen Kvaal's method for time-dependent CC, change time to temperature)
- CC for other observables in cartesian momentum coordinates?
- Extract a density functional??
- Relativistic coupled-cluster theory for infintie nuclear matter (similar to RBHF)?

Bibliography

[1] M. Arnould, S. Goriely, and K. Takahashi. The r-process of stellar nucleosynthesis: Astrophysics and nuclear physics achievements and mysteries. *Physics Reports*, 450(46):97 – 213, 2007.

[2] S. Goriely, A. Bauswein, and H.-T. Janka. R-process nucleosynthesis during the decompression of neutron star crust material. *Journal of Physics: Conference Series*, 337(1):012039, 2012.

[3] Hans-Thomas Janka. Explosion mechanisms of core-collapse supernovae. *Annual Review of Nuclear and Particle Science*, 62(1):407–451, 2012.

[4] The Committee on the Assessment of, Outlook for Nuclear Physics; Board on Physics, Astronomy; Division on Engineering, and Physical Sciences; National Research Council. *Nuclear Physics: Exploring the Heart of Matter*. The National Academies Press, 2013.

[5] V. Bârsan and A. Aldea, editors. *Trends in Nanophysics. Theory, experiment and Technology*. Springer, 2010.

[6] F. Mandl and G. Shaw. *Quantum Field Theory*. John Wiley & Sons, 1984.

[7] B. R. Martin. *Nuclear and Particle Physics. An Introduction*. John Wiley & Sons Ltd, second edition, 2009.

[8] Michael Riordan. The discovery of quarks. *Science*, 256(5061):pp. 1287–1293, 1992.

[9] P. Braun-Munzinger and J. Wambach. Colloquium: Phase diagram of strongly interacting matter. *Rev. Mod. Phys.*, 81:1031–1050, Jul 2009.

[10] B. D. Day. *Rev. Mod. Phys.*, 39(4):719, 1967.

[11] S. S. M. Wong. *Introductory Nuclear Physics*. Prentice Hall, 1990.

[12] H. Heiselberg and M. Hjorth-Jensen. *Phys. Rep.*, 328:237, 2000.

[13] J. M. Lattimer. *Ann. Rev. Nucl. Part. Sci.*, 62:485, 2012.

[14] Heavy ions and quark-gluon plasma. `http://home.web.cern.ch/about/physics/heavy-ions-and-quark-gluon-plasma`. Accessed: 2013-11-28.

[15] A new area of physics. `http://www.bnl.gov/rhic/newPhysics.asp`. Accessed: 2013-11-28.

[16] J. M. Lattimer and M. Prakash. The physics of neutron stars. *Science*, 304(5670):536–542, 2004.

[17] R. N. Boyd. *An Introduction to Nuclear Astrophysics*. The University of Chicago Press, 2008.

[18] H. A. Bethe. Supernova mechanisms. *Rev. Mod. Phys.*, 62:801–866, Oct 1990.

[19] J. M. Lattimer and M. Prakash. *Astrophys. J.*, 550:426, 2001.

[20] A. Akmal, V. R. Pandharipande, and D. G. Ravenhall. Equation of state of nucleon matter and neutron star structure. *Phys. Rev. C*, 58:1804–1828, Sep 1998.

[21] T. Frick and H. Müther. Self-consistent solution to the nuclear many-body problem at finite temperature. *Phys. Rev. C*, 68:034310, Sep 2003.

[22] Z. H. Li, U. Lombardo, H.-J. Schulze, W. Zuo, L. W. Chen, and H. R. Ma. Nuclear matter saturation point and symmetry energy with modern nucleon-nucleon potentials. *Phys. Rev. C*, 74:047304, 2006.

[23] Stefano Gandolfi, Francesco Pederiva, Stefano Fantoni, and Kevin E. Schmidt. Quantum monte carlo calculations of symmetric nuclear matter. *Phys. Rev. Lett.*, 98:102503, Mar 2007.

[24] V. Somà and P. Bożek. In-medium t matrix for nuclear matter with three-body forces: Binding energy and single-particle properties. *Phys. Rev. C*, 78:054003, Nov 2008.

[25] E. N. E. van Dalen and H. Müther. Nuclear saturation with low momentum interactions. *Phys. Rev. C*, 80:037303, Sep 2009.

[26] K. Hebeler, S. K. Bogner, R. J. Furnstahl, A. Nogga, and A. Schwenk. *Phys. Rev. C*, 83:031301, 2011.

[27] M. Baldo, A. Polls, A. Rios, H.-J. Schulze, and I. Vidaña. Comparative study of neutron and nuclear matter with simplified argonne nucleon-nucleon potentials. *Phys. Rev. C*, 86:064001, Dec 2012.

[28] Francesca Sammarruca, B. Chen, L. Coraggio, N. Itaco, and R. Machleidt. Dirac-brueckner-hartree-fock versus chiral effective field theory. *Phys. Rev. C*, 86:054317, Nov 2012.

[29] Arianna Carbone, Artur Polls, and Arnau Rios. Symmetric nuclear matter with chiral three-nucleon forces in the self-consistent green's functions approach. *Phys. Rev. C*, 88:044302, Oct 2013.

[30] G. Hagen, T. Papenbrock, A. Ekström, K.A. Wendt, G. Baardsen, et al. Coupled-cluster calculations of nucleonic matter. 2013.

[31] H. Müther, M. Prakash, and T.L. Ainsworth. The nuclear symmetry energy in relativistic brueckner-hartree-fock calculations. *Physics Letters B*, 199(4):469 – 474, 1987.

[32] L. Engvik, M. Hjorth-Jensen, R. Machleidt, H. Müther, and A. Polls. *Nucl. Phys. A*, 627:85, 1997.

[33] C.-H. Lee, T. T. S. Kuo, G. Q. Li, and G. E. Brown. Nuclear symmetry energy. *Phys. Rev. C*, 57:3488–3491, Jun 1998.

[34] I. Vidaña, C. Providência, A. Polls, and A. Rios. Density dependence of the nuclear symmetry energy: A microscopic perspective. *Phys. Rev. C*, 80:045806, 2009.

[35] A. Carbone, A. Polls, and A. Rios. High-momentum components in the nuclear symmetry energy. *EPL (Europhysics Letters)*, 97(2):22001, 2012.

[36] James M. Lattimer and Madappa Prakash. Nuclear matter and its role in supernovae, neutron stars and compact object binary mergers. *Physics Reports*, 333334(0):121 – 146, 2000.

[37] A.S. Botvina and I.N. Mishustin. Formation of hot heavy nuclei in supernova explosions. *Physics Letters B*, 584(34):233 – 240, 2004.

[38] Pawe Danielewicz, Roy Lacey, and William G. Lynch. Determination of the equation of state of dense matter. *Science*, 298(5598):1592–1596, 2002.

[39] W.G. Lynch, M.B. Tsang, Y. Zhang, P. Danielewicz, M. Famiano, Z. Li, and A.W. Steiner. Probing the symmetry energy with heavy ions. *Progress in Particle and Nuclear Physics*, 62(2):427 – 432, 2009. ¡ce:title¿Heavy-Ion Collisions from the Coulomb Barrier to the Quark-Gluon Plasma¡/ce:title¿ ¡ce:subtitle¿30th Course¡/ce:subtitle¿ ¡xocs:full-name¿International Workshop on Nuclear Physics¡/xocs:full-name¿.

[40] Andrea Maselli, Leonardo Gualtieri, and Valeria Ferrari. Constraining the equation of state of nuclear matter with gravitational wave observations: Tidal deformability and tidal disruption. *Phys. Rev. D*, 88:104040, Nov 2013.

[41] I. Tews, T. Krüger, K. Hebeler, and A. Schwenck. *Phys. Rev. Lett.*, 110:032504, 2013.

[42] K. A. Brueckner, C. A. Levinson, and H. M. Mahmoud. Two-body forces and nuclear saturation. i. central forces. *Phys. Rev.*, 95:217–228, Jul 1954.

[43] K. A. Brueckner and J. L. Gammel. *Phys. Rev.*, 109(4):1023, 1958.

[44] C. Fuchs. *Extended Density Functionals in Nuclear Structure Physics*, chapter The Relativistic Dirac-Brueckner Approach to Nuclear Matter. Springer, Berlin, 2004.

[45] J.R. Stone and P.-G. Reinhard. The skyrme interaction in finite nuclei and nuclear matter. *Progress in Particle and Nuclear Physics*, 58(2):587 – 657, 2007.

[46] H. Müther and A. Polls. *Progress in Particle and Nuclear Physics*, 45(1):243 – 334, 2000.

[47] Michael Bender, Paul-Henri Heenen, and Paul-Gerhard Reinhard. Self-consistent mean-field models for nuclear structure. *Rev. Mod. Phys.*, 75:121–180, Jan 2003.

[48] E. van Dalen and H. Müther. Relativistic effects in nuclear matter and nuclei. *International Journal of Modern Physics E*, 19(11):2077–2122, 2010.

[49] R. Machleidt and I. Slaus. *J. Phys. G: Nucl. Part. Phys.*, 27:R69, 2001.

[50] R. Machleidt and D. R. Entem. *Phys. Rep.*, 503:1, 2011.

[51] A. Lejeune, U. Lombardo, and W. Zuo. Nuclear matter {EOS} with a three-body force. *Physics Letters B*, 477(13):45 – 50, 2000.

[52] S. Gandolfi, A. Yu. Illarionov, S. Fantoni, J. C. Miller, F. Pederiva, and K. E. Schmidt. Microscopic calculation of the equation of state of nuclear matter and neutron star structure. *Monthly Notices of the Royal Astronomical Society: Letters*, 404(1):L35–L39, 2010.

[53] E. K. U. Gross and R. M. Dreizler. *Density Functional Theory*. Springer, 1995.

[54] M. Baldo, C. Maieron, P. Schuck, and X. Vias. Low densities in nuclear and neutron matters and in the nuclear surface. *Nuclear Physics A*, 736(34):241 – 254, 2004.

[55] L. G. Cao, U. Lombardo, C. W. Shen, and Nguyen Van Giai. From brueckner approach to skyrme-type energy density functional. *Phys. Rev. C*, 73:014313, Jan 2006.

[56] J.E. Drut, R.J. Furnstahl, and L. Platter. Toward ab initiodensity functional theory for nuclei. *Progress in Particle and Nuclear Physics*, 64(1):120 – 168, 2010.

[57] Steven C. Pieper and R. B. Wiringa. Quantum monte carlo calculations of light nuclei1. *Annual Review of Nuclear and Particle Science*, 51(1):53–90, 2001.

[58] W. H. Dickhoff and C. Barbieri. *Prog. Part. Nucl. Phys.*, 52:377, 2004.

[59] Petr Navrtil, Sofia Quaglioni, Ionel Stetcu, and Bruce R Barrett. Recent developments in no-core shell-model calculations. *Journal of Physics G: Nuclear and Particle Physics*, 36(8):083101, 2009.

[60] G. Hagen, T. Papenbrock, M. Hjorth-Jensen, and D.J. Dean. Coupled-cluster computations of atomic nuclei. 2013.

[61] G. Hagen, M. Hjorth-Jensen, G. R. Jansen, R. Machleidt, and T. Papenbrock. Evolution of shell structure in neutron-rich calcium isotopes. *Phys. Rev. Lett.*, 109:032502, Jul 2012.

[62] Robert Roth, Angelo Calci, Joachim Langhammer, and Sven Binder. Evolved Chiral NN+3N Hamiltonians for Ab Initio Nuclear Structure Calculations. 2013.

[63] Hans-Werner Hammer, Andreas Nogga, and Achim Schwenk. ¡i¿colloquium¡/i¿: Three-body forces: From cold atoms to nuclei. *Rev. Mod. Phys.*, 85:197–217, Jan 2013.

[64] A. Cipollone, C. Barbieri, and P. Navrátil. Isotopic chains around oxygen from evolved chiral two- and three-nucleon interactions. *Phys. Rev. Lett.*, 111:062501, Aug 2013.

[65] J. D. Walecka. *Theoretical Nuclear and Subnuclear Physics*. World Scientific, 2004.

[66] E. Chabanat, P. Bonche, P. Haensel, J. Meyer, and R. Schaeffer. A skyrme parametrization from subnuclear to neutron star densities. *Nuclear Physics A*, 627(4):710 – 746, 1997.

[67] C. Mahaux and R. Sartor. *Nuclear Matter and Heavy Ion Collisions, in: NATO ASI Series B. Physics, vol. 205*, chapter Nuclear Matter with Nonrelativistic Potentials: Present status. Plenum Press, New York, 1989.

[68] H. A. Bethe. *Annual Review of Nuclear Science*, 21(1):93–244, 1971.

[69] B. D. Day. *Rev. Mod. Phys.*, 50(3):495, 1978.

[70] M. I. Haftel and F. Tabakin. *Nucl. Phys. A*, 158:1, 1970.

[71] C. Mahaux, P. F. Bortignon, and R. A. Broglia. *Phys. Rep.*, 120:1, 1985.

[72] C. Mahaux and R. Sartor. *Phys. Rev. C*, 40(4):1833, 1989.

[73] M.R. Anastasio, L.S. Celenza, W.S. Pong, and C.M. Shakin. Relativistic nuclear structure physics. *Physics Reports*, 100(6):327 – 392, 1983.

[74] R. Brockmann and R. Machleidt. Nuclear saturation in a relativistic brueckner-hartree-fock approach. *Physics Letters B*, 149(45):283 – 287, 1984.

[75] C.J. Horowitz and Brian D. Serot. Two-nucleon correlations in a relativistic theory of nuclear matter. *Physics Letters B*, 137(56):287 – 293, 1984.

[76] Bernard ter Haar and Rudi Malfliet. Nucleons, mesons and deltas in nuclear matter a relativistic dirac-brueckner approach. *Physics Reports*, 149(4):207 – 286, 1987.

[77] C.J. Horowitz and Brian D. Serot. The relativistic two-nucleon problem in nuclear matter. *Nuclear Physics A*, 464(4):613 – 699, 1987.

[78] R. Brockmann and R. Machleidt. Relativistic nuclear structure. i. nuclear matter. *Phys. Rev. C*, 42:1965–1980, Nov 1990.

[79] F. Coester, S. Cohen, B. Day, and C. M. Vincent. *Phys. Rev. C*, 1:769, 1970.

[80] I. Shavitt and R. J. Bartlett. *Many-Body Methods in Chemistry and Physics*. Cambridge University Press, 2009.

[81] H. Q. Song, M. Baldo, G. Giansiracusa, and U. Lombardo. *Phys. Rev. Lett.*, 81(8):1584, 1998.

[82] K. A. Brueckner and C. A. Levinson. *Phys. Rev.*, 97(5):1344, 1955.

[83] K. A. Brueckner. *Phys. Rev.*, 100(1):36, 1955.

[84] A. D. Jackson. *Annual Review of Nuclear and Particle Science*, 33(1):105–142, 1983.

[85] A. Lejeune, P. Grange, M. Martzolff, and J. Cugnon. Hot nuclear matter in an extended brueckner approach. *Nuclear Physics A*, 453(2):189 – 219, 1986.

[86] M. Baldo, I. Bombaci, G. Giansiracusa, and U. Lombardo. *Journal of Physics G: Nuclear and Particle Physics*, 16(11):L263, 1990.

[87] L. Engvik, E. Osnes, M. Hjorth-Jensen, G. Bao, and E. Østgaard. *Astr. J.*, 469(2):794, 1996.

[88] E. Schiller, H. Müther, and P. C. Czerski. *Physical Review C*, 60:059901(E), 1999.

[89] I. Vidaña, A. Polls, A. Ramos, M. Hjorth-Jensen, and V. G. J. Stoks. Strange nuclear matter within brueckner-hartree-fock theory. *Phys. Rev. C*, 61:025802, Jan 2000.

[90] K. Suzuki, R. Okamoto, M. Kohno, and S. Nagata. *Nucl. Phys. A*, 665:92, 2000.

[91] W. Zuo, A. Lejeune, U. Lombardo, and J.F. Mathiot. Interplay of three-body interactions in the {EOS} of nuclear matter. *Nuclear Physics A*, 706(34):418 – 430, 2002.

[92] W. Zuo, Z. H. Li, A. Li, and G. C. Lu. Hot nuclear matter equation of state with a three-body force. *Phys. Rev. C*, 69:064001, Jun 2003.

[93] G F Burgio. The equation of state of dense matter: from nuclear collisions to neutron stars. *Journal of Physics G: Nuclear and Particle Physics*, 35(1):014048, 2008.

[94] Isaac Vidaña, Artur Polls, and Constan ça Providência. Nuclear symmetry energy and the role of the tensor force. *Phys. Rev. C*, 84:062801, Dec 2011.

[95] Takashi Inoue, Sinya Aoki, Takumi Doi, Tetsuo Hatsuda, Yoichi Ikeda, Noriyoshi Ishii, Keiko Murano, Hidekatsu Nemura, and Kenji Sasaki. Equation of state for nucleonic matter and its quark mass dependence from the nuclear force in lattice qcd. *Phys. Rev. Lett.*, 111:112503, Sep 2013.

[96] I. Bombaci and U. Lombardo. Asymmetric nuclear matter equation of state. *Phys. Rev. C*, 44:1892–1900, Nov 1991.

[97] W. Zuo, A. Lejeune, U. Lombardo, and J.F. Mathiot. Microscopic three-body force for asymmetric nuclear matter. *The European Physical Journal A - Hadrons and Nuclei*, 14(4):469–475, 2002.

[98] H.-J. Schulze, M. Baldo, U. Lombardo, J. Cugnon, and A. Lejeune. Hyperonic nuclear matter in brueckner theory. *Phys. Rev. C*, 57:704–713, Feb 1998.

[99] B. D. Day. *Phys. Rev. C*, 24(3):1203, 1981.

[100] H.Q. Song, M. Baldo, G. Giansiracusa, and U. Lombardo. Three hole-line contribution in nuclear matter revisited. *Physics Letters B*, 411(34):237 – 243, 1997.

[101] R. Rajaraman and H. A. Bethe. *Rev. Mod. Phys.*, 39(4):745, 1967.

[102] F. Coester. *Nucl. Phys.*, 7:421, 1958.

[103] F. Coester and H. Kümmel. *Nucl. Phys.*, 17:477, 1960.

[104] Jiri Cizek. On the correlation problem in atomic and molecular systems. calculation of wavefunction components in ursell-type expansion using quantum-field theoretical methods. *The Journal of Chemical Physics*, 45(11):4256–4266, 1966.

[105] J. Čížek and J. Paldus. Correlation problems in atomic and molecular systems III. Rederivation of the coupled-pair many-electron theory using the traditional quantum chemical methods. *Int. J. Quant. Chem.*, 5:359, 1971.

[106] R. Bartlett and M. Musiał. *Rev. Mod. Phys.*, 79:291, 2007.

[107] H. Kümmel, K. H. Lührmann, and J. G. Zabolitzky. *Phys. Rep.*, 36(1):1, 1978.

[108] B. D. Day and G. Zabolitzky. *Nucl. Phys. A*, 366:221, 1981.

[109] G. Baardsen, A. Ekström, G. Hagen, and M. Hjorth-Jensen. Coupled-cluster studies of infinite nuclear matter. *Phys. Rev. C*, 88:054312, Nov 2013.

[110] F. E. Harris, H. J. Monkhorst, and D. L. Freeman. *Algebraic and diagrammatic methods in many-fermion theory*. Oxford University Press, 1992.

[111] S. K. Bogner, A. Schwenk, R. J. Furnstahl, and A. Nogga. *Nucl. Phys. A*, 763:59, 2005.

[112] S.K. Bogner, R.J. Furnstahl, and A. Schwenk. From low-momentum interactions to nuclear structure. *Progress in Particle and Nuclear Physics*, 65(1):94 – 147, 2010.

[113] K. Hebeler and A. Schwenk. Chiral three-nucleon forces and neutron matter. *Phys. Rev. C*, 82:014314, Jul 2010.

[114] R. J. Furnstahl and K. Hebeler. New applications of renormalization group methods in nuclear physics. *Reports on Progress in Physics*, 76(12):126301, 2013.

[115] W.H. Dickhoff, Amand Faessler, and H. Mther. Multiple (3, 3) excitation and the binding energy of nuclear matter. *Nuclear Physics A*, 389(3):492 – 508, 1982.

[116] Z.Y. Ma and T.T.S. Kuo. Theory of model-space single-particle potential and its application to nuclear matter calculations. *Physics Letters B*, 127(34):137 – 143, 1983.

[117] T. T. S. Kuo, Z. Y. Ma, and R. Vinh Mau. Model-space nuclear matter calculations with the paris nucleon-nucleon potential. *Phys. Rev. C*, 33:717–724, Feb 1986.

[118] L. Engvik, E. Osnes, M. Hjorth-Jensen, and T.T.S. Kuo. Nuclear and neutron matter calculations with different model spaces. *Nucl. Phys. A*, 622:553, 1997.

[119] H.Q. Song, S.D. Yang, and T.T.S. Kuo. Infinite order summation of particle-particle ring diagrams in a model-space approach for nuclear matter. *Nucl. Phys. A*, 462:491 – 526, 1987.

[120] M. F. Jiang, T. T. S. Kuo, and H. Müther. Ring diagram nuclear matter calculations using bonn and V_{14} potentials. *Phys. Rev. C*, 38:2408, 1988.

[121] L.-W. Siu, J. W. Holt, T. T. S. Kuo, and G. E. Brown. Low-momentum *NN* interactions and all-order summation of ring diagrams of symmetric nuclear matter. *Phys. Rev. C*, 79:054004, 2009.

[122] W. H. Dickhoff and H. Müther. Nucleon properties in the nuclear medium. *Reports on Progress in Physics*, 55(11):1947, 1992.

[123] P. Boek. Short-range correlations in asymmetric nuclear matter. *Physics Letters B*, 586(34):239 – 243, 2004.

[124] Kh. S. A. Hassaneen and H. Müther. Correlations and spectral functions in asymmetric nuclear matter. *Phys. Rev. C*, 70:054308, Nov 2004.

[125] T. Frick, H. Müther, A. Rios, A. Polls, and A. Ramos. Correlations in hot asymmetric nuclear matter. *Phys. Rev. C*, 71:014313, Jan 2005.

[126] P. Bożek, D. J. Dean, and H. Müther. Correlations and effective interactions in nuclear matter. *Phys. Rev. C*, 74:014303, Jul 2006.

[127] V. Somà and P. Bożek. Diagrammatic calculation of thermodynamical quantities in nuclear matter. *Phys. Rev. C*, 74:045809, Oct 2006.

[128] Kh. Gad and Kh.S.A. Hassaneen. Equation of state for neutron-rich matter with self-consistent green function approach. *Nuclear Physics A*, 793(14):67 – 78, 2007.

[129] V. Somà and P. Bożek. Thermodynamic properties of nuclear matter with three-body forces. *Phys. Rev. C*, 80:025803, Aug 2009.

[130] V. Som and P. Boek. Modifications of single-particle properties in nuclear matter induced by three-body forces. *Progress in Particle and Nuclear Physics*, 62(2):371 – 372, 2009. ¡ce:title¿Heavy-Ion Collisions from the Coulomb Barrier to the Quark-Gluon Plasma¡/ce:title¿ ¡ce:subtitle¿30th Course¡/ce:subtitle¿ ¡xocs:full-name¿International Workshop on Nuclear Physics¡/xocs:full-name¿.

[131] A. Rios, A. Polls, and I. Vidaña. Hot neutron matter from a self-consistent green's-functions approach. *Phys. Rev. C*, 79:025802, 2009.

[132] S. Fantoni and A. Faborchini. *Microscopic Quantum Many-Body Theories and Their Applications. Lecture Notes in Physics*, chapter Correlated Basis Function Theory for Fermion Systems. Springer, Berlin, 1998.

[133] S. C. Pieper. *Microscopic Quantum Many-Body Theories and Their Applications. Lecture Notes in Physics*, chapter Monte Carlo Calculations of Nuclei. Springer, Berlin, 1998.

[134] V. R. Pandharipande and R. B. Wiringa. Variations on a theme of nuclear matter. *Rev. Mod. Phys.*, 51:821–861, Oct 1979.

[135] R. B. Wiringa, V. Fiks, and A. Fabrocini. Equation of state for dense nucleon matter. *Phys. Rev. C*, 38:1010–1037, Aug 1988.

[136] A. Akmal and V. R. Pandharipande. Spin-isospin structure and pion condensation in nucleon matter. *Phys. Rev. C*, 56:2261–2279, Oct 1997.

[137] J. Carlson, J. Morales, V. R. Pandharipande, and D. G. Ravenhall. Quantum monte carlo calculations of neutron matter. *Phys. Rev. C*, 68:025802, Aug 2003.

[138] S. Gandolfi, A. Yu. Illarionov, K. E. Schmidt, F. Pederiva, and S. Fantoni. Quantum monte carlo calculation of the equation of state of neutron matter. *Phys. Rev. C*, 79:054005, May 2009.

[139] B. S. Pudliner, V. R. Pandharipande, J. Carlson, Steven C. Pieper, and R. B. Wiringa. Quantum monte carlo calculations of nuclei with $A \leq 7$. *Phys. Rev. C*, 56:1720–1750, Oct 1997.

[140] Alexandros Gezerlis and J. Carlson. Low-density neutron matter. *Phys. Rev. C*, 81:025803, Feb 2010.

[141] K.E. Schmidt and S. Fantoni. A quantum monte carlo method for nucleon systems. *Physics Letters B*, 446(2):99 – 103, 1999.

[142] S. Gandolfi, A. Yu. Illarionov, F. Pederiva, K. E. Schmidt, and S. Fantoni. Equation of state of low-density neutron matter, and the $^1S_0$ pairing gap. *Phys. Rev. C*, 80:045802, Oct 2009.

[143] B. Borasoy, E. Epelbaum, H. Krebs, D. Lee, and U.-G. Meißner. *Eur. Phys. J. A*, 35:357, 2008.

[144] E. Epelbaum, H. Krebs, D. Lee, and U.-G. Meißner. *Eur. Phys. J. A*, (40):199, 2009.

[145] Jeremy W. Holt, Norbert Kaiser, and Wolfram Weise. Nuclear chiral dynamics and thermodynamics. *Progress in Particle and Nuclear Physics*, 73(0):35 – 83, 2013.

[146] Kazuhiro Oyamatsu and Kei Iida. Saturation of nuclear matter and radii of unstable nuclei. *Progress of Theoretical Physics*, 109(4):631–650, 2003.

[147] A. Schwenk and C. J. Pethick. Resonant fermi gases with a large effective range. *Phys. Rev. Lett.*, 95:160401, Oct 2005.

[148] B. E. Vonderfecht, W. H. Dickhoff, A. Polls, and A. Ramos. *Nucl. Phys. A*, 555:1, 1993.

[149] T. Alm, G. Røpke, A. Schnell, N. H. Kwong, and H. S. Køhler. *Phys. Rev. C*, 53:2181, 1996.

[150] P. Bożek. *Nucl. Phys. A*, 657:187, 1999.

[151] P. Bożek and P. Czerski. *Eur. Phys. J. A*, 11:271, 2001.

[152] G. Shen, C. J. Horowitz, and S. Teige. Equation of state of nuclear matter in a virial expansion of nucleons and nuclei. *Phys. Rev. C*, 82:045802, Oct 2010.

[153] Alexandros Gezerlis and J. Carlson. Strongly paired fermions: Cold atoms and neutron matter. *Phys. Rev. C*, 77:032801, Mar 2008.

[154] A. L. Fetter and J. D. Walecka. *Quantum theory of many-particle systems*. McGraw-Hill Book Company, 1971.

[155] F. Schwabl. *Advanced Quantum Mechanics*. Springer-Verlag, fourth edition, 2008.

[156] R. L. Liboff. *Introductory Quantum Mechanics*. Addison Wesley, fourth edition, 2003.

[157] J. J. MacKenzie. *Phys. Rev.*, 179(4):1002, 1969.

[158] K. L. G. Heyde. *The Nuclear Shell Model*. Springer-Verlag, first edition, 1990.

[159] D. A. Varshalovich, A. N. Moskalev, and V. K. Khersonskii. *Quantum Theory of Angular Momentum*. World Scientific, 1988.

[160] T. D. Crawford and H. F. Schaefer. *Rev. Comp. Chem.*, 14:33, 2000.

[161] J. Goldstone. *Proc. R. Soc. Lond. A*, 239:267, 1957.

[162] M. Hjorth-Jensen, T. T. S. Kuo, and E. Osnes. *Phys. Rep. 261*, 261:125, 1995.

[163] A. Ramos, A. Polls, and W. H. Dickhoff. *Nucl. Phys. A*, 503:1, 1989.

[164] Àngels Ramos Gómez. PhD thesis, University of Barcelona, 1988.

[165] W. H. Press, S. A. Teukolosky, W. T. Vetterling, and B. P. Flannery. *Numerical Recipes in Fortran 77*. Cambridge University Press, second edition, 1992.

[166] L. E. Engvik. PhD thesis, University of Oslo, 1999.

[167] D. J. Dean and M. Hjorth-Jensen. *Phys. Rev. C*, 69:054320, 2004.

[168] Jochen H. Heisenberg and Bogdan Mihaila. Ground state correlations and mean field in ^{16}O. *Phys. Rev. C*, 59:1440–1448, Mar 1999.

[169] G. Hagen, T. Papenbrock, D. J. Dean, A. Schwenk, A. Nogga, M. Włoch, and P. Piecuch. *Phys. Rev. C*, 76:034302, 2007.

[170] G. Hagen, D. J. Dean, M. Hjorth-Jensen, T. Papenbrock, and A. Schwenk. *Phys. Rev. C*, 76:044305, 2007.

[171] Robert Roth, Jeffrey R. Gour, and Piotr Piecuch. *Ab initio* coupled-cluster and configuration interaction calculations for ^{16}O using the V_{ucom} interaction. *Phys. Rev. C*, 79:054325, May 2009.

[172] G. Hagen, P. Hagen, H.-W. Hammer, and L. Platter. Efimov physics around the neutron-rich ^{60}Ca isotope. *Phys. Rev. Lett.*, 111:132501, Sep 2013.

[173] Ø. Jensen, G. Hagen, T. Papenbrock, D. J. Dean, and J. S. Vaagen. Computation of spectroscopic factors with the coupled-cluster method. *Phys. Rev. C*, 82:014310, Jul 2010.

[174] D. A. Pigg, G. Hagen, H. Nam, and T. Papenbrock. Time-dependent coupled-cluster method for atomic nuclei. *Phys. Rev. C*, 86:014308, Jul 2012.

[175] R. Rajaraman. Three-body effect in nuclear matter to all orders of perturbation. *Phys. Rev.*, 131:1244–1248, Aug 1963.

[176] H. A. Bethe. Three-body correlations in nuclear matter. *Phys. Rev.*, 138:B804–B822, May 1965.

[177] R. F. Bishop and K. H. Lührmann. Electron correlations: I. ground-state results in the high-density regime. *Phys. Rev. B*, 17:3757–3780, May 1978.

[178] R F Bishop and W A Lahoz. Two-component fermi systems. i. fluid coupled cluster theory. *J. Phys. A: Math. Gen.*, 20(13):4203, 1987.

[179] D. L. Freeman. Coupled-cluster expansion applied to the electron gas: Inclusion of ring and exchange effects. *Phys. Rev. B*, 15:5512, 1977.

[180] G. H. Golub and C. F. van Loan. *Matrix Computations*. The John Hopkins University Press, third edition, 1996.

[181] W. Gropp, E. Lusk, and A. Skjellum. *Using MPI: portable parallel programming with the message-passing interface*. MIT Press, second edition, 1999.

[182] J. L. Träff, S. Benkner, and J. J. Dongarra. *Recent Advances in the Messsage Passing Interface. 19th European MPI Users' Group Meeting, EuroMPI 2012, Vienna, Austria, September 23-26, 2012. Proceedings*. Springer, 2012.

[183] B. Chapman, G. Jost, and R. van der Pas. *Using OpenMP. Portable Shared Memory Parallel Programming*. The MIT Press, 2008.

[184] G. Hagen, T. Papenbrock, D. J. Dean, and M. Hjorth-Jensen. *Ab initio* coupled-cluster approach to nuclear structure with modern nucleon-nucleon interactions. *Phys. Rev. C*, 82:034330, Sep 2010.

[185] P. Ring and P. Schuck. *The Nuclear Many-Body Problem*. Springer-Verlag, first edition, 2004.

[186] C.W. Wong and D.M. Clement. Vector bracket and transformed wave function of a few-body state. *Nuclear Physics A*, 183(1):210 – 224, 1972.

[187] C. L. Kung, T. T. S. Kuo, and K. F. Ratcliff. Converged values of second-order core-polarization diagrams with orthogonalized-plane-wave intermediate states. *Phys. Rev. C*, 19:1063–1082, Mar 1979.

[188] R. Balian and E. Brezin. *Nuovo Cim.*, 61:403, 1969.

[189] M. Hjorth-Jensen, M. Borromeo, H. Müther, and A. Polls. Isobar contributions to the imaginary part of the optical-model potential for finite nuclei. *Nuclear Physics A*, 551(4):580 – 610, 1993.

[190] R. D. Lawson. *Theory of the Nuclear Shell Model*. Oxford University Press, 1980.

[191] G. Racah. Theory of complex spectra. ii. *Phys. Rev.*, 62:438–462, Nov 1942.

[192] T. Papenbrock. Private communication.

[193] G. Hagen, M. Hjorth-Jensen, and N. Michel. Gamow shell model and realistic nucleon-nucleon interactions. *Phys. Rev. C*, 73:064307, Jun 2006.

[194] James J. Shepherd, Andreas Grüneis, George H. Booth, Georg Kresse, and Ali Alavi. Convergence of many-body wave-function expansions using a plane-wave basis: From homogeneous electron gas to solid state systems. *Phys. Rev. B*, 86:035111, Jul 2012.

[195] Alessandro Roggero, Abhishek Mukherjee, and Francesco Pederiva. Quantum monte carlo with coupled-cluster wave functions. *Phys. Rev. B*, 88:115138, Sep 2013.

[196] James J. Shepherd, George Booth, Andreas Grüneis, and Ali Alavi. Full configuration interaction perspective on the homogeneous electron gas. *Phys. Rev. B*, 85:081103, Feb 2012.

[197] James J. Shepherd, George H. Booth, and Ali Alavi. Investigation of the full configuration interaction quantum monte carlo method using homogeneous electron gas models. *The Journal of Chemical Physics*, 136(24):–, 2012.

[198] M. Abramowitz and I. A. Stengun. *Handbook of Mathematical Functions With Formulas, Graphs, and Mathematical Tables*. National Bureau of Standards, 1972.

[199] I. S. Gradshteyn and I. M. Ryzhik. *Table of integrals, series and products*. Elsvier, seventh edition, 2007.

[200] C. Hamaguchi. *Basic Semiconductor Physics*. Springer, 2010.

[201] T.T.S Kuo, J Shurpin, K.C Tam, E Osnes, and P.J Ellis. A simple method for evaluating goldstone diagrams in an angular momentum coupled representation. *Annals of Physics*, 132(2):237 – 276, 1981.

[202] J. J. Callahan. *Advanced Calculus. A Geometric View*. Springer, 2010.

Appendix A

Technical details

A.1 Antisymmetrization

When transforming the Brueckner-Hartree-Fock and coupled-cluster equations to a coupled angular momentum - relative momentum basis, one needs to consider antisymmetrized interaction matrix elements

$$\begin{aligned}
&\langle \mathbf{k}_p m_{s_p} m_{t_p} \mathbf{k}_q m_{s_q} m_{t_q} | \hat{v} | \mathbf{k}_r m_{s_r} m_{t_r} \mathbf{k}_s m_{s_s} m_{t_s} \rangle_{AS} \\
=&\langle \mathbf{k}_p m_{s_p} m_{t_p} \mathbf{k}_q m_{s_q} m_{t_q} | \hat{v} | \mathbf{k}_r m_{s_r} m_{t_r} \mathbf{k}_s m_{s_s} m_{t_s} \rangle \\
-&\langle \mathbf{k}_p m_{s_p} m_{t_p} \mathbf{k}_q m_{s_q} m_{t_q} | \hat{v} | \mathbf{k}_s m_{s_s} m_{t_s} \mathbf{k}_r m_{s_r} m_{t_r} \rangle . \qquad \text{(A.1)}
\end{aligned}$$

Let us transform only the ket vector of Eq. (A.1) to the coupled angular momentum - relative momentum basis

$$|k \mathcal{J} m_{\mathcal{J}} (lS) m_{t_1} m_{t_2} \rangle .$$

Using the angular momentum algebra relations of Eqs. (3.34) - (3.36) and (3.38) - (3.40) and assuming that the two nucleons are both either protons

or neutrons, we get

$$\begin{aligned}
&\left[|\mathbf{k}_p m_{s_p} \mathbf{k}_q m_{s_q}\rangle - |\mathbf{k}_q m_{s_q} \mathbf{k}_p m_{s_p}\rangle\right] \\
=&\left[|\mathbf{kK} m_{s_p} m_{s_q}\rangle - |-\mathbf{kK} m_{s_q} m_{s_p}\rangle\right] \\
=&\sum_{SM_S} \left[|\mathbf{kK}\rangle - (-1)^{1-S}|-\mathbf{kK}\rangle\right] \\
&\times |SM_S\rangle\langle SM_S| s m_{s_p} s m_{s_q}\rangle \\
=&\sum_{SM_S} \sum_{lm_l} \left[|\mathbf{kK}\rangle - (-1)^{1-S+l}|-\mathbf{kK}\rangle\right] \\
&\times \langle lm_l|\hat{\mathbf{k}}\rangle |SM_S lm_l\rangle\langle SM_S| s m_{s_p} s m_{s_q}\rangle \\
=&\sum_{SM_S} \sum_{lm_l} \sum_{\mathcal{J}m_\mathcal{J}} (1-(-1)^{1-S+l})|k\mathbf{K}\mathcal{J}m_\mathcal{J} lS\rangle \\
&\times \langle lm_l|\hat{\mathbf{k}}\rangle\langle SM_S| s m_{s_p} s m_{s_q}\rangle\langle \mathcal{J}m_\mathcal{J} lS|lm_l SM_S\rangle, \qquad \text{(A.2)}
\end{aligned}$$

where $\mathbf{k}$ and $\mathbf{K}$ are relative and CM momenta, respectively, as defined in Eq. (3.30). Whereas two creation operators related to one type of particle anticommute, creation operators of different particle species commute with each other [178]. Instead of antisymmetric matrix elements as defined in Eq. (A.1), we get matrix elements

$$2\langle \mathbf{k}_p m_{s_p} m_{t_p} \mathbf{k}_q m_{s_q} m_{t_q}|\hat{v}|\mathbf{k}_r m_{s_r} m_{t_r} \mathbf{k}_s m_{s_s} m_{t_s}\rangle \qquad \text{(A.3)}$$

when the particles r and s are of different nucleon types. The ket vector then becomes

$$\begin{aligned}
&2|\mathbf{k}_p m_{s_p} \mathbf{k}_q m_{s_q}\rangle \\
=&2\sum_{SM_S} \sum_{lm_l} \sum_{\mathcal{J}m_\mathcal{J}} |k\mathbf{K}\mathcal{J}m_\mathcal{J} lS\rangle \\
&\times \langle lm_l|\hat{\mathbf{k}}\rangle\langle SM_S| s m_{s_p} s m_{s_q}\rangle\langle \mathcal{J}m_\mathcal{J} lS|lm_l SM_S\rangle, \qquad \text{(A.4)}
\end{aligned}$$

where we now have a factor 2 insted of the antisymmetrization factor $(1-(-1)^{1-S+l})$. In the proton-neutron representation, we define the antisymmetrization operator

$$\mathcal{A}^{lSM_T} = \begin{cases} \sqrt{2}, & \text{if } M_T = 0, \\ \left(1-(-1)^{l+S+1}\right)/\sqrt{2}, & \text{if } |M_T| = 1. \end{cases} \qquad \text{(A.5)}$$

When written in the basis (A.2), all interaction matrix elements are assumed to be multiplied by a product $\mathcal{A}^{lSM_T}\mathcal{A}^{l'SM_T}$ to get the correct antisymmetrization. Observe that the antisymmetrization operator $\mathcal{A}$ is defined differently here than in Paper II.

The antisymmetrization operator $\mathcal{B}^{M_T,\pm}$ is defined for symmetric nuclear matter as

$$\mathcal{B}^{M_T,\pm}\langle k\mathcal{J}(lS)|\hat{O}|k\mathcal{J}(lS)\rangle = \langle k\mathcal{J}(lS)|\hat{O}(M_{T'}=0)|k\mathcal{J}(lS)\rangle + \left(1-(-1)^{1+l+S}\right)\langle k\mathcal{J}(lS)|\hat{O}(M_{T'}=M_T\pm\delta_{M_T0})|k\mathcal{J}(lS)\rangle \quad \text{(A.6)}$$

and for pure neutron matter as

$$\mathcal{B}^{M_T,\pm}\langle k\mathcal{J}(lS)|\hat{O}|k\mathcal{J}(lS)\rangle = \left(1-(-1)^{1+l+S}\right) \times \langle k\mathcal{J}(lS)|\hat{O}(M_{T'}=1)|k\mathcal{J}(lS)\rangle, \quad \text{(A.7)}$$

where $\hat{O}$ is a general two-particle operator.

Appendix B

Mathematical tools

B.1 Coupled delta distributions

Assume that $f : (x, y) \to \mathbb{R}$ and $g : (x, y) \to \mathbb{R}$ are functions with continuous derivatives on the domain $(x, y) \in \Omega(x, y) \subset \mathbb{R}^2$, and $h : (x, y) \to \mathbb{R}$ is an arbitrary function. We want to calculate an integral with two coupled delta distributions

$$\begin{aligned} &\iint_{\Omega(x,y)} \delta(f(x,y))\delta(g(x,y))h(x,y)dxdy \\ &\quad = \iint_{\Omega(x,y)} \delta^{(2)}(f(x,y), g(x,y))h(x,y)dxdy. \end{aligned} \tag{B.1}$$

On right-hand side we have defined the two-dimensional delta distribution $\delta^{(2)}(s, t)$. This integral can be evaluated by changing to the variables

$$s = f(x, y), \qquad t = g(x, y). \tag{B.2}$$

The integration measure transforms accordingly as [202]

$$dxdy \quad \longrightarrow \quad \left| \begin{array}{cc} \frac{\partial x}{\partial s} & \frac{\partial x}{\partial t} \\ \frac{\partial y}{\partial s} & \frac{\partial y}{\partial t} \end{array} \right| dsdt, \tag{B.3}$$

where the new measure contains the absolute value of a Jacobian determinant. Let the direction of integration of the new integration domain $\tilde{\Omega}(s, t)$ be the same as in the old domain $\Omega(x, y)$. If the initial integration domain $\Omega(x, y)$ is chosen such that there exist unique inverse mappings

$$\begin{aligned} \eta &= x(s, t), \\ \xi &= y(s, t), \end{aligned} \tag{B.4}$$

we can write the integral as

$$\begin{aligned}
&\iint_{\Omega(x,y)} \delta(f(x,y))\delta(g(x,y))h(x,y)dxdy \\
&\quad = \iint_{\tilde{\Omega}(s,t)} \delta^{(2)}(s,t)\tilde{h}(s,t) \left| \begin{array}{cc} \frac{\partial x}{\partial s} & \frac{\partial x}{\partial t} \\ \frac{\partial y}{\partial s} & \frac{\partial y}{\partial t} \end{array} \right| dsdt \\
&\quad = \tilde{h}(s,t) \left| \frac{\partial x}{\partial s} \cdot \frac{\partial y}{\partial t} - \frac{\partial x}{\partial t} \cdot \frac{\partial y}{\partial s} \right| \Bigg|_{s=t=0} \\
&\quad = \frac{\tilde{h}(s,t)}{\left| \frac{\partial s}{\partial x} \cdot \frac{\partial t}{\partial y} - \frac{\partial t}{\partial x} \cdot \frac{\partial s}{\partial y} \right|} \Bigg|_{s=t=0},
\end{aligned} \tag{B.5}$$

where we have defined $\tilde{h}(s,t) \equiv h(x(s,t), y(s,t))$. In the last equality we have applied the inverse function theorem [202].